

**PROBABILISTIC DESIGN AND RELIABILITY ANALYSIS WITH
KRIGING AND ENVELOPE METHODS**

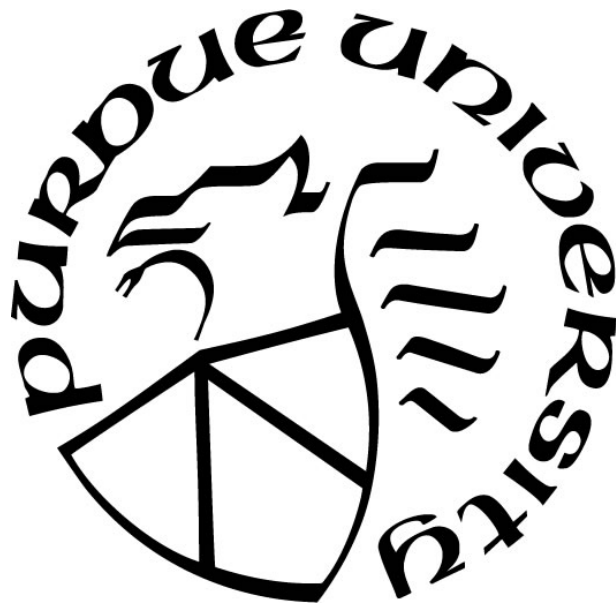
by
Hao Wu

A Dissertation

Submitted to the Faculty of Purdue University

In Partial Fulfillment of the Requirements for the degree of

Doctor of Philosophy



School of Mechanical Engineering

West Lafayette, Indiana

May 2022

THE PURDUE UNIVERSITY GRADUATE SCHOOL
STATEMENT OF COMMITTEE APPROVAL

Dr. Xiaoping Du, Co-Chair

Department of Mechanical and Energy Engineering

Dr. Ilias Bilonis, Co-Chair

School of Mechanical Engineering

Dr. Whitney Yu

Department of Mechanical and Energy Engineering

Dr. Qifan Song

Department of Statistics

Approved by:

Dr. Nicole L. Key

For my parents.

ACKNOWLEDGMENTS

First and foremost, I am extremely grateful to my advisor, Prof. Xiaoping Du for the invaluable advice, continuous support, and guidance during my PhD study. There are lots of ups and downs in this PhD journey, without his immense knowledge and plentiful support, I would not be where I am today, and this work would not have been possible. His diligence and rigorous attitude to work will have a significant influence on my future life.

The dissertation is supported by the National Science Foundation under Grants NO.1923799. I would also like to thank my committee members, Prof. Whitney Yu, Prof. Ilias Bilionis and Prof. Qifan Song for their insightful comments and support on my dissertation.

Besides, I would like to thank my labmates and friends, Dr. Zhengwei Hu, Dr. Zhangli Hu, Dr. Xinpeng Wei, Jianhua Yin, and Huiru Li for their support and help. I will remember this precious time in Rolla, MO and Indianapolis, IN.

Finally, I would like to express my gratitude to my parents. Without their tremendous love and support in the past few years, it would be impossible for me to complete my study.

TABLE OF CONTENTS

LIST OF TABLES	9
LIST OF FIGURES	11
ABSTRACT	12
1. INTRODUCTION	13
1.1 Background	13
1.2 Research Objective and Contributions.....	15
1.3 Organization of Dissertation	16
2. SYSTEM RELIABILITY ANALYSIS WITH AUTOCORRELATED KRIGING PREDICTIONS	18
2.1 Background.....	18
2.2 Methodologies Review	23
2.2.1 Kriging Method	23
2.2.2 Review of AK-SYS and EGRA-SYS	25
2.2.3 Review of Dependent Kriging Method for Component Reliability	27
2.3 Dependent Kriging Method for System Reliability.....	29
2.3.1 Estimate of ρ_{sf}	29
2.3.2 Learning Function.....	32
2.3.3 Stopping Criterion	33
2.3.4 Implementation	33
2.3.5 Parallel Systems.....	35
2.4 Examples.....	36
2.4.1 Example 1	36
2.4.2 Exmample 2	39
2.4.3 Example 3	41
2.4.4 Example 4	44
2.5 Summary.....	48
3. SYSTEM RELIABILITY ANALYSIS WITH SECOND ORDER SADDLEPOINT APPROXIMATION	49

3.1	Background.....	49
3.2	Review of Second Order SPA	52
3.2.1	MPP Search	52
3.2.2	Quadratic Limit-state Function.....	53
3.2.3	Saddlepoint Approximation.....	55
3.3	System Reliability with Second Order SPA	57
3.4	Examples.....	60
3.4.1	Example 1	60
3.4.2	Example 2	62
3.4.3	Example 3	64
3.4.4	Example 4	67
3.5	Summary.....	71
4.	TIME-DEPENDENT SYSTEM RELIABILITY ANALYSIS WITH SECOND ORDER RELIABILITY METHOD.....	72
4.1	Background.....	73
4.2	Methodologies Review	76
4.2.1	Time-Dependent Component Reliability.....	76
4.3	Proposed Methods	79
4.3.1	Overview.....	79
4.3.2	Hessian Matrix of the Envelope Function	80
4.3.3	System Reliability with SOSPA	83
4.3.4	Extension to the Problems with Input Random Process	87
4.3.5	Parallel Systems.....	88
4.4	Examples.....	88
4.4.1	Example 1: A Math Problem	88
4.4.2	Example 2: A Roof Truss Structure.....	92
4.4.3	Example 3: A Function Generator Mechanism System	94
4.5	Summary.....	97
5.	ENVELOPE METHOD FOR TIME- AND SPACE-DEPENDENT RELIABILITY PREDICTION.....	99
5.1	Background.....	99

5.2	Review Fundamental Methodologies	101
5.2.1	Problem Statement.....	101
5.2.2	First Order Reliability Method (FORM)	102
5.2.3	Time- and Space-independent Reliability Problem.....	102
5.2.4	Time-Dependent Reliability Problem.....	103
5.3	Envelope Method for Time- and Space-dependent Problem.....	103
5.3.1	Problems with Random Variables, and Temporal/Spatial Parameters	104
5.3.2	Problems with Random Variables, Random Fields, and Temporal/Spatial Parameters	111
5.3.3	Implementation	112
5.4	Examples.....	113
5.4.1	Example 1: A Math Problem	113
5.4.2	Example 2: A Truss Structure.....	116
5.4.3	Example 3: An Electron Accelerator.....	118
5.5	Summary.....	120
6.	ENVELOPE METHOD FOR TIME- AND SPACE-DEPENDENT RELIABILITY- BASED DESIGN.....	122
6.1	Background.....	123
6.2	Problem Statement.....	125
6.2.1	Problem Statement.....	125
6.2.2	Review of Sequential RBD.....	126
6.3	Sequential RBDO with the Envelope Method.....	127
6.3.1	Overview.....	127
6.3.2	Time- and Space-dependent Reliability Analysis.....	128
6.3.3	Extension to Case 2	134
6.3.4	Procedure of Sequential RBDO with Envelope Method	135
6.4	Examples.....	136
6.4.1	Example 1: A Mathematical Problem.....	137
6.4.2	Example 2: Three Bar System	138
6.4.3	Example 3: A Cantilever Beam	141
6.4.4	Example 4: Thermal Deflection of a Bimetallic Beam	144

6.5	Summary.....	145
7.	CONCLUSIONS AND FUTURE WORK.....	147
7.1	Conclusions.....	147
7.2	Future Work.....	148
	REFERENCES	149
	VITA.....	162

LIST OF TABLES

Table 2.1 Average results from 20 runs based on direct MCS	38
Table 2.2 Average results from 20 runs based on Latin hypercube sampling.....	39
Table 2.3 Random variables of example two.....	40
Table 2.4 Comparison of average results from 20 runs	40
Table 2.5 Random variables of example 3.....	42
Table 2.6 Deterministic parameters	43
Table 2.7 Comparison of average results from 20 runs	44
Table 2.8 Random variables	46
Table 2.9 Deterministic parameter.....	47
Table 2.10 Comparison of average results from 20 runs	47
Table 3.1 MPP, reliability index and directional vector	61
Table 3.2 Probability of system failure in Example 1	62
Table 3.3 Distribution of random variables	63
Table 3.4 Probability of system failure in Example 2	64
Table 3.5 Distribution of random variables	66
Table 3.6 Probability of system failure in Example 3	67
Table 3.7 Distribution of random variables	68
Table 3.8 Probability of system failure in Example 4	70
Table 4.1 Iteration history of MPP search for g_1	91
Table 4.2 Probability of system failure in Example 1	91
Table 4.3 Distribution of random variables	92
Table 4.4 Probability of system failure in Example 2	94
Table 4.5 Parameters in Example 3	96
Table 4.6 Probability of system failure in Example 3	97
Table 5.1 Iteration history of searching for the worst-case MPP	115
Table 5.2 Results of Example 1	116
Table 5.3 Random variables of Example 3	118

Table 5.4 Results of Example 3	118
Table 5.5 Results of Example 2	120
Table 6.1 Results of Example 1	137
Table 6.2 Random variables of Example 2.....	139
Table 6.3 Results of Example 2	141
Table 6.4 Distributions of variables in Example 3	143
Table 6.5 Results of Example 3	143
Table 6.6 Random variables	145
Table 6.7 Results of Example 4	145

LIST OF FIGURES

Figure 1.1 Organization of the dissertation.....	17
Figure 2.1 Flowchart of DKM-SYS.....	35
Figure 2.2 Training points and surrogate models of AK-SYS.....	37
Figure 2.3 Training points and surrogate models of DKM-SYS	38
Figure 2.4 A cantilever beam.....	41
Figure 2.5 A crank-slider system	44
Figure 3.1 A cantilever bar	67
Figure 4.1 Relationship between the worst-case limit-state function and envelope function	79
Figure 4.2 Flowchart of time-dependent system reliability	86
Figure 4.3 Envelope function formed by instantaneous limit-state surfaces	89
Figure 4.4 System extreme limit-state function.....	90
Figure 4.5 A roof truss	92
Figure 4.6 A Function Generator Mechanism System.....	95
Figure 5.1 The envelope function	114
Figure 5.2 Convergence history of reliability index β	115
Figure 5.3 A truss structure.....	117
Figure 5.4 An electron accelerator.....	119
Figure 6.1 Search for equivalent MPP with the envelope method	127
Figure 6.2 Sequential RBDO with the envelope method.....	136
Figure 6.3 Iterative process of the objective function and design variables	138
Figure 6.4 A truss structure.....	139
Figure 6.5 A cantilever beam.....	142
Figure 6.6 Deflection of the Bimetallic Beam	144

ABSTRACT

In the mechanical design stage, engineers always meet with uncertainty, such as random variables, stochastic processes, and random processes. Due to the uncertainty, products may behave randomly with respect to time and space, and this may result in a high probability of failure, low lifetime, and low robustness. Although extensive research has been conducted on the component reliability methods, time- and space-dependent system reliability methods are still limited. This dissertation is motivated by the need of efficient and accurate methods for addressing time- and space-dependent system reliability and probabilistic design problems.

The objective of this dissertation is to develop efficient and accurate methods for reliability analysis and design. There are five research tasks for this objective. The first research task develops a surrogate model with an active learning method to predict the time- and space-independent system reliability. In the second research task, the time- and space-independent system reliability is estimated by the second order saddlepoint approximation method. In the third research task, the time-dependent system reliability is addressed by an envelope method with efficient global optimization. In the fourth research task, a general time- and space-dependent problem is investigated. The envelope method converts the time- and space-dependent problem into time- and space-independent one, and the second order approximation is used to predict results. The last task proposes a new sequential reliability-based design with the envelope method for time- and space-dependent reliability. The accuracy and efficiency of our proposed methods are demonstrated through a wide range of mathematics problems and engineering problems.

1. INTRODUCTION

1.1 Background

Uncertainty always exists in the product design and development, and operations of engineering systems [1-5]. Uncertainty may significantly affect the reliability of products and systems. It is vital to predict system reliability in the design stage to maintain low lifecycle costs and avoid tragic system failures [6, 7]. System reliability is the probability that the system can work properly without any failure. Since a system is composed of multiple components, its reliability depends on the reliability of each component and the dependency between component states.

Uncertainty can be classified into time- and space-independent uncertainty, namely static uncertainty, and time- and space-dependent uncertainty. Static uncertainty exists in random variables, which do not vary with respect to time and space, such as the randomness in dimensions of mechanical components. Time- and space-dependent uncertainty exists in random processes and random fields that change randomly over time and in space. Examples include random material properties, random loadings that vary at different time instances and locations, and random operation conditions.

There are three types of methods for the system reliability analysis, and they are numerical methods, sampling-based methods, and surrogate model methods. Among numerical methods, the traditional first-order reliability method (FORM) is the most common method as it has a good trade-off between efficiency and accuracy [8-12]. When the limit-state functions (the functions to predict the state of a component and system for reliability analysis) are non-linear, using the second-order reliability method (SORM) can achieve higher accuracy in estimating the probabilities [13-15]. The saddlepoint approximation (SPA) method can also achieve higher accuracy without sacrificing computational efficiency [14, 16-20].

Sampling-based methods can produce accurate results if the sample size is large enough. Such methods include Monte Carlo simulation (MCS) [21-23], importance sampling (IS) [24, 25], and subset simulation (SS) [26-28]. The advantage of MCS is its easy implementation and high accuracy. MCS can deal with highly nonlinear problems. But the computational cost will be extremely high if the reliability is high. IS provides a way to reduce the computational cost since

it generates more samples in the failure area. SS is also a powerful simulation tool for estimating small failure probabilities, which are expressed as a product of larger conditional failure probabilities by introducing intermediate failure events.

Surrogate modeling methods overcome the drawbacks of the inefficiency of sampling methods [29-35]. A surrogate model as an approximate model is constructed based on inputs and outputs of the chosen training points. If the inexpensive surrogate model is close to the limit-state function, it can replace the expensive limit-state function for reliability analysis. Popular surrogate modeling methods include support vector machines [25][34], polynomial response surface method [26], neural networks [27], and Kriging [35-37].

The above three types of methods are for reliability prediction. Reliability should also be considered in the design process. Reliability-based design (RBD) aims to mitigate the effects of uncertainty upon system performance and reduce the risk and cost in the design stage. When the system information is completely known, RBD determines optimal design variables by minimizing the cost and ensuring the satisfaction of the reliability requirement. It involves both optimization and reliability analysis. There are many mature RBD methodologies, such as double-loop methods [38], single loop approaches [39], sequential optimization method [40], and safety-factor approaches [41].

Most of the above methods are for static problems. There are still research needs in improving their performance. For instance, the most popular methods of the first and second-order reliability methods (FORM and SORM) for system reliability analysis may introduce large errors when limit-state functions are highly nonlinear [42]. Therefore, the surrogate-based methods are used [43]. But the surrogate-based methods still have some limitations. For instance, the Kriging method [35] does not account for the covariance between responses at different inputs, which may affect the efficiency and accuracy of the results.

Time- and space-dependent uncertainty, such as stochastic processes and random fields [44], is common in engineering applications. Time-dependent reliability methods can be solved by MCS, but the computational cost is much higher than those for static reliability methods [45-49]. The most common method is the Rice formula method [50]. It is efficient but may not be accurate when upcrossings (failure) events are strongly dependent [51]. Surrogate-modeling methods have therefore been proposed to improve the accuracy [52], but the accuracy is still not satisfactory for highly nonlinear limit-state functions. For the most general time- and space-dependent reliability

methods, MCS will be computationally expensive [53-55]. There is a critical need to develop methodologies to improve the accuracy and efficiency of time- and space-dependent reliability prediction.

As for the time- and space-dependent RBD, to our best knowledge, there is no practical way to efficiently perform optimization with time- and space-dependent reliability constraints. There is a need to extend the time- and space-dependent reliability analysis into time- and space-dependent RBD to achieve efficient time- and space-dependent RBD.

1.2 Research Objective and Contributions

The objective of this research is to predict component and system reliability and conduct reliability-based design efficiently and accurately with Kriging and Envelope methods. To achieve this objective, we propose five research tasks. The first research task develops a Kriging method with active learning to predict system reliability. The second research task employs a second order saddlepoint method to predict system reliability. The third research task proposes an envelope method with efficient global optimization to estimate time-dependent system reliability. The fourth research task extends the envelope method to deal with the most general time- and space-dependent problem. The fifth research task is reliability-based design under time- and space-dependent uncertainty with the envelope method. The five research tasks together improve the accuracy of reliability prediction results and enable time- and space-dependent reliability-based design, and the specific contributions of each research task are summarized below.

Research task 1 proposes a new system reliability method that combines Monte Carlo simulation and the kriging method with improved accuracy and efficiency. A new learning function is proposed to select training points to relieve the computational burden greatly without jeopardizing the accuracy of the reliability prediction. Accurate surrogate models are created for limit-state functions with the minimal variance in the estimate of the system reliability, thereby producing high accuracy for the system reliability prediction.

Research task 2 extends the second order SPA to system reliability analysis. The joint distribution of all the component responses is approximated by a multivariate normal distribution. To maintain high accuracy of the approximation, the proposed method employs the second-order SPA to accurately generate the marginal distributions of the component responses. The proposed

method estimates the covariance matrix of the multivariate normal distribution with the first order approximation to the component responses to achieve high efficiency. With the estimated marginal component distributions and covariance matrix, the very fast estimation for system reliability can be achieved.

Research task 3 develops a time-dependent system reliability method, which uses the envelope method and second-order reliability method. The component reliability index is estimated using the existing second-order component reliability method for high accuracy. The covariance between component responses is estimated with the first-order approximations for high efficiency. The accurate prediction result is achieved by approximating the joint probability of all the component responses as a multivariate normal distribution with its mean vector being component reliability indexes and covariance being those calculated by the first order reliability method.

Research task 4 proposes an envelope method for predicting the component reliability under time- and space-dependent reliability. It at first searches for the most probable point (MPP) of the envelope function using the sequential efficient global optimization in the domain of the space and time under consideration. The distinctive feature of the new method is the true second order approximation to envelope functions with its accurate Hessian matrix calculation, and then the envelope function of the time- and space-dependent limit-state function is evaluated at its worst-case MPP with high accuracy.

Research task 5 aims at introducing the envelope method into time- and space-dependent RBD. Sequential optimization is used to decouple the double-loop structure of optimization for releasing the computational cost. The accurate design results are achieved by a series cycle of deterministic optimization and reliability analysis with the envelope method.

In summary, the results of the above research will enable engineers to accurately predict the reliability of engineering systems and to identify the optimal design results by ensuring satisfied reliability in the early design stage. Other areas that can benefit include uncertainty quantification, design under uncertainty, and reliability engineering.

1.3 Organization of Dissertation

The sequence of the dissertation is shown in Figure 1.1. The first four tasks are system reliability analysis, and the last task is reliability-based design. Tasks I and II address the gaps in

existing static reliability methodologies and prepare for time-dependent reliability analysis. Task III deals with gaps in time-dependent reliability. Task VI focuses on the time- and space-dependent reliability problem. Task V uses the above reliability analysis methods for the time- and space-dependent reliability-based design problem.

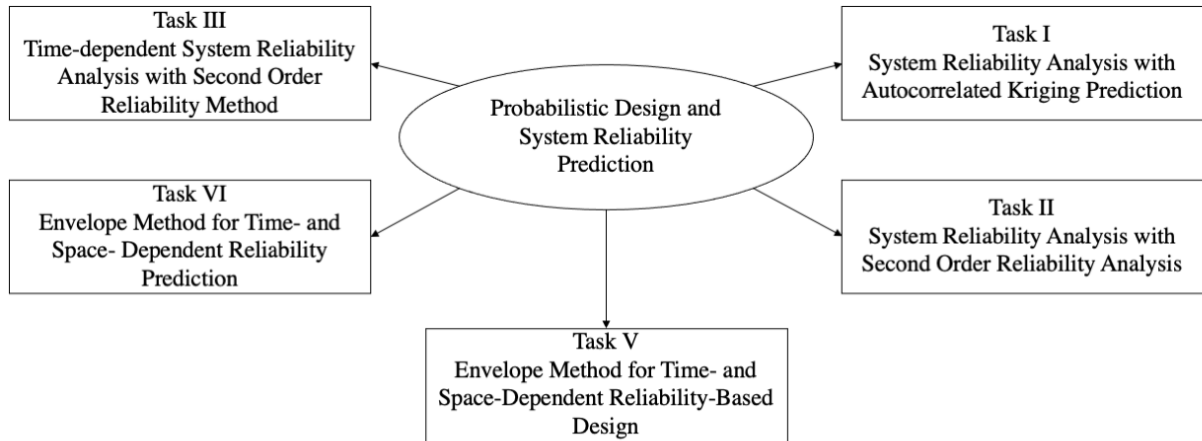


Figure 1.1 Organization of the dissertation

2. SYSTEM RELIABILITY ANALYSIS WITH AUTOCORRELATED KRIGING PREDICTIONS

Hao Wu¹, Xiaoping Du²

¹School of Mechanical Engineering, Purdue University, West Lafayette, IN, United States

²Department of Mechanical and Energy Engineering, Indiana University - Purdue University Indianapolis, IN, United States

Published in ASME. J. Mech., doi: <https://doi.org/10.1115/1.4046648>

Authors' contribution: H.W. and X.D. designed the study and contributed to the writing of the manuscript. H.W. developed detailed methodology and the code.

When limit-state functions are highly nonlinear, traditional reliability methods, such as the first order and second-order reliability methods, are not accurate. Monte Carlo simulation (MCS), on the other hand, is accurate if sufficient sample size is used, but is computationally intensive. This research proposes a new system reliability method that combines MCS and the Kriging method with improved accuracy and efficiency. Accurate surrogate models are created for limit-state functions with the minimal variance in the estimate of the system reliability, thereby producing high accuracy for the system reliability prediction. Instead of employing global optimization, this method uses MCS samples from which training points for the surrogate models are selected. By considering the autocorrelation of a surrogate model, this method captures the more accurate contribution of each MCS sample to the uncertainty in the estimate of the serial system reliability and therefore chooses training points efficiently. Good accuracy and efficiency are demonstrated by four examples.

2.1 Background

With the increasing complexity of engineering systems, the cost of system failures may also increase. To maintain low lifecycle costs and avoid tragic system failures, it is vital to predict the system reliability accurately in the design process. System reliability is the probability that a system performs its intended function without failures under given working conditions. With the

system reliability available, designers can make more reliable decisions on maintenance plans, warranty policies, and cost assessment [56, 57].

In general, system reliability methods are classified into two major groups: analytical methods and sampling-based methods. The most popular analytical methods are the First and Second-Order Reliability Methods (FORM and SORM) [58-61], which employ a first and second-order approximation, respectively, to a limit-state function in the vicinity of the Most Probable Point (MPP). But for limit-state functions that are not linear or quadratic, significant errors could be introduced by FORM and SORM. Both methods may also produce large errors if multiple MPPs exist. Higher accuracy can be achieved by sampling-based methods. They include Monte Carlo simulation [62] and importance sampling [63-68]. MCS is widely used due to its easy implementation and high accuracy if a sufficiently large number of samples is used. MCS can deal with problems with almost any level of nonlinearity, but the computational cost is extremely high if reliability is high. Importance sampling methods could be used to reduce the computational cost because they generate more samples in the failure region. The importance sampling methods require the MPP to center the sample distributions at the MPP. For a large-scale problem, searching for the MPP is expensive, and this reduces the efficiency of importance sampling.

In addition to the above two groups of methods, surrogate-based methods are increasingly used due to their ability to reduce computational cost by creating surrogate models, or meta-models [69, 70]. A surrogate model is a computationally inexpensive model created to substitute the original expensive limit-state function. The goal of metamodeling is to make the surrogate model accurate at an affordable computational cost. The general process of metamodeling starts with generating a small number of initial sample points (training points or TPs) by Design of Experiments (DOE) [71]. Based on these samples, an initial surrogate model is built by a metamodeling technique. Then more TPs are added to improve the accuracy of the surrogate model. Learning functions are employed to select the best TPs intelligently, and the surrogate model is refined in a most efficient manner.

Popular metamodeling techniques include the polynomial response surface method [72, 73], neural networks [74-76], support vector machines [77-79], polynomial chaos expansion [80], Kriging [81-83], etc. Kriging method could be used for interpolation. The prediction of an existing training point produces the exact value of the response at the point. Besides, due to its stochastic characteristics, Kriging provides not only the prediction of an untried point, but also the variance

of the prediction. The variance indicates the uncertainty of the prediction. Based on Kriging, Jones et al. developed the Efficient Global Optimization (EGO) method [84]. EGO uses the Expected Improvement Function (EIF) to achieve a good balance between exploiting areas of the design space where good solutions have been found, and exploring the design space where the uncertainty is high. Later, Bichon et al. proposed the Efficient Global Reliability Analysis (EGRA) [85] and extended it to system reliability prediction with multiple failure modes [86]. The latter method is called EGRA-SYS. The method uses the Expected Feasibility Function (EFF) to choose new TPs in the vicinity of the limit state and helps build an accurate surrogate model with fewer function evaluations. EGRA needs global optimization to find the optimum training point. Recently, Echard et al. proposed an active learning method to avoid global optimization. The method takes advantage of Kriging and Monte Carlo simulation (AK-MCS) [87], which chooses new TPs from a pre-sampled MCS population; as a result, no global optimization is needed. Fauriat and Gayton then applied AK-MCS to system reliability analysis [88].

The above methods make the Kriging predictions without exploiting the covariance between pairs of given points, and we referred to them as Independent Kriging Methods (IKM). As a matter of fact, the predictions from Kriging are realizations of a Gaussian process and therefore are dependent on one another. Considering the dependence could further improve the efficiency and accuracy of the active learning methods. Based on this strategy, Zhu and Du proposed a reliability method with MCS and dependent Kriging predictions, called Dependent Kriging Method (DKM) [89]. Accounting for dependence between Kriging predictions and focusing directly on the accuracy of reliability estimation, DKM achieves better accuracy and efficiency.

DKM is applicable only for component reliability analysis. The objective of the present study is to extend DKM to system reliability analysis. The contributions of this study include the following: (1) the extension of the component DKM to system problems so that multiple failure modes can be considered, (2) a new learning function that uses selected candidate points to relieve the computational burden greatly without jeopardizing the accuracy of reliability estimation, and (3) the development of a numerical procedure allows for accurate system reliability prediction at an affordable cost. Since the proposed method is based on Kriging and DKM, we briefly review them in Section 2. In Section 3, the dependent Kriging method for systems (DKM-SYS) is explained in detail. Section 4 provides four examples to illustrate the implementation process and the effectiveness of the new method. Conclusions are made in Section 5.

With the increasing complexity of engineering systems, the cost of system failures may also increase. To maintain low lifecycle costs and avoid tragic system failures, it is vital to predicting the system reliability accurately in the design process. System reliability is the probability that a system performs its intended function without failures under given working conditions. With the system reliability available, designers can make more reliable decisions on maintenance plans, warranty policies, and cost assessment [56, 57].

In general, system reliability methods are classified into two major groups: analytical methods and sampling-based methods. The most popular analytical methods are the First and Second-Order Reliability Methods (FORM and SORM) [58-61], which employ a first and second-order approximation, respectively, to a limit-state function in the vicinity of the Most Probable Point (MPP). But for limit-state functions that are not linear or quadratic, significant errors could be introduced by FORM and SORM. Both methods may also produce large errors if multiple MPPs exist.

Higher accuracy can be achieved by sampling-based methods. They include Monte Carlo simulation [62] and importance sampling [63-68]. MCS is widely used due to its easy implementation and high accuracy if a sufficiently large number of samples is used. MCS can deal with problems with almost any level of nonlinearity, but the computational cost is extremely high if reliability is high. Importance sampling methods could be used to reduce the computational cost because they generate more samples in the failure region. Most importance sampling methods require the MPP to center the sample distributions at the MPP. For a large-scale problem, searching for the MPP is expensive, and this reduces the efficiency of importance sampling.

In addition to the above two groups of methods, surrogate-based methods are increasingly used due to their ability to reduce computational cost by creating surrogate models, or meta-models [69, 70]. A surrogate model is a computationally inexpensive model created to substitute the original expensive limit-state function. The goal of metamodeling is to make the surrogate model accurate at an affordable computational cost. The general process of metamodeling starts with generating a small number of initial sample points (training points or TPs) by Design of Experiments (DOE) [71]. Based on these samples, an initial surrogate model is built by a metamodeling technique. Then more TPs are added to improve the accuracy of the surrogate model. Learning functions are employed to select the best TPs intelligently, and the surrogate model is refined in a most efficient manner.

Popular metamodeling techniques include the polynomial response surface method [72, 73], neural networks [74-76], support vector machines [77-79], polynomial chaos expansion [80], Kriging [81-83], etc. Kriging method could be used for interpolation. The prediction of an existing training point produces the exact value of the response at the point. Besides, due to its stochastic characteristics, Kriging provides not only the prediction of an untried point, but also the variance of the prediction. The variance indicates the uncertainty of the prediction. Based on Kriging, Jones et al. developed the Efficient Global Optimization (EGO) method [84]. EGO uses the Expected Improvement Function (EIF) to achieve a good balance between exploiting areas of the design space where good solutions have been found, and exploring the design space where the uncertainty is high. Later, Bichon et al. proposed the Efficient Global Reliability Analysis (EGRA) [85] and extended it to system reliability prediction with multiple failure modes [86]. The latter method is called EGRA-SYS. The method uses the Expected Feasibility Function (EFF) to choose new TPs in the vicinity of the limit state and helps build an accurate surrogate model with less function evaluations. EGRA needs global optimization to find the optimum training point. Recently, Echard et al. proposed an active learning method to avoid global optimization. The method takes advantage of Kriging and Monte Carlo simulation (AK-MCS) [87], which chooses new TPs from a pre-sampled MCS population; as a result, no global optimization is needed. Fauriat and Gayton then applied AK-MCS to system reliability analysis [88].

The above methods make the Kriging predictions without exploiting the covariance between pairs of given points, and we referred to them as Independent Kriging Methods (IKM). As a matter of fact, the predictions from Kriging are realizations of a Gaussian process and therefore are dependent on one another. Accounting for dependence between Kriging predictions and focusing directly on the accuracy of reliability estimation, DKM achieves better accuracy and efficiency.

DKM is applicable only for component reliability analysis. The objective of the present study is to extend DKM to system reliability analysis. The contributions of this study include the following: (1) the extension of the component DKM to system problems so that multiple failure modes can be considered; (2) a new learning function that uses selected candidate points to relieve the computational burden greatly without jeopardizing the accuracy of reliability estimation, and (3) the development of a numerical procedure allows for accurate system reliability prediction at an affordable cost.

Since the proposed method is based on Kriging and DKM, we briefly review them in Section 2. In Section 3, the dependent Kriging method for systems (DKM-SYS) is explained in detail. Section 4 provides four examples to illustrate the implementation process and the effectiveness of the new method. Conclusions are made in Section 5.

2.2 Methodologies Review

In this work, the component reliability is defined by

$$R = \Pr\{y = g(\mathbf{x}) > 0\} \quad (1)$$

where y is a component response and \mathbf{x} is a random vector. If $y > 0$, the failure mode does not occur; otherwise, the failure occurs.

Next, we herein review the methods that are needed by the proposed method.

2.2.1 Kriging Method

Kriging is an interpolation method since its prediction at an existing TP is the exact value of the response at the point. For a performance function $y = f(\mathbf{x})$, Kriging considers $y = f(\mathbf{x})$ being a realization of Gaussian process defined by

$$G(\mathbf{x}) = \mathbf{f}(\mathbf{x})^T \boldsymbol{\beta} + Z(\mathbf{x}) \quad (2)$$

where $\mathbf{f}(\mathbf{x})^T \boldsymbol{\beta}$ is a determination term for the mean response, $\mathbf{f}(\mathbf{x})$ is a vector of regression functions, and $\boldsymbol{\beta}$ is a vector regression coefficient. $Z(\cdot)$ is a stationary Gaussian process with zero mean and covariance

$$\text{Cov}[Z(\mathbf{x}_i), Z(\mathbf{x}_j)] = \sigma_Z^2 R(\mathbf{x}_i, \mathbf{x}_j) \quad (3)$$

where σ_Z^2 is the process variance, and $R(\cdot, \cdot)$ is the correlation function. The commonly used Gaussian correlation is the anisotropic squared exponential model, which is given by

$$R(\mathbf{x}_i, \mathbf{x}_j) = \exp \left[- \sum_{k=1}^d \theta_k (x_{ik} - x_{jk})^2 \right] \quad (4)$$

where x_{ik} and x_{jk} are the k -th components of \mathbf{x}_i and \mathbf{x}_j , respectively, d is the dimensionality of \mathbf{x} , and θ_k is a parameter that indicates the correlation between the points in dimension k . Due to the stochastic characteristics, Kriging provides not only the prediction at an untried point but also the variance of the prediction. The variance indicates the uncertainty of the prediction. At an untried point \mathbf{x} , the Kriging predictor $\hat{g}(\mathbf{x})$ follows a Gaussian distribution denoted by

$$\hat{g}(\mathbf{x}) \sim N(\mu_G(\mathbf{x}), \sigma_G^2(\mathbf{x})) \quad (5)$$

where $\mu_G(\mathbf{x})$ and $\sigma_G^2(\mathbf{x})$ are the prediction and its variance, respectively. They are computed by [81]

$$\mu_G(\mathbf{x}) = \mathbf{f}(\mathbf{x})^\top \hat{\boldsymbol{\beta}} + \mathbf{r}(\mathbf{x})\mathbf{R}^{-1}(\mathbf{y} - \mathbf{F}\hat{\boldsymbol{\beta}}) \quad (6)$$

$$\sigma_G^2 = \hat{\sigma}_Z^2 \{1 - \mathbf{r}(\mathbf{x})^\top \mathbf{R}^{-1} \mathbf{r}(\mathbf{x}) + [\mathbf{F}^\top \mathbf{R}^{-1} \mathbf{r}(\mathbf{x}) - \mathbf{f}(\mathbf{x})]^\top (\mathbf{F}^\top \mathbf{R}^{-1} \mathbf{F})^{-1} [\mathbf{F}^\top \mathbf{R}^{-1} \mathbf{r}(\mathbf{x}) - \mathbf{f}(\mathbf{x})]\} \quad (7)$$

in which \mathbf{y} is a vector of responses at the TPs, \mathbf{F} is a $m \times p$ matrix with rows $\mathbf{f}(\mathbf{x})^\top$, m is the number of TPs, and $\mathbf{r}(\cdot)$ is the correlation vector containing the correlation between \mathbf{x} and each of the TPs.

$$\mathbf{r}(\mathbf{x}) = [R(\mathbf{x}, \mathbf{x}_1), R(\mathbf{x}, \mathbf{x}_2), \dots, R(\mathbf{x}, \mathbf{x}_m)]^\top \quad (8)$$

\mathbf{R} is the correlation matrix, which is composed of correlation functions evaluated at each possible combination of the m TPs. \mathbf{R} is given by

$$\mathbf{R} = [R(\mathbf{x}_i, \mathbf{x}_j)], \quad 1 \leq i \leq m; 1 \leq j \leq m \quad (9)$$

$\hat{\boldsymbol{\beta}}$ is the least square estimate of $\boldsymbol{\beta}$ given by

$$\hat{\boldsymbol{\beta}} = (\mathbf{F}^\top \mathbf{R}^{-1} \mathbf{F})^{-1} \mathbf{F}^\top \mathbf{R}^{-1} \mathbf{y} \quad (10)$$

and $\hat{\sigma}_Z^2$ are determined through

$$\hat{\sigma}_Z^2 = \frac{1}{m} (\mathbf{y} - \mathbf{F}\hat{\boldsymbol{\beta}})^\top \mathbf{R}^{-1} (\mathbf{y} - \mathbf{F}\hat{\boldsymbol{\beta}}) \quad (11)$$

The parameters θ_k are determined through the maximum likelihood estimation, details of which are available in Ref. [81, 82].

2.2.2 Review of AK-SYS and EGRA-SYS

Both AK-SYS [88] and EGRA-SYS [86] are system reliability methods and are based on the Kriging method. Once surrogate models of all the limit-state functions are built, the two methods use MCS to estimate the system reliability using the surrogate models. They at first generate a sufficient number of sample points \mathbf{x}_{MCS} by MCS and use a few initial TPs to create initial surrogate models. New TPs are then added one by one so that the surrogate models are continually updated. AK-SYS and EGRA-SYS select new TPs using the strategies in AK-MCS [87] and EGRA [30], respectively. AK-MCS selects a new TP with a learning function defined by

$$U(\mathbf{x}) = \frac{|\mu_g(\mathbf{x})|}{\sigma_g(\mathbf{x})} \quad (12)$$

U is related to the chance of making a mistake on the sign of the prediction. The smaller is U , the higher is the likelihood. Consequently, the sample point with the smallest U is selected as a new TP. For a system with multiple components, a composite learning function U^* is used by AK-SYS [88] and is given by $U^*(\mathbf{x}) = |\mu_g^*(\mathbf{x})| / \sigma_g^*(\mathbf{x})$. For a series system, $\mu_g^*(\mathbf{x})$ is the minimal value among the predictions of all components at \mathbf{x} , and $\sigma_g^*(\mathbf{x})$ is the corresponding standard deviation. EGRA-SYS [31] uses a different learning function, which is called the expected feasibility function (*EFF*) and is defined by

$$\begin{aligned} EFF(\mathbf{x}) = & (\mu_g^*(\mathbf{x}) - e) \left[2\Phi\left(\frac{e - \mu_g^*(\mathbf{x})}{\sigma_g^*(\mathbf{x})}\right) - \Phi\left(\frac{e^- - \mu_g^*(\mathbf{x})}{\sigma_g^*(\mathbf{x})}\right) - \Phi\left(\frac{e^+ - \mu_g^*(\mathbf{x})}{\sigma_g^*(\mathbf{x})}\right) \right] \\ & - \sigma_g^*(\mathbf{x}) \left[2\phi\left(\frac{e - \mu_g^*(\mathbf{x})}{\sigma_g^*(\mathbf{x})}\right) - \phi\left(\frac{e^- - \mu_g^*(\mathbf{x})}{\sigma_g^*(\mathbf{x})}\right) - \phi\left(\frac{e^+ - \mu_g^*(\mathbf{x})}{\sigma_g^*(\mathbf{x})}\right) \right] \\ & + \delta \left[\Phi\left(\frac{e^+ - \mu_g^*(\mathbf{x})}{\sigma_g^*(\mathbf{x})}\right) - \Phi\left(\frac{e^- - \mu_g^*(\mathbf{x})}{\sigma_g^*(\mathbf{x})}\right) \right] \end{aligned} \quad (13)$$

where $e^- = e - \delta$, $e^+ = e + \delta$, in which e is the failure threshold, and δ is usually chosen by $\delta = 2\sigma_g^*(\mathbf{x})$. $\Phi(\cdot)$ and $\phi(\cdot)$ are the cumulative density function (CDF) and probability density function (PDF) of a standard normal random variable.

The process of AK-SYS and EGRA-SYS is as follows:

(1) Generate a small number of initial TPs, denoted by \mathbf{x}_{kT} ; evaluate the limit-state functions $\mathbf{y}_{kT} = \mathbf{g}_k(\mathbf{x}_{kT})$, where $k = 1, 2, \dots, M$, and M is the number of components.

(2) Build surrogate models $\hat{y}_k = \hat{g}_k(\mathbf{x}_{kT})$.

(3) Generate Monte Carlo samples for input random variables \mathbf{x}_{MCS} .

(4) Evaluate the composite U function and EFF function at \mathbf{x}_{MCS} using the predictions and standard deviations from $\hat{y}_k = \hat{g}_k(\mathbf{x}_{kT})$.

(5) Find the minimal value of the composite U learning function among those at all points in \mathbf{x}_{MCS} . For the EGRA method, find the maximal value of the composite EFF learning function among those at all points in \mathbf{x}_{MCS} .

(6) Check the convergence: The process converges if $U_{\min}^* \geq 2$ or $EFF_{\max}^* \leq 0.001$, and then perform reliability analysis using $\hat{y}_k = \hat{g}_k(\mathbf{x}_{kT})$; otherwise, go to Step (7).

(7) Identify a new TP \mathbf{x}_{new} with the minimal composite learning function value U_{\min}^* or the maximal composite learning function EFF_{\max}^* .

(8) Calculate the component U_k or EFF_k with high uncertainty at \mathbf{x}_{new} , and check $U_k < 2$ or $EFF_k > 0.001$.

(9) Add \mathbf{x}_{new} and the responses at \mathbf{x}_{new} to the existing training point set and update the surrogate models.

Repeat steps (2) through (9) till convergence.

As discussed previously, the larger is U or EFF , the higher is the chance that the Kriging model is accurate. In Step 8, the threshold of 2 is taken for U to check the convergence. The threshold of EFF is taken 0.001.

The size of \mathbf{x}_{MCS} is determined by the estimate of the probability of system failure p_{sf} and the coefficient of variation COV_{psf} . The relationship is given by

$$COV_{psf} = \sqrt{\frac{1-p_{sf}}{p_{sf}N_{MCS}}} \quad (14)$$

where N_{MCS} is the size of \mathbf{x}_{MCS} . N_{MCS} may vary so that $COV_{psf} \leq 5\%$.

Without the consideration of correlation, AK-SYS and EGRA-SYS use only mean predictions as shown in the following indicator function

$$I(\mathbf{x}) = \begin{cases} 1, & \mu_g^*(\mathbf{x}) < 0 \\ 0, & \text{otherwise} \end{cases} \quad (15)$$

Then p_f is estimated by

$$p_f = \frac{1}{N} \sum_{i=1}^N I(\mathbf{x}_i) \quad (16)$$

where N is the number of samples in \mathbf{x}_{MCS} .

2.2.3 Review of Dependent Kriging Method for Component Reliability

The dependent Kriging method (DKM) accounts for dependence between predictions to achieve better accuracy and efficiency. DKM uses all the information of the surrogate model $\hat{y} = \hat{g}(\mathbf{x}) = \mu(\mathbf{x}) + \varepsilon(\mathbf{x})$, where $\varepsilon(\mathbf{x}) \sim N(0, \sigma^2(\mathbf{x}))$ with correlation matrix \mathbf{R} . DKM computes p_f by

$$p_f = \int_{\mu(x)+\varepsilon(x)<0} f(\mathbf{x})d\mathbf{x} = \int I(\mathbf{x})f(\mathbf{x})d\mathbf{x} = E[I(\mathbf{x})] \quad (17)$$

where $I(\cdot)$ is the indicator function defined by

$$I(x) = \begin{cases} 1, & \hat{y} = \hat{g}(\mathbf{x}) = \mu(\mathbf{x}) + \varepsilon(\mathbf{x}) < 0 \\ 0, & \text{otherwise} \end{cases} \quad (18)$$

p_f is a random variable since the domain of integration in Eq. (17) is random. The expectation of p_f is used to the estimate of the probability of failure [89]

$$E[p_f] = \frac{1}{N} \sum_{i=1}^N E(I_i) = \frac{1}{N} \sum_{i=1}^N e_i \quad (19)$$

where

$$e_i = \Phi\left(-\frac{\mu(\mathbf{x}_i)}{\sigma(\mathbf{x}_i)}\right) \quad (20)$$

The variance of p_f is used to estimate the error of p_f and is given by

$$Var(p_f) = \frac{1}{N^2} \sum_{i=1}^N [e_i(1-e_i) + \sum_{i=1, j \neq i}^N (e_{ij} - e_i e_j)] \quad (21)$$

where $e_{ij} = \Pr\{\hat{g}(\mathbf{x}_i) < 0, \hat{g}(\mathbf{x}_j) < 0\}$ is the CDF of the bivariate normal distribution defined by means $[\mu_i, \mu_j]$, standard deviations $[\sigma_i, \sigma_j]$, and correlation r_{ij} . Eq. (21) indicates that $Var(p_f)$ is the sum of N terms of the N sample points. Each term can be considered as the contribution from each sample. The contribution of one sample i is defined as the learning function below.

$$c_i = e_i(1-e_i) + \sum_{i=1, j \neq i}^N (e_{ij} - e_i e_j) \quad (22)$$

The learning function uses all the information of a Gaussian process, including its mean, variance, and correlation. As a result, it provides a more accurate and efficient way of select TPs to build surrogate models. In [89], selected candidate points (SCPs) are used to relieve the computational burden of the bivariate joint probability evaluation in Eq. (22). e_{ij} is not calculated for all points in \mathbf{x}_{MCS} , and a smaller number of points in \mathbf{x}_{MCS} are selected to form the SCPs. Then the evaluations of e_{ij} are performed with only SCPs. The SCPs are selected based on two criteria. The first criterion is a small error in the estimate of p_f , and this criterion requires a significant number of points fall into the failure region. The second criterion is a high contribution to $Var(p_f)$.

Therefore, the SCPs consist of all the points in the failure region and other points with the highest indicator function variances in the safe region. Details of the implementation is given in [89].

2.3 Dependent Kriging Method for System Reliability

The new dependent Kriging method for systems (DKM-SYS) is the extension of component DKM to system reliability analysis. Similar to the component DKM, DKM-SYS consists of the same components: the estimate of probability of failure, a learning function, a stopping criterion, and an implementation process.

2.3.1 Estimate of p_{sf}

In this work, we consider a series system with k failure modes. For a series system, if at least one failure mode occurs, the system fails, and then the system reliability is computed by

$$R_s = \Pr\{g_1(\mathbf{x}) > 0 \cap g_2(\mathbf{x}) > 0 \cap \dots \cap g_k(\mathbf{x}) > 0\} \quad (23)$$

where \cap denotes intersection. The safe region Ω is therefore defined by

$$\Omega = \{\mathbf{x} \mid g_1(\mathbf{x}) > 0 \cap g_2(\mathbf{x}) > 0 \cap \dots \cap g_k(\mathbf{x}) > 0\} \quad (24)$$

The system is safe at point \mathbf{x} if \mathbf{x} falls into Ω . Thus R_s is computed by

$$R_s = \int_{\Omega} f(\mathbf{x}) d\mathbf{x} = \int I_s(\mathbf{x}) f(\mathbf{x}) d\mathbf{x} = E[I_s(\mathbf{x})] \quad (25)$$

where the system indicator function is defined by

$$I_s(\mathbf{x}) = \begin{cases} 1, & \mathbf{x} \in \Omega \\ 0, & \text{otherwise} \end{cases} \quad (26)$$

R_s can be estimated by

$$R_s = \frac{1}{N} \sum_{i=1}^N I_s(\mathbf{x}_i) = \frac{1}{N} \sum_{i=1}^N I_{si} \quad (27)$$

where $I_{si} = I_s(\mathbf{x}_i)$. The system reliability at $\mathbf{x}_i \in \mathbf{x}_{MCS}$ is

$$\Pr\{I_{si} = 1\} = \Pr\{\hat{g}_1(\mathbf{x}_i) > 0 \cap \hat{g}_2(\mathbf{x}_i) > 0 \cap \dots \cap \hat{g}_k(\mathbf{x}_i) > 0\} \quad (28)$$

Thus, the probability of system failure at $\mathbf{x}_i \in \mathbf{x}_{MCS}$ is

$$p_{sf} = 1 - R_s = 1 - \frac{1}{N} \sum_{i=1}^N I_{si} \quad (29)$$

In this work, we generate surrogate models for limit-state functions separately and assume the predictions of the k responses at the same point are independent. (The responses of a single limit-state function at two points, however, are still dependent.) Thus the joint probability density functions (PDF) of the k responses at point \mathbf{x}_i are the product of their marginal PDFs. Eq. (28) is then rewritten as

$$\Pr\{I_{si} = 1\} = \prod_{k=1}^M \Pr\{\hat{g}_k(\mathbf{x}_i) > 0\} \quad (30)$$

At point \mathbf{x}_i , the reliability of component k is

$$\Pr\{\hat{g}_k(\mathbf{x}_i) > 0\} = \Phi\left(\frac{\mu_k(\mathbf{x}_i)}{\sigma_k(\mathbf{x}_i)}\right) = r_{ki} \quad (31)$$

Thus

$$\Pr\{I_{si} = 1\} = \prod_{k=1}^M r_{ki} \quad (32)$$

$$\Pr\{I_{si} = 0\} = 1 - \prod_{k=1}^M r_{ki} \quad (33)$$

The expectation of the system indicator at \mathbf{x}_i is

$$E[I_{si}] = 1 \cdot (\Pr\{I_{si} = 1\}) + 0 \cdot (\Pr\{I_{si} = 0\}) = \prod_{k=1}^M r_{ki} \quad (34)$$

The variance of the system indicator is

$$\text{Var}[I_{si}] = E[(I_{si})^2] - (E[I_{si}])^2 = \prod_{k=1}^M r_{ki} - \left(\prod_{k=1}^M r_{ki}\right)^2 = \left(1 - \prod_{k=1}^M r_{ki}\right) \prod_{k=1}^M r_{ki} \quad (35)$$

Since R_s is a random variable, its expectation is used for the estimate of the system reliability; namely

$$E[R_s] = \frac{1}{N} \sum_{i=1}^N E[I_{Si}] = \frac{1}{N} \sum_{i=1}^N \left(\prod_{k=1}^M r_{ki} \right) \quad (36)$$

The probability of system failure p_{sf} is

$$E[p_{sf}] = 1 - \frac{1}{N} \sum_{i=1}^N \left(\prod_{k=1}^M r_{ki} \right) \quad (37)$$

The variance of p_{sf} is the same with the variance of R_s , which is calculated by

$$Var[p_{sf}] = Var[R_s] = \frac{1}{N^2} Var \sum_{i=1}^N I_{Si} = \frac{1}{N^2} \left[\sum_{i=1}^N Var[I_{Si}] + 2 \sum_{i=1}^N \sum_{j>i}^N cov(I_{Si}, I_{Sj}) \right] \quad (38)$$

$Var[p_{sf}]$ is determined by the covariance $cov(I_{Si}, I_{Sj})$, which is given by

$$cov(I_{Si}, I_{Sj}) = E[I_{Si} I_{Sj}] - E[I_{Si}] E[I_{Sj}] = \Pr\{I_{Si} = 1, I_{Sj} = 1\} - E[I_{Si}] E[I_{Sj}] \quad (39)$$

where

$$E[I_{Si}] E[I_{Sj}] = \prod_{k=1}^M r_{ki} \prod_{k=1}^M r_{kj} \quad (40)$$

Let $H = \Pr\{I_{Si} = 1, I_{Sj} = 1\}$, Eq. (38) becomes

$$Var[p_{sf}] = \frac{1}{N^2} \left\{ \sum_{i=1}^N \left[\left(1 - \prod_{k=1}^M r_{ki} \right) \prod_{k=1}^M r_{kj} \right] + 2 \sum_{i=1}^N \sum_{j>i}^N \left(H - \prod_{k=1}^M r_{ki} \prod_{k=1}^M r_{kj} \right) \right\} \quad (41)$$

where

$$H = \Pr\{I_{Si} = 1, I_{Sj} = 1\} = \Pr\{[\hat{g}_1(\mathbf{x}_i) > 0 \cap \dots \cap \hat{g}_k(\mathbf{x}_i) > 0] \cap [\hat{g}_1(\mathbf{x}_j) > 0 \cap \dots \cap \hat{g}_k(\mathbf{x}_j) > 0]\} \quad (42)$$

Eq. (42) is the probability of system safety at points \mathbf{x}_i and \mathbf{x}_j . Since the predictions of all the responses are independent, H is given by

$$H = \Pr\{I_{Si} = 1, I_{Sj} = 1\} = \prod_{k=1}^M \Pr\{\hat{g}_{ki} > 0, \hat{g}_{kj} > 0\} = r_{kij} \quad (43)$$

where r_{kij} is the probability that component k is safe at point i and j .

Eq. (41) can be rewritten as

$$Var[p_{sf}] = \frac{1}{N^2} \sum_{i=1}^N \left\{ \left(1 - \prod_{k=1}^M r_{ki} \right) \prod_{k=1}^M r_{ki} + 2 \sum_{j=1, j \neq i}^N \left(\prod_{k=1}^M r_{kij} - \prod_{k=1}^M r_{ki} \prod_{k=1}^M r_{kj} \right) \right\} \quad (44)$$

or

$$Var[p_{sf}] = \frac{1}{N^2} \sum_{i=1}^N c_i \quad (45)$$

where

$$c_i = \frac{1}{N^2} \sum_{i=1}^N \left\{ \left(1 - \prod_{k=1}^M r_{ki} \right) \prod_{k=1}^M r_{ki} + 2 \sum_{j=1, j \neq i}^N \left(\prod_{k=1}^M r_{kij} - \prod_{k=1}^M r_{ki} \prod_{k=1}^M r_{kj} \right) \right\} \quad (46)$$

Therefore, the standard deviation of p_{sf} is

$$\sigma_{p_{sf}} = \frac{1}{N} \sqrt{\sum_{i=1}^N c_i} \quad (47)$$

$\sigma_{p_{sf}}$ is an indicator of the uncertainty associated with the estimate of the system reliability. If there was no model uncertainty, $\sigma_{p_{sf}}$ would be zero. The higher $\sigma_{p_{sf}}$ is, the higher the uncertainty associated with the system reliability estimated based on the surrogate models is. We therefore use $\sigma_{p_{sf}}$ to measure the error of the system reliability prediction.

2.3.2 Learning Function

A learning function is used to select new TPs to refine the surrogate model. As indicated in Eq. (44), each TP contributes to $\sigma_{p_{sf}}$ or $Var[p_{sf}]$. The sum of terms involving \mathbf{x}_i in $Var[p_{sf}]$ is c_i in Eq. (46). Thus, we use c_i as the learning function. Maximizing c_i identifies a new TP that has the highest contribution to the uncertainty of the estimate of system reliability; namely

$$\begin{cases} \mathbf{x}_{new} = \mathbf{x}_h \\ h = \arg \max_{i=1,2,\dots,N_{MCS}} \{c_i\} \end{cases} \quad (48)$$

where \mathbf{x}_h is the h -th point in \mathbf{x}_{MCS} . Adding the highest contribution point as new TP is the most effective way to refine the surrogate model with fast convergence [89].

2.3.3 Stopping Criterion

When $\sigma_{p_{sf}}$ is small enough, no more new TPs are needed. Then the surrogate models are used to calculate p_{sf} . Let the confidence of the probability of system failure be $1 - \alpha$ and the allowable relative error be ε , and then the confidence interval of the estimate is computed by

$$E[p_{sf}] \pm \Phi(\alpha/2)\sigma_{p_{sf}}.$$

The relative error is defined by

$$\eta = \frac{|E[p_{sf}] \pm \Phi^{-1}(\alpha/2)\sigma_{p_{sf}} - E[p_{sf}]|}{E[p_{sf}]} = \left| \frac{\Phi^{-1}(\alpha/2)\sigma_{p_{sf}}}{E[p_{sf}]} \right| \quad (49)$$

If η is smaller than the allowable error, the process terminates. Thus, the stopping criterion is determined by

$$\frac{\sigma_{p_{sf}}}{E[p_{sf}]} \leq \left| \frac{\eta}{\Phi^{-1}(\alpha/2)} \right| \quad (50)$$

2.3.4 Implementation

Accounting for the dependence between responses requires calculations of bivariate probabilities given by

$$r_{kij} = \Pr\{g_{ki} > 0, g_{kj} > 0\}, (k = 1, \dots, M; i, j = 1, 2, \dots, N, i \neq j) \quad (51)$$

Calculating r_{kij} is time consuming. For example, if the size of \mathbf{x}_{MCS} is 10^5 , the number of calculating the joint probability in r_{kij} is $\frac{N(1+N)}{2} = \frac{10^5(1+10^5)}{2} \approx 1.5 \times 10^{10}$. To relieve the computational burden, we use the so-called selected candidate points (SCPs), denoted by \mathbf{x}_s ,

which are selected from \mathbf{x}_{MCS} . The size of \mathbf{x}_S is much smaller than that of \mathbf{x}_{MCS} . To ensure a significant number of points fall into the failure region, we adjust the size of SCPs N_{sel} using the following condition.

$$25\% \leq r = \frac{N_{F,sel}}{N_{sel}} \leq 75\% \quad (52)$$

where $N_{F,sel}$ is the number of failure points in the SCPs. SCPs consist of all points in the failure region and the other points with highest indicator function variances in the safe region. Using SCPs, the computational effort needed is greatly reduced. In the examples in Sec.4, we use 200 SCPs.

The stopping criterion in Eq. (50) needs to be modified accordingly. The probability of system failure using \mathbf{x}_S is calculated by

$$E[p_{sf,sel}] = 1 - \frac{1}{N_{sel}} \sum_{i=1}^{N_{sel}} r_i \quad (53)$$

and

$$\sigma_{P_{sf,sel}} = \frac{1}{N_{sel}} \sqrt{\sum_{i=1}^{N_{sel}} c_i} \quad (54)$$

The stopping criterion becomes

$$\frac{\sigma_{P_{sf,sel}}}{E[p_{sf,sel}]} \leq \left| \frac{\eta}{\Phi^{-1}(\alpha/2)} \right| \quad (55)$$

The flowchart of the DKM-SYS is provided in Fig. 2.1

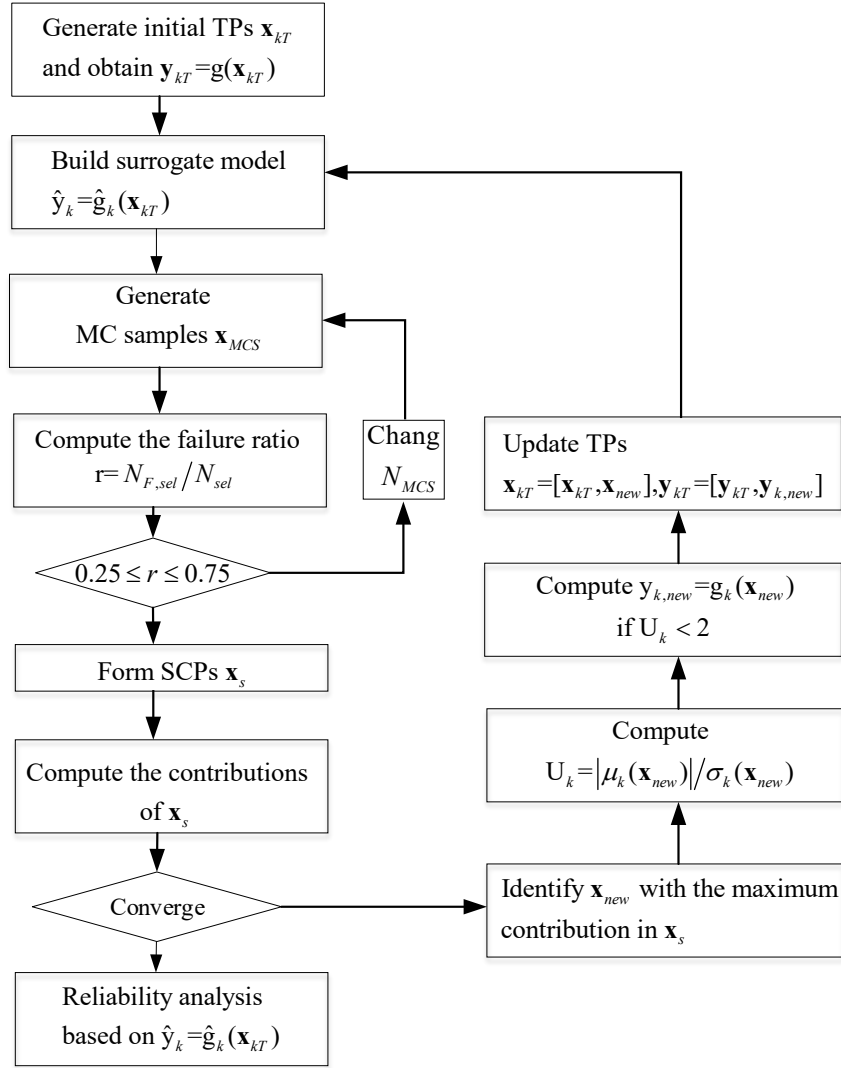


Figure 2.1 Flowchart of DKM-SYS

2.3.5 Parallel Systems

The above results can be extended to parallel systems. For a parallel system with k failure modes, the probability of failure can be computed by

$$p_{fs} = \Pr\{g_1(\mathbf{x}) < 0 \cap g_2(\mathbf{x}) < 0 \cap \dots \cap g_k(\mathbf{x}) < 0\} \quad (56)$$

Let $G_i(\mathbf{x}) = -g_i(\mathbf{x})$, then

$$p_{fs} = \Pr\{G_1(\mathbf{x}) > 0 \cap G_2(\mathbf{x}) > 0 \cap \dots \cap G_k(\mathbf{x}) > 0\} \quad (57)$$

Eq. (57) evaluates the probability of a union of n -events as Eq. (23) does. Hence the proposed method can be used to calculate Eq. (57), which leads to the parallel system reliability $R_s = 1 - p_{fs}$.

2.4 Examples

The proposed method is evaluated with four examples. The first example is a mathematical problem, which clearly demonstrates the application details and effectiveness of DKM-SYS, while the other three examples show possible engineering applications.

In all examples, initial TPs are generated by the Latin hypercube sampling (LHS) [90], and the initial sample size is 12. The efficiency is measured by the number of limit-state function calls. The accuracy is measured by the percentage error with respect to the direct MCS. The error is calculated by

$$\varepsilon = \frac{|p_{sf} - p_{sf}^{MCS}|}{p_{sf}^{MCS}} \times 100\% \quad (58)$$

where p_{sf}^{MCS} and p_{sf} are probabilities of system failure from the direct MCS and the other method, respectively. Since Kriging-based reliability methods are stochastic methods, we run each method 20 independently, and the average results are used for comparison. The standard deviation of the number of function calls and probabilities of system failure are also provided. A smaller standard deviation means that the results are concentrated closer to their mean values, and this indicates that the method tends to produce more stable results. We therefore use the standard deviation as an indicator of the robustness of the method.

2.4.1 Example 1

This example involves two random variables and three mathematical equations. For this two-dimensional problem, it is easy to demonstrate the effectiveness of the proposed method. The three limit-state functions are given by [91]

$$g_1(\mathbf{x}) = (x_2^2 + 11)(x_1 - 1) / 5 - \cos(3x_2) - 5 \quad (59)$$

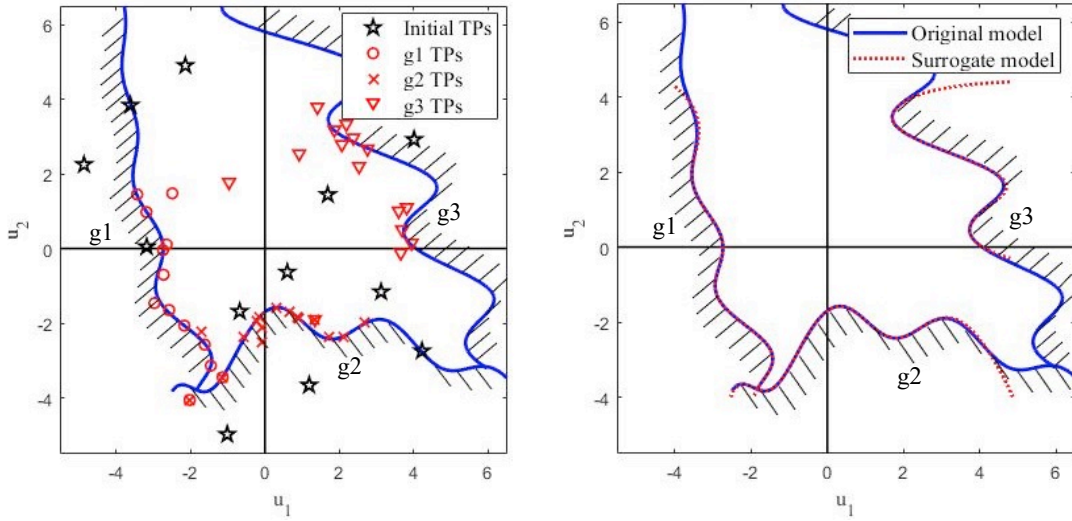
$$g_2(\mathbf{x}) = (x_1 + x_2 - 5)^2 / 30 + (x_1 - x_2 - 12)^2 / 120 - 1 - \cos(3x_1) / 10 \quad (60)$$

$$g_3(\mathbf{x}) = 80 / (x_1^2 + 8x_2 - 5) - \cos(3x_2) / 10 - 1 \quad (61)$$

where $x_i \sim N(4, 0.7^2)$, $i = 1, 2$. Figs. 2.2 and 2.3 show the TPs and surrogate models using AK-SYS and DKM-SYS method, respectively.

The average numbers of function calls and the average probabilities of system reliability based on direct MCS and LHS are provided in Table 2.1 and Table 2.2, respectively. The difference of results from the two sampling methods is not significant since the sample size is large. For this reason, we compare two different sampling methods for only this example.

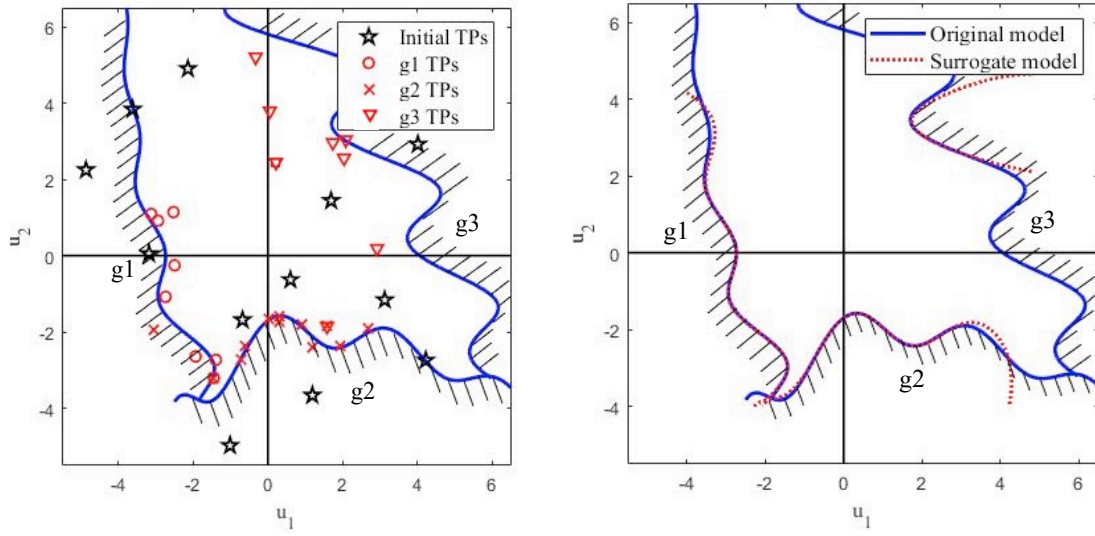
We also compare the probabilities of system failure from DKM-SYS, AK-SYS and EGRA-SYS with those from the direct MCS and LHS. In both tables, the results show that DKM-SYS is more accurate than AK-SYS and EGRA-SYS. DKM-SYS is also more efficient than AK-SYS and DKM-SYS since the former method has smaller average numbers of function calls. Limit-state function 3 is far away from the origin as shown in Figs. 2.2 and 2.3, and it is hard to obtain an accurate surrogate model. This function consumes most of the computational effort by DKM-SYS, AK-SYS and EGRA-SYS.



(a) Training points

(b) Final surrogate models

Figure 2.2 Training points and surrogate models of AK-SYS



(a) Training points

(b) Final surrogate models

Figure 2.3 Training points and surrogate models of DKM-SYS

Table 2.1 Average results from 20 runs based on direct MCS

Method	p_{sf}	ε (%)	Number of function calls		
			N_1	N_2	N_3
AK-SYS	2.7249×10^{-2}	1.94	25.30	28.20	30.60
EGRA-SYS	2.7241×10^{-2}	1.97	26.05	29	32.05
DKM-SYS	2.7403×10^{-2}	1.37	17.85	22.25	22.45
MCS	2.750×10^{-2}	N/A	5×10^6	5×10^6	5×10^6

Table 2.2 Average results from 20 runs based on Latin hypercube sampling

Method	p_{sf}	ε (%)	Number of function calls		
			N_1	N_2	N_3
AK-SYS	2.7389×10^{-2}	1.24	25.5	28.5	30.0
EGRA-SYS	2.7472×10^{-2}	1.26	26.4	28.7	29.4
DKM-SYS	2.7403×10^{-2}	1.23	18.8	22.6	23.6
LHS	2.7474×10^{-2}	N/A	5×10^6	5×10^6	5×10^6

2.4.2 Exmapple 2

This is an engineering problem with a small probability of system failure. This problem involves a liquid hydrogen fuel tank that is used on a space launch vehicle [86, 92, 93]. The tank has a honeycomb sandwich deign. It is subjected to stress caused by ullage pressure, head pressure, axial force due to acceleration, and bending and shear stress due to the weight of the fuel. There are three failure modes related to the von Mises strength, isotropic strength, and honeycomb buckling. The limit-state functions for the von Mises and isotropic strength are given by

$$g_1(\mathbf{X}) = \frac{84000t_{plate}}{\sqrt{N_x^2 + N_y^2 - N_x N_y + 3N_{xy}^2}} - 1 \quad (62)$$

$$g_2(\mathbf{X}) = \frac{84000t_{plate}}{|N_y|} - 1 \quad (63)$$

The limit-state function of honeycomb buckling is defined by a response surface generated from the structural sizing program and is given by [86, 93].

$$g_3(\mathbf{X}) = 0.847 + 0.96y_1 + 0.986y_2 - 0.216y_3 + 0.077y_1^2 + 0.11y_2^2 + 0.007y_3^2 + 0.378y_1y_2 - 0.106y_1y_3 - 0.11y_2y_3 \quad (64)$$

where

$$y_1 = 4(t_{plate} - 0.075) \quad (65)$$

$$y_2 = 20(t_h - 0.1) \quad (66)$$

$$y_3 = -6000\left(\frac{1}{N_{xy}} + 0.003\right) \quad (67)$$

The five independent random variables are given in Table 2.3. The reliability analysis results are provided in Table 4.

Table 2.3 Random variables of example two

	Random variables	Distribution
X_1	t_{plate}	$N(0.07433, 0.005)$
X_2	t_h	$N(0.1, 0.01)$
X_3	N_x	$N(13, 60)$
X_4	N_y	$N(4751, 48)$
X_5	N_{xy}	$N(-684, 11)$

Table 2.4 shows that the average total function call of AK-SYS and EGRA-SYS are 56.1 and 43.35 respectively, while the average total function call of DKM-SYS is 42.45. This demonstrates that DKM-SYS is more efficient. DKM-SYS is also more accurate than AK-SYS and EGRA-SYS, because the error of DKM-SYS is only 0.57% and the errors of the other two methods are relatively large.

Table 2.4 Comparison of average results from 20 runs

Method	p_{sf}	ε (%)	Number of function calls		
			N_1	N_2	N_3
AK-SYS	6.9756×10^{-4}	1.52	12	31.50	12.60
EGRA-SYS	6.9603×10^{-4}	2.01	12	18.10	13.25
DKM-SYS	7.0107×10^{-4}	0.57	12	19.10	12.40
MCS	6.9855×10^{-4}	N/A	2×10^7	2×10^7	2×10^7

2.4.3 Example 3

This is an engineering problem that involves a relatively large set of input random variables. As shown in Fig. 2.4, a cantilever beam [19] with ten random variables is used to prove the robustness of DKM-SYS method.

The beam is subjected to external forces F_1 and F_2 , external moments M_1 and M_2 , and external distributed loads denoted by (q_{L1}, q_{R1}) and (q_{L2}, q_{R2}) . These forces, moments, distributed loads, together with the yield strength S and the maximum allowable shear stress τ_{\max} are normally distributed random variables. Their information is given in Table 2.5. The deterministic parameters are listed in Table 2.6.

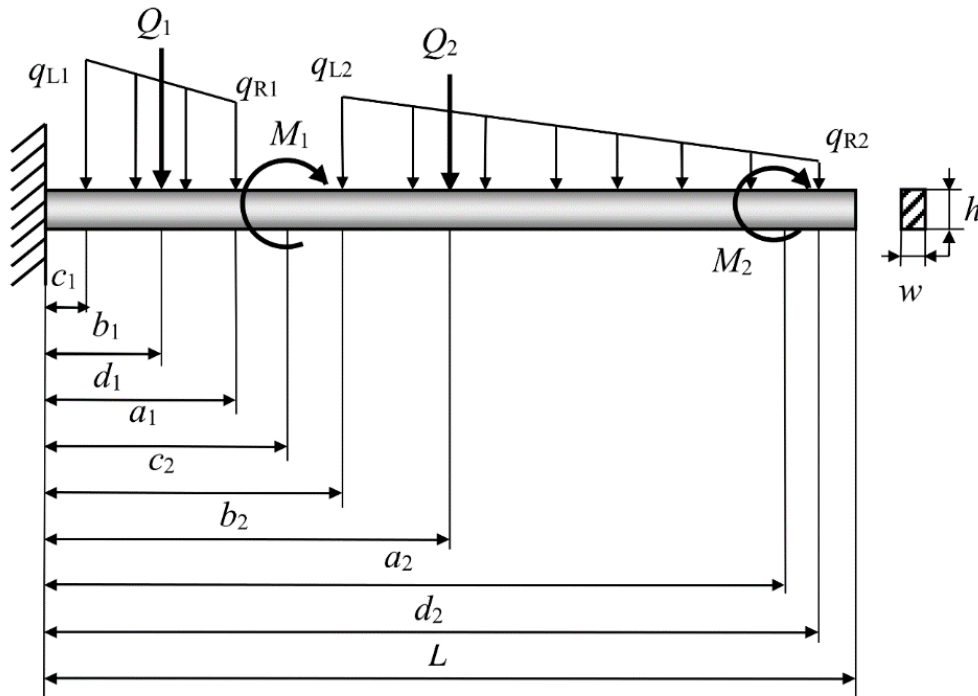


Figure 2.4 A cantilever beam

Table 2.5 Random variables of example 3

	Random Variables	Distribution
X_1	$M_1(\text{Nm})$	$N(50 \times 10^3, 5 \times 10^3)$
X_2	$M_2(\text{Nm})$	$N(30 \times 10^3, 3 \times 10^3)$
X_3	$F_1(\text{m})$	$N(1.8 \times 10^4, 2 \times 10^3)$
X_4	$F_2(\text{m})$	$N(3 \times 10^4, 3 \times 10^3)$
X_5	$q_{L1}(\text{N/m})$	$N(3 \times 10^4, 1 \times 10^3)$
X_6	$q_{R1}(\text{N/m})$	$N(2 \times 10^4, 1 \times 10^3)$
X_7	$q_{L2}(\text{N/m})$	$N(2 \times 10^4, 1 \times 10^3)$
X_8	$q_{R2}(\text{N/m})$	$N(1 \times 10^3, 10)$
X_9	$S(\text{Pa})$	$N(4.5 \times 10^7, 4.5 \times 10^6)$
X_{10}	$\tau_{\max}(\text{Pa})$	$N(3.5 \times 10^6, 5 \times 10^5)$

The maximum normal stress of the beam should be smaller than its yield strength, and this is given by

$$g_1(\mathbf{X}) = S - \frac{6M}{wh^2} \quad (68)$$

where the bending moment at the left end point of the beam is

$$M = \sum_{i=1}^2 M_i + \sum_{i=1}^2 F_i b_i + \sum_{i=1}^2 \frac{q_{Li}(d_i - c_i)(d_i + c_i)}{2} + \sum_{i=1}^2 \frac{(q_{Ri} - q_{Li})(d_i - c_i)(2d_i + c_i)}{6} \quad (69)$$

The deflection of the right end point of the beam should not greater than the allowable deflection $\delta_{allowable} = 2$ cm.

$$g_2(\mathbf{X}) = \delta - \delta_{allowable} \quad (70)$$

where δ is computed by

$$\delta = \frac{1}{EI} \left[\frac{ML^2}{2} + \frac{PL^3}{6} + \sum_{i=1}^2 \frac{M_i(L-a_i)^2}{2} - \sum_{i=1}^2 \frac{F_i(L-b_i)^3}{6} - \sum_{i=1}^2 \frac{q_{Li}(L-c_i)^4}{24} \right. \\ \left. - \sum_{i=1}^2 \frac{(q_{Ri} - q_{Li})(L-c_i)^5}{120(d_i - c_i)} + \sum_{i=1}^2 \frac{q_{Ri}(L-d_i)^4}{24} + \sum_{i=1}^2 \frac{(q_{Ri} - q_{Li})(L-d_i)^5}{120(d_i - c_i)} \right] \quad (71)$$

where the Young's modulus is $E = 2 \times 10^{11}$ Pa, and the moment of inertia is $I = wh^3 / 12$. P is the reaction force at the fixed end, which is given by

$$P = \sum_{i=1}^2 F_i + \sum_{i=1}^2 q_{Li}(d_i - c_i) + \sum_{i=1}^2 \frac{(q_{Ri} - q_{Li})(d_i - c_i)}{2} \quad (72)$$

The last limit-state function specifies that the shear stress should not be greater than the maximum allowable shear stress

$$g_3(\mathbf{X}) = \tau_{\max} - \tau = \tau_{\max} - \frac{3P}{2wh} \quad (73)$$

Table 2.6 Deterministic parameters

Parameters	Values
a_1 (m)	1.5
a_2 (m)	4.5
b_1 (m)	0.75
b_2 (m)	2.5
c_1 (m)	0.25
c_2 (m)	1.75
d_1 (m)	1.25
d_2 (m)	4.75
L (m)	5
w (m)	0.2
h (m)	0.4

The results from Table 2.7 also show that DKM-SYS has better performance than AK-SYS and EGRA-SYS in accuracy, efficiency. The significant advantage of DKM-SYS over AK-SYS and EGRA-SYS in this example is the efficiency. On average, the total function calls of AK-SYS and EGRA-SYS are 353.64 and 477, while DKM-SYS just needs 129.5 function calls.

Table 2.7 Comparison of average results from 20 runs

Method	p_{sf}	$\varepsilon(\%)$	Number of function calls		
			N_1	N_2	N_3
AK-SYS	5.2592×10^{-3}	1.74	245.89	12	95.75
EGRA-SYS	5.2542×10^{-3}	1.71	355	15	107
DKM-SYS	5.2657×10^{-3}	0.94	70.80	13.05	45.65
MCS	5.2567×10^{-3}	N/A	1×10^7	1×10^7	1×10^7

2.4.4 Example 4

This problem involves more failure modes than the previous examples. A crank-slider system is considered which has four components shown in Fig. 2.5 [94]. An external moment is applied to joint A to drive link AB rotating around A. The task is to predict the system reliability when $\theta_2 = \pi/2$ and five failure modes are considered for this system.

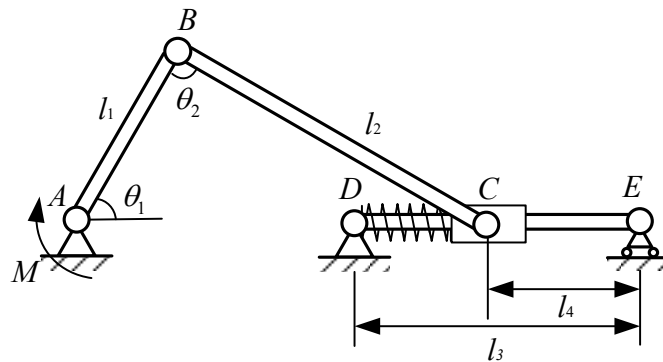


Figure 2.5 A crank-slider system

For link AB, the length is l_1 , and the width and height of the cross section are b_1 and h_1 . The

maximal normal stress $S_1 = \frac{M(h_1/2)}{b_1 h_1^3/12}$ developed in the link AB should be smaller than the

allowable normal stress S_{a1} and this is given by

$$g_1(\mathbf{X}) = S_{a1} - S_1 \quad (74)$$

For link BC, the length is l_2 , and the width and height of the cross section are b_2 and h_2 . The force developed in the link F_{BC} should be smaller than the critical force for buckling P_{cr} .

$$g_2(\mathbf{X}) = P_{cr} - F_{BC} \quad (75)$$

where $F_{BC} = M/l_1$, $P_{cr} = \frac{\pi^2 E_2 I_2}{(K l_2)^2}$ and $I_2 = \frac{b_2 h_2^3}{12}$.

For shaft DE, the length and diameter are l_3 and d_4 . It has two failure modes caused by excessive deflection and excessive normal stress, respectively. The corresponding limit-state functions are given by

$$\begin{cases} g_3(\mathbf{X}) = \delta_{a3} - \delta_3 \\ g_4(\mathbf{X}) = S_{a4} - S_4 \end{cases} \quad (76)$$

where δ_{a3} is the allowable deflection, and δ_3 is the maximal deflection given by

$$\delta_3 = \frac{F_{BC} \sin(\pi/2 - \theta_1) l_4 (l_3^2 - l_4^2)^{3/2}}{9\sqrt{3} l_3 E_4 (\pi/4) (d_4/2)^4} \quad (77)$$

where E_4 is the Young's modulus of shaft DE. S_{a4} is the allowable normal stress, and S_4 is the maximal normal stress developed in the shaft and is calculated by

$$S_4 = \frac{M_{\max} c}{I_4} = \frac{F_{BC} \sin(\pi/2 - \theta_1) (l_3 - l_4) (d_4/2)}{(\pi/4) (d_4/2)^4} \quad (78)$$

For spring DE, the outer diameter and inner diameter of the spring are D and d . The developed maximal shear stress τ_5 should not be greater than the allowable shear stress of the spring coils τ_{a5} .

$$g_5(\mathbf{X}) = \tau_{a5} - \tau_5 \quad (79)$$

where τ_5 is computed by

$$\tau_5 = \frac{F_{BC} \cos(\pi/2 - \theta_1) D}{\pi d^3} \left(\frac{4D - d}{4D - 4d} + \frac{0.615d}{D} \right) \quad (80)$$

All the random variables are listed in Table 2.8, and the deterministic parameters are listed in Table 2.9. The reliability analysis results are provided in Table 2.10.

Table 2.8 Random variables

	Random Variables	Distribution
X_1	$M_1(\text{Nm})$	$N(350, 65)$
X_2	$l_1(\text{m})$	$N(0.3, 10^{-4})$
X_3	$l_2(\text{m})$	$N(0.9, 2 \times 10^{-3})$
X_4	$b_1(\text{m})$	$N(0.022, 5 \times 10^{-4})$
X_5	$h_1(\text{m})$	$N(0.019, 5 \times 10^{-4})$
X_6	$b_2(\text{m})$	$N(0.015, 5 \times 10^{-4})$
X_7	$h_2(\text{m})$	$N(0.009, 5 \times 10^{-4})$
X_8	$d_4(\text{m})$	$N(0.0228, 1 \times 10^{-4})$
X_9	$D(\text{m})$	$N(34.7 \times 10^{-3}, 1 \times 10^{-4})$
X_{10}	$\tau_{a5}(\text{m})$	$N(50 \times 10^6, 10 \times 10^6)$

Table 2.9 Deterministic parameter

Deterministic Parameters	Values
E_2 (Pa)	200×10^9
E_4 (Pa)	200×10^9
K	1
l_3 (m)	0.95
l_4 (m)	0.30
S_{a1} (Pa)	400×10^6
S_{a4} (Pa)	460×10^6
δ_{a3} (m)	0.0053
d (m)	29.5×10^{-3}

Table 2.10 Comparison of average results from 20 runs

Method	p_{sf}	ε (%)	Number of function calls				
			N_1	N_2	N_3	N_4	N_5
AK-SYS	1.3638×10^{-2}	1.92	149.95	215	12	12	77.45
EGRA-SYS	1.3655×10^{-2}	1.91	214.75	303.70	12	17.40	110.95
DKM-SYS	1.3713×10^{-2}	0.81	54.35	76.25	12.05	12.15	38.90
MCS	1.3643×10^{-2}	N/A	5×10^6	5×10^6	5×10^6	5×10^6	5×10^6

Table 2.10 shows the comparison between AK-SYS, EGRA-SYS, DKM-SYS, and MCS. It is obvious that DKM-SYS can achieve better accuracy and efficiency than AK-SYS and EGRA-SYS. In particular, the total average function call of DKM-SYS is 193.7, while that of AK-SYS and EGRA-SYS are 466.4 and 658.8, respectively.

2.5 Summary

This work develops a new system reliability method for series systems with multiple dependent failure modes using the Kriging method. High efficiency and accuracy are achieved through the following means: 1) the use of surrogate models from Kriging, 2) the use of all information from Kriging, such as the prediction and its standard deviation, in the estimate of the system reliability, and 3) an efficient way for selecting training points for refining surrogate models. Since the dependence between Kriging predictions at different points are considered and the error of system reliability estimate is directly quantified (instead of the error of surrogate models), the new method improves the performance of Kriging-based system reliability methods.

The proposed method extends the Kriging method from component reliability analysis to system reliability in an efficient manner. It can be potentially used for system reliability-based design and robust system design.

3. SYSTEM RELIABILITY ANALYSIS WITH SECOND ORDER SADDLEPOINT APPROXIMATION

Hao Wu¹, Xiaoping Du²

¹School of Mechanical Engineering, Purdue University, West Lafayette, IN, United States

²Department of Mechanical and Energy Engineering, Indiana University - Purdue University
Indianapolis, IN, United States

Published in ASME. ASME J. Risk Uncertainty Part B, doi: <https://doi.org/10.1115/1.4047217>

Authors' contribution: H.W. and X.D. designed the study and contributed to the writing of the manuscript. H.W. detailed methodology and the code.

The second order saddlepoint approximation (SPA) has been used for component reliability analysis for higher accuracy than the traditional second order reliability method. This work extends the second order SPA to system reliability analysis. The joint distribution of all the component responses is approximated by a multivariate normal distribution. To maintain high accuracy of the approximation, the proposed method employs the second order SPA to accurately generate the marginal distributions of the component responses; to simplify computations and achieve high efficiency, the proposed method estimates the covariance matrix of the multivariate normal distribution with the first order approximation to the component responses. Examples demonstrate the high effectiveness of the second order SPA method for system reliability analysis.

3.1 Background

One of the criteria for systems design is to avoid system failures or minimize the probability of system failures. It is therefore necessary to predict system reliability accurately and efficiently during the design process [95]. System reliability is typically measured by the probability that the system fulfills its intended function without failures [96]. There are multiple components in the system, and each component may have multiple failure modes. Suppose the i -th failure model has a limit-state function given by

$$Y_i = g_i(\mathbf{X}) \quad (i = 1, \dots, m) \quad (1)$$

where Y_i is a component response, and \mathbf{x} is the vector of random variables. If $Y_i < 0$, the failure model does not occur; otherwise, the failure mode occurs. If we consider a failure model as a component, component reliability is then computed by

$$R_i = \Pr(g_i(\mathbf{X}) < 0) = \int_{\Omega_i} f(\mathbf{x}) d\mathbf{x} \quad (i = 1, 2, \dots, m) \quad (2)$$

where Ω_i is the component safe domain or the domain defined by $\{\mathbf{X} : Y_i = g_i(\mathbf{X}) < 0\}$, and $f(\mathbf{x})$ is the joint probability density function (PDF) of \mathbf{x} . For a series system, if one failure mode occurs, the system fails. System reliability is therefore given by

$$R_S = \Pr\left(\bigcap_{i=1}^m g_i(\mathbf{X}) < 0\right) = \int_{\Omega_S} \dots \int f_{\mathbf{X}}(\mathbf{x}) d\mathbf{x} \quad (3)$$

where Ω_S is the system safe domain or the domain defined by $\left\{\mathbf{X} : \bigcap_{i=1}^m g_i(\mathbf{X}) < 0\right\}$, and m is the number of components in the system.

In practice, it is difficult to integrate a multidimensional PDF over the safe domain in Eq. (3). Different approaches have therefore been developed to approximate the multi-dimensional integral. They include the bound approximation, surrogate approaches, and analytical approaches.

Bound approximation methods predict system reliability with lower and upper bounds. The first order bound method for series systems assumes that all the component responses are completely dependent or mutually exclusive. Based on this assumption, upper and lower bounds are derived. Ditlevsen [97] developed the second-order bound method by taking into account all the single mode failure probabilities and all the pairwise mode intersection failure probabilities to narrow the first order bound. Song and Der Kiureghian [98] proposed a linear programming (LP) method to compute the system reliability bound. The LP bounds are independent of the ordering of the components and are guaranteed to produce the narrowest possible bounds. Another reliability bound method is the complementary intersection method [99]. It approximates the reliability of series systems with eigenvector dimension reduction and produces more accurate results compared with the first and the second order bound methods. More studies on system reliability bound methods can be found in Refs. [100, 101].

Surrogate approaches predict single-valued system reliability by creating surrogate models for component responses and using Monte Carlo simulation (MCS). Surrogate models are created first,

and then system reliability is estimated with MCS based on the surrogate models. The surrogate modeling methods include the polynomial chaos expansion (PCE) [102], Support Vector Machine (SVM) [103], and Kriging method [104-106]. The recent development in this area is to perform surrogate modeling and MCS simultaneously. For example, Bichon et al. [104, 105] applied the efficient global optimization to reliability assessment. This method uses the active learning function called the Expected Feasibility Function (EFF) to choose new training points in the vicinity of the limit state, resulting in building an accurate surrogate model with fewer function evaluations. Fauriat and Gayton [106] proposed to build the initial Kriging surrogate model and continually refine the model by choosing new training points from a pre-sampled MCS population. Wu and Du proposed a new kriging method to predict system reliability that combines MCS and the Kriging method with improved accuracy and efficiency[37].

Analytical methods use neither surrogate models nor MCS and also produce single-valued system reliability. They approximate nonlinear limit-state functions so that the system probability integral can be easily computed. The methods include the use of the First Order Reliability Method (FORM) [107, 108], Second Order Reliability Method (SORM) [109, 110], and Saddlepoint Approximation Method (SPA) [108, 111]. FORM is the most well-known method due to its good balance between accuracy and efficiency. It at first transforms random variables into standard normal variables and then it identifies the reliability index, which is the minimum distance from the origin to the linearized and transformed limit-state function at the most probable point (MPP). System reliability is then approximated by the multidimensional integration of the joint probability density function after the marginal distributions and correlation coefficients of component states are obtained by the first order approximation [107, 112]. Although the efficiency of such method is good, the accuracy may not be good if limit-state functions are highly nonlinear. Therefore, Madsen [110] presented an extension of FORM based on a more accurate approximation of the limit-state function, and the result shows smaller differences between the second order approximation and the exact result.

Among the above methods, SPA can improve accuracy for problems with or without the non-normal to normal transformation. Du estimated the system reliability by SPA without any transformation on random input variables, leading to more accurate result than the FORM [100]. But the method is still the first order approximation and produces bounds of system reliability. An extension of the first order SPA to the second order SPA on component reliability analysis has

also been proposed to accommodate quadratic functions, and the method is more accurate than the first order SPA and SORM without sacrificing computational efficiency [113]. Papadimitriou et al. proposed a new mean-value second-order saddlepoint approximation method for reliability analysis of nonlinear systems with correlated non-Gaussian and multimodal random variables, and the result is more accurate than FORM and SORM [114]. But these methods are for only the component reliability analysis.

The purpose of this work is to extend the second-order SPA to system reliability analysis in order to achieve high accuracy. The joint distribution of all the component responses is approximated by a multivariate normal distribution. The second order SPA is used to approximate the marginal distributions of the component responses for higher accuracy. The covariance matrix of the multivariate normal distribution is estimated using the first order approximation.

The second-order SPA for component reliability analysis is briefly reviewed in Section 2. The extension of the second-order SPA to system reliability analysis is discussed in Section 3 followed by examples in Section 4. Conclusions are made in Section 5.

3.2 Review of Second Order SPA

In this section, we review the second order SPA for component reliability analysis [113]. It is the basis of the proposed system reliability method in this work.

3.2.1 MPP Search

The method first approximates the limit-state function with a second order polynomial. It is the same approximation in the original SORM [115], which involves the MPP search in the standard normal space using FORM. With the assumption that all variables in \mathbf{X} are independent, they are transformed into the standard normal variables \mathbf{U} . The transformation is given by

$$F_i(X_i) = \Phi(U_i) \quad (4)$$

where $F_i(\cdot)$ and $\Phi(\cdot)$ are the cumulative distribution functions (CDFs) of X_i and U_i , respectively. Then the transformed standard normal variables are

$$U_i = \Phi^{-1}[F_i(X_i)] \quad (5)$$

After the transformation, the limit state function becomes

$$Y = g(\mathbf{X}) = G(\mathbf{U}) \quad (6)$$

Then, the minimum distance from the original to the limit-state surface $G(\mathbf{U}) = 0$ is identified. The distance is the reliability index β . The minimum distance point is called the MPP. The model for searching for the MPP is given by

$$\begin{cases} \min \|\mathbf{u}\| \\ \text{subject to } G(\mathbf{u}) = 0 \end{cases} \quad (7)$$

where $\|\cdot\|$ means the length of a vector, namely

$$\beta = \|\mathbf{u}\| = \sqrt{u_1^2 + u_2^2 + \dots + u_n^2} = \sum_{i=1}^n u_i^2 \quad (8)$$

The solution from Eq. (7) is the MPP $\mathbf{u}^* = (u_1^*, u_2^*, \dots, u_n^*)$.

3.2.2 Quadratic Limit-state Function

After the MPP is found, the limit-state function is approximated by

$$Q(\mathbf{U}) = \frac{1}{2}(\mathbf{u}^*)^T \nabla^2 G(\mathbf{u}^*) \mathbf{u}^* - \nabla G(\mathbf{u}^*)^T \mathbf{u}^* + (\nabla G(\mathbf{u}^*) - \nabla^2 G(\mathbf{u}^*) \mathbf{u}^*)^T \mathbf{U} + \frac{1}{2} \mathbf{U}^T \nabla^2 G(\mathbf{u}^*) \mathbf{U} \quad (9)$$

where $\nabla G(\mathbf{u}^*) = \left(\left. \frac{\partial G}{\partial U_1} \right|_{\mathbf{u}^*}, \dots, \left. \frac{\partial G}{\partial U_n} \right|_{\mathbf{u}^*} \right)$ is the gradient, and $\nabla^2 G(\mathbf{u}^*)$ is the Hessian matrix,

given by

$$\nabla^2 G(\mathbf{u}^*) = \begin{bmatrix} \frac{\partial^2 G}{\partial U_1^2} & \frac{\partial^2 G}{\partial U_1 U_2} & \dots & \frac{\partial^2 G}{\partial U_1 U_n} \\ \frac{\partial^2 G}{\partial U_2 U_1} & \frac{\partial^2 G}{\partial U_2^2} & \dots & \frac{\partial^2 G}{\partial U_2 U_n} \\ \vdots & \vdots & \ddots & \vdots \\ \frac{\partial^2 G}{\partial U_n U_1} & \frac{\partial^2 G}{\partial U_n U_2} & \dots & \frac{\partial^2 G}{\partial U_n^2} \end{bmatrix}_{\mathbf{u}^*} \quad (10)$$

The independent standard normal vector $\tilde{\mathbf{U}} = (\tilde{U}_1, \tilde{U}_2, \dots, \tilde{U}_n)$ can be easily generated as follows:

$$\tilde{\mathbf{U}} = \mathbf{D}^{-1} \mathbf{U} \quad (11)$$

where \mathbf{D} is an orthogonal matrix whose column vectors are the eigenvectors of $\frac{1}{2}\nabla^2 G(\mathbf{u}^*)$,

and $\tilde{\mathbf{U}} = (\tilde{U}_1, \tilde{U}_2, \dots, \tilde{U}_n)$ is a vector of independent standard normal random variables.

Thus, Eq. (9) is expressed in the form of a quadratic polynomial function, as follows:

$$Q(\tilde{\mathbf{U}}) = a + \tilde{\mathbf{b}}^T \tilde{\mathbf{U}} + \tilde{\mathbf{U}}^T \tilde{\mathbf{C}} \tilde{\mathbf{U}} \quad (12)$$

in which

$$\begin{cases} a = \frac{1}{2} (\mathbf{u}^*)^T \nabla^2 G(\mathbf{u}^*) \mathbf{u}^* - \nabla G(\mathbf{u}^*)^T \mathbf{u}^* \\ \tilde{\mathbf{b}} = \mathbf{D}^T \mathbf{b} = (\tilde{b}_1, \tilde{b}_2, \dots, \tilde{b}_n) \\ \tilde{\mathbf{C}} = \mathbf{D}^T \mathbf{C} \mathbf{D} = \text{diag}(\tilde{c}_1, \tilde{c}_2, \dots, \tilde{c}_n) \end{cases} \quad (13)$$

Since $\tilde{\mathbf{C}}$ is diagonal, Eq. (12) can be written as sum of quadratic functions of different standard normal variables.

$$Q(\mathbf{U}) = \sum_{i=1}^n Q_i(\tilde{\mathbf{U}}) = \sum_{i=1}^n (\tilde{a}_i + \tilde{b}_i \tilde{U}_i + \tilde{c}_i \tilde{U}_i^2) \quad (14)$$

where

$$\tilde{a}_i = \frac{a}{n} \quad (15)$$

and n is the total number of random variables.

$Q_i(\tilde{\mathbf{U}})$ is further rewritten as follows

$$Q_i(\tilde{\mathbf{U}}) = \begin{cases} (\sqrt{\tilde{c}_i} \tilde{U}_i + \frac{\tilde{b}_i}{2\sqrt{\tilde{c}_i}})^2 + \tilde{a}_i - \frac{\tilde{b}_i^2}{4\tilde{c}_i} & \tilde{c}_i > 0 \\ -(\sqrt{-\tilde{c}_i} \tilde{U}_i - \frac{\tilde{b}_i}{2\sqrt{-\tilde{c}_i}})^2 + \tilde{a}_i - \frac{\tilde{b}_i^2}{4\tilde{c}_i} & \tilde{c}_i < 0 \\ \tilde{a}_i + \tilde{b}_i \tilde{U}_i & \tilde{c}_i = 0 \end{cases} \quad (16)$$

where d_i is constant and is determined by the following equation

$$d_i = \tilde{a}_i - \frac{\tilde{b}_i^2}{4\tilde{c}_i} \quad (17)$$

Z_i is obtained by a linear transformation of \tilde{U}_i

$$\begin{cases} Z_i = \sqrt{\tilde{c}_i} \tilde{U}_i + \frac{\tilde{b}_i}{2\sqrt{\tilde{c}_i}} & \tilde{c}_i > 0 \\ Z_i = \sqrt{-\tilde{c}_i} \tilde{U}_i - \frac{\tilde{b}_i}{2\sqrt{-\tilde{c}_i}} & \tilde{c}_i < 0 \end{cases} \quad (18)$$

Z_i is normally distributed and is denoted by $Z_i \sim N(\mu_{Z_i}, \sigma_{Z_i})$, where the mean μ_{Z_i} is given by

$$\mu_{Z_i} = \begin{cases} \frac{\tilde{b}_i}{2\sqrt{\tilde{c}_i}} & \tilde{c}_i > 0 \\ -\frac{\tilde{b}_i}{2\sqrt{-\tilde{c}_i}} & \tilde{c}_i < 0 \end{cases} \quad (19)$$

and the standard deviation σ_{Z_i} is given by

$$\sigma_{Z_i} = \begin{cases} \sqrt{\tilde{c}_i} & \tilde{c}_i > 0 \\ \sqrt{-\tilde{c}_i} & \tilde{c}_i < 0 \end{cases} \quad (20)$$

$V_i = (Z_i / \sigma_{Z_i})^2$ follows a noncentral chi-square distribution with freedom of 1 [116, 117]; namely $V_i \sim \chi^2(1, \lambda)$, where λ is a non-centrality parameter and given by

$$\lambda = \left(\frac{\mu_{Z_i}}{\sigma_{Z_i}} \right)^2 \quad (21)$$

The limit-state function in Eq. (16) is finally expressed by a linear combination of either noncentral chi-square variables or standard normal variables.

$$Q_i(\tilde{\mathbf{U}}) = \begin{cases} \sigma_{Z_i}^2 V_i + d_i & \tilde{c}_i > 0 \\ -\sigma_{Z_i}^2 V_i + d_i & \tilde{c}_i < 0 \\ \tilde{a}_i + \tilde{b}_i \tilde{U}_i & \tilde{c}_i = 0 \end{cases} \quad (22)$$

3.2.3 Saddlepoint Approximation

Saddlepoint approximation is used to recover a PDF from its cumulant generating function (CGF). The CGF of the noncentral chi-square V_i in Eq. (22) is given by

$$K_{V_i}(t) = \frac{\lambda_i t}{1-2t} - \frac{1}{2} \log(1-2t) \quad (23)$$

The CGF of the standard normal variable \tilde{U}_i in Eq. (22) is given by

$$K_{\tilde{U}_i} = \frac{1}{2}t^2 \quad (24)$$

The CGF of $Q_i(\tilde{\mathbf{U}})$ in Eq. (22) is then given by

$$K_{Q_i}(t) = \begin{cases} \frac{\lambda_i \sigma_{Z_i}^2 t}{1 - 2\sigma_{Z_i}^2 t} - \frac{1}{2} \log(1 - 2\sigma_{Z_i}^2 t) + d_i t & \tilde{c}_i > 0 \\ -\frac{\lambda_i \sigma_{Z_i}^2 t}{1 + 2\sigma_{Z_i}^2 t} - \frac{1}{2} \log(1 + 2\sigma_{Z_i}^2 t) + d_i t & \tilde{c}_i < 0 \\ \tilde{a}t + \frac{1}{2} \tilde{b}_i^2 t^2 & \tilde{c}_i = 0 \end{cases} \quad (25)$$

With all the above CGFs available, the CGF of the limit-state function in Eq. (12) $Q(\tilde{\mathbf{U}})$ is then computed by

$$K_Q(t) = \sum_{i=1}^n K_{Q_i}(t) \quad (26)$$

After the CGF $K_Q(t)$ is obtained, it is straightforward to find the PDF of the limit-state function, and this requires to find the saddlepoint t_s , which is found by solving the following equation

$$K'_Q(t) = 0 \quad (27)$$

where $K'_Q(t)$ is the first derivative of $K_Q(t)$. According to the Lugannani and Rice's formula [118], the component reliability R_{SPA} is computed by

$$R_{\text{SPA}} = \Pr\{Q(\tilde{\mathbf{U}}) < 0\} = \Phi(w) + \phi(w) \left(\frac{1}{w} - \frac{1}{v} \right) \quad (28)$$

where $\Phi(\cdot)$ and $\phi(\cdot)$ are CDF and PDF of a standard normal distribution, respectively.

$$w = \text{sgn}(t_s) \{2[-K_Q(t_s)]\}^{1/2} \quad (29)$$

$$v = t_s [K''_Q(t_s)]^{1/2} \quad (30)$$

where $\text{sgn}(t_s) = +1, -1$ or 0 , depending on whether t_s is positive, negative or zero; $K''_Q(t)$ is the second derivative of $K_Q(t)$ with respect to t .

3.3 System Reliability with Second Order SPA

In this section, we discuss the new second-order SPA method for system reliability analysis. We focus on only series systems; the method, however, can also be extended to parallel systems and the combination of series and parallel systems.

System reliability can be estimated by integrating the joint PDF of all the input random variables in the safe region as indicated Eq. (3). To use SPA, we consider the PDF of component responses directly. The system state is determined by component responses predicted from component limit-state functions $Y_i = g_i(\mathbf{X})$ ($i = 1, 2, \dots, m$). System reliability is then computed by

$$R_S = \Pr\left(\bigcap_{i=1}^m Y_i = g_i(\mathbf{X}) < 0, i = 1, 2, \dots, m\right) \quad (31)$$

Eq. (31) requires the joint distribution of Y_i ($i = 1, 2, \dots, m$). This means that we need to consider both component reliability and dependencies between component responses. Hereby, we approximate the joint distribution of all the component responses as a multivariate normal distribution.

If we consider only the first order terms of Eq. (9), the component limit-state function becomes

$$Q_i(\mathbf{U}) = -\nabla G(\mathbf{u}_i^*)^T \mathbf{u}_i^* + \nabla G_i(\mathbf{u}_i^*) \mathbf{U} \quad (32)$$

If we divide both sides of Eq. (32) by the magnitude of the gradient, we obtain

$$\frac{Q_i(\mathbf{U})}{\|\nabla G(\mathbf{u}_i^*)\|} = -\frac{\nabla G(\mathbf{u}_i^*)^T}{\|\nabla G(\mathbf{u}_i^*)\|} \mathbf{u}_i^* + \frac{\nabla G_i(\mathbf{u}_i^*)}{\|\nabla G(\mathbf{u}_i^*)\|} \mathbf{U} \quad (33)$$

Or

$$\frac{Q_i(\mathbf{U})}{\|\nabla G(\mathbf{u}_i^*)\|} = -\beta_i + \boldsymbol{\alpha}_i \mathbf{U} \quad (34)$$

The event of the safe component $Q_i(\mathbf{U}) < 0$ is equivalent to the event $-\beta_i + \boldsymbol{\alpha}_i \mathbf{U} < 0$. We then define a new variable

$$Z_i = -\beta_i + \boldsymbol{\alpha}_i \mathbf{U} \quad (35)$$

where $\boldsymbol{\alpha}_i$ is the directional vector and is given by

$$\boldsymbol{\alpha}_i = \frac{\nabla G_i(\mathbf{u}_i^*)}{\|\nabla G(\mathbf{u}_i^*)\|} = \frac{\mathbf{u}_i^*}{\beta_i} \quad (36)$$

We call Z_i an equivalent component response. It is obvious that Z_i follows a normal distribution. As a result, all the equivalent component responses follow a multivariate normal distribution.

System reliability is then approximated by

$$R_S = \Pr\left(\bigcap_{i=1}^m Q_i(\mathbf{U}) < 0\right) = \Pr\left(\bigcap_{i=1}^m \boldsymbol{\alpha}_i \mathbf{U} - \beta_i < 0\right) = \Pr\left(\bigcap_{i=1}^m Z_i < 0\right) \quad (37)$$

The multivariate normal distribution is denoted by $N(\boldsymbol{\mu}_Z, \boldsymbol{\Sigma}_Z)$, where $\boldsymbol{\mu}_Z$ is the mean vector of $\mathbf{Z} = (Z_1, Z_2, \dots, Z_m)$ and $\boldsymbol{\Sigma}_Z$ is the covariance matrix. System reliability thus becomes the CDF $\Phi_m(\mathbf{0}; \boldsymbol{\mu}_Z, \boldsymbol{\Sigma}_Z)$ of \mathbf{Z} at $\mathbf{0}$; namely

$$R_S = \Phi_m(\mathbf{0}; \boldsymbol{\mu}_Z, \boldsymbol{\Sigma}_Z) = \int_{-\infty}^0 \dots \int_{-\infty}^0 f_Z(\mathbf{z}) d\mathbf{z} \quad (38)$$

where $f_Z(\mathbf{z})$ is the joint PDF of \mathbf{Z} .

Since we use the first approximation directly as indicated in Eq. (9), the method we have just discussed is the existing FORM for system reliability analysis.

The accuracy of the multivariate normal integration in Eq. (38) is closely related to the accuracy of the mean vector $\boldsymbol{\mu}_Z$ and covariance matrix $\boldsymbol{\Sigma}_Z$. In addition to high accuracy, we would also like to maintain high efficiency. There are mainly two ways to make the integration accurate and efficient. First, we improve the accuracy by determining $\boldsymbol{\mu}_Z$ with the second order component reliability obtained from the second order SPA. This strategy is adapted from Ref. [119] where the traditional SORM is used. Since the second-order SPA is in general more accurate than the traditional SORM, the new method has higher accuracy. We use the second order SPA to approximate the marginal CDF of Z_i at 0, which is the component reliability

$$F_{Z_i}(\mathbf{0}) = \Pr(Z_i < 0) = R_{\text{SPA}i} \quad (39)$$

where $R_{\text{SPA}i}$ is calculated by the second-order SPA method given in Eq. (28). Then the associated reliability index is determined by

$$R_{\text{SPA}i} = \Phi(\beta_i^{\text{SPA}}) \quad (40)$$

We call β_i^{SPA} an equivalent reliability index, which is given by

$$\beta_i^{\text{SPA}} = \Phi^{-1}(R_{\text{SPA}i}) \quad (41)$$

Since β_i^{SPA} is obtained from a more accurate reliability estimate, we use it to replace β_i in Eq. (35), resulting in $Z_i = -\beta_i^{\text{SPA}} + \mathbf{a}_i \mathbf{U}$. The mean vector of the multivariable distribution of \mathbf{Z} is then obtained.

$$\boldsymbol{\mu}_Z = (\beta_1^{\text{SPA}}, \beta_2^{\text{SPA}}, \dots, \beta_m^{\text{SPA}}) \quad (42)$$

The above treatment ensures that the component reliability or the marginal distributions of component responses are accurately estimated by the second order approximation.

In order to simplify computations and achieve high efficiency, we use the same strategy in Ref. [119] to estimate the covariance matrix $\boldsymbol{\Sigma}_Z$. The idea is to use the first order approximation in Eq. (32). Let the components of $\boldsymbol{\Sigma}_Z$ be ρ_{ij} , $i, j = 1, 2, \dots, m$, $i \neq j$. The covariance is given by

$$\rho_{ij} = \mathbf{a}_i^T \mathbf{a}_j \quad (43)$$

Then $\boldsymbol{\Sigma}_Z$ is given by

$$\boldsymbol{\Sigma}_Z = \begin{bmatrix} 1 & \rho_{12} & \cdots & \rho_{1m} \\ \rho_{21} & 1 & \cdots & \rho_{2m} \\ \vdots & \vdots & \rho_{ij} & \vdots \\ \rho_{m1} & \rho_{m2} & \cdots & 1 \end{bmatrix}_{m \times m} \quad (44)$$

The joint distribution of all component responses is now approximated by a multivariate normal distribution. With $\boldsymbol{\mu}_Z$ and $\boldsymbol{\Sigma}_Z$ available, the joint PDF of $\mathbf{Z} = (Z_1, Z_2, \dots, Z_m)$ is expressed as

$$f_Z(\mathbf{z}) = \frac{1}{\sqrt{(2\pi)^m |\boldsymbol{\Sigma}_Z|}} \exp\left(-\frac{1}{2}(\mathbf{z} - \boldsymbol{\mu}_Z)^T \boldsymbol{\Sigma}_Z^{-1}(\mathbf{z} - \boldsymbol{\mu}_Z)\right) \quad (45)$$

Then system reliability R_S can be easily calculated by integrating the PDF in Eq. (38) from $(-\infty, \dots, -\infty)$ to $(0, \dots, 0)$ and the system probability of failure is

$$p_{Sf} = 1 - R_S \quad (46)$$

Many algorithms are available for integrating $f_Z(\mathbf{z})$ in Eq. (45) such as the first order multi-normal approximation (FOMN) [120], the product of conditional marginal method (PCM) [121], and Alan Genz method [122]. The proposed method provides a new way to estimate the system reliability with nonlinear limit-state functions. The dependencies between component responses are automatically accommodated in the system covariance matrix, and component marginal CDFs can be obtained accurately by using the second-order SPA. Thus this method not only achieves

high accuracy in estimating system reliability but also simplifies the computations while maintaining high efficiency.

The procedure of the system reliability analysis with the second-order SPA is briefly summarized below.

- (1) Transform random variable \mathbf{X} into \mathbf{U} in the standard normal space.
- (2) Search for MPPs \mathbf{u}_i^* ; obtain the reliability index β_i and first and second derivatives of component limit-state functions at the MPPs.
- (3) Perform the second-order SPA for all components.
- (4) Use SPA results to find the means of equivalent component responses.
- (5) Use MPPs and reliability indexes to find the covariance matrix.
- (6) Form the multivariate normal PDF and integrate it to obtain system reliability.

3.4 Examples

In this section, four examples are presented. The first example is used to demonstrate the proposed method while the other three examples show possible engineering applications. The accuracy is measured by the percentage error with respect to a solution from MCS. The error is calculated by

$$\varepsilon = \frac{|p_{sf} - p_{sf}^{\text{MCS}}|}{p_{sf}^{\text{MCS}}} \times 100\% \quad (47)$$

where p_{sf}^{MCS} and p_{sf} are probabilities of system failure from MCS and second order SPA method, FORM method or SORM method, respectively.

3.4.1 Example 1

The first example is mathematical example. A system consists of two physical components, and each component has one limit-state function. There are two basic random variables denoted by $\mathbf{X} = (X_1, X_2)$. X_1 is normally distributed with mean $\mu_1 = 4$ and standard deviation $\sigma_1 = 0.7$, and the distribution is denoted by $X_1 \sim N(4, 0.7)$. X_2 is lognormally distributed with mean

$\mu_2 = 4$ and standard deviation $\sigma_2 = 1$, and the distribution is denoted by $X_2 \sim LN(4,1)$. The two limit-state functions are given by

$$g_1(\mathbf{X}) = 5 - X_1 X_2 \quad (48)$$

$$g_2(\mathbf{X}) = -X_1^2 - X_2^2 - 7X_1 + 16X_2 - 40 \quad (49)$$

At first, MPPs, reliability indexes, and directional vectors of the two limit-state functions are obtained. The results are given in Table 3.1.

Table 3.1 MPP, reliability index and directional vector

	\mathbf{u}^*	β	$\boldsymbol{\alpha}$
g_1	(-2.6981,-2.0057)	3.3602	(0.8025,0.5966)
g_2	(-2.5485, 1.8429)	3.1450	(0.8103,-0.5869)

Next, the reliability of each component is calculated by the second-order SPA with $R_1 = 0.9995$ and $R_2 = 0.9994$. The mean values of the two equivalent component responses $\mathbf{Z} = (Z_1, Z_2)$ are then calculated by

$$\boldsymbol{\mu}_Z = \boldsymbol{\beta}^{\text{SPA}} = (\beta_i^{\text{SPA}})_{i=1,2} = (\Phi^{-1}(R_i))_{i=1,2} = (3.3083, 3.2358)$$

The correlation coefficients ρ_{ij} are calculated by Eq. (43). For example, $\rho_{12} = \boldsymbol{\alpha}_1 \boldsymbol{\alpha}_2^T = 0.3007$. Therefore, the covariance matrix is obtained.

$$\boldsymbol{\Sigma}_Z = \begin{bmatrix} 1 & \rho_{12} \\ \rho_{21} & 1 \end{bmatrix} = \begin{bmatrix} 1 & 0.3007 \\ 0.3007 & 1 \end{bmatrix}$$

Using Eq. (38), we obtain the system probability of failure $p_{sf} = 1 - R_s = 1.0702 \times 10^{-3}$.

When FORM and SORM are used, the covariance matrices are the same as $\boldsymbol{\Sigma}_Z$, and the mean values of the two equivalent component responses are $\boldsymbol{\mu}_Z = \boldsymbol{\beta}^{\text{FORM}} = (3.3620, 3.1450)$ and $\boldsymbol{\mu}_Z = \boldsymbol{\beta}^{\text{SORM}} = (3.3086, 3.2274)$ Based on Eq. (38), the system probabilities of failure based on FORM and SORM are $p_{sf} = 1.2111 \times 10^{-3}$ and $p_{sf} = 1.0878 \times 10^{-3}$ respectively.

For MCS, a large sample size of 10^7 is used to compute the system reliability. All results are listed in Table 2, which shows that the errors of SOSPA, SORM and FORM are 0.289%, 1.35% and 12.% respectively. The results indicate that SOSPA is more accurate than FORM and SORM.

The number of function calls in Table 3.2 indicate that FORM is more efficient than SOSPA and SORM. 1.0878×10^{-3}

Table 3.2 Probability of system failure in Example 1

Method	p_{sf}	ε (%)	Total function calls
SOSPA	1.0702×10^{-3}	0.29	45
SORM	1.0878×10^{-3}	1.35	45
FORM	1.2111×10^{-3}	12.80	39
MCS	1.0733×10^{-3}	N/A	10^7

3.4.2 Example 2

Example 2 is an engineering example. Consider a roof structure [123], whose top boom and compression bars are made by concrete, while the bottom boom and all the tension bars are made of steel. Assume the bars bear a uniformly distributed load q . Let A_c and E_c be the cross-sectional area and elastic modulus of the concrete bars, respectively. Let A_s and E_s be the cross-sectional area and elastic modulus of the steel bars, respectively. The perpendicular deflection of the roof peak node C is calculated by

$$\Delta C = \frac{ql^2}{2} \left(\frac{3.81}{A_c E_c} + \frac{1.13}{A_s E_s} \right) \quad (52)$$

A failure event occurs when the perpendicular deflection ΔC exceeds 1.5 cm. The limit-state function is then defined by

$$g_1(\mathbf{X}) = \frac{ql^2}{2} \left(\frac{3.81}{A_c E_c} + \frac{1.13}{A_s E_s} \right) - 0.015 \quad (53)$$

The second failure mode is that the internal force of bar AD exceeds its ultimate stress. The internal force of bar AD is $N_{AD} = 1.35ql$, and the ultimate strength of the bar is $f_c A_c$, where f_c is the compressive stress of the bar. The second limit-state function is given by

$$g_2(\mathbf{X}) = 1.185ql - f_c A_c \quad (54)$$

A failure occurs when the internal force of bar EC $N_{EC} = 1.3ql$ exceeds its ultimate stress $f_s A_s$, where f_s is the tensile strength of the bar. Therefore, the third limit-state function is formulated by

$$g_3(\mathbf{X}) = 0.65ql - f_s A_s \quad (55)$$

E_C and E_s are lognormally distributed, and the rest of random variables q , l , A_s , A_C , f_C , and f_s are normally distributed. They are listed in Table 3.3.

Table 3.3 Distribution of random variables

	Variables	Distribution
X_1	q (N/m)	N(14000,1400)
X_2	L (m)	N(12,0.12)
X_3	A_s (m ²)	N(9.00×10^{-4} , 0.54×10^{-4})
X_4	A_C (m ²)	N(5×10^{-2} , 4×10^{-3})
X_5	E_s (N/m ²)	LN(2×10^{11} , 0.12×10^{11})
X_6	E_C (N/m ²)	LN(3×10^{11} , 0.18×10^{11})
X_7	f_s (N/m ²)	N(3.35×10^8 , 0.60×10^8)
X_8	f_C (N/m ²)	N(1.34×10^7 , 0.24×10^7)

After the MPPs are found, the reliability indexes and directional vectors are available.

$$\beta_1 = 4.6396$$

$$\beta_2 = 3.8122$$

$$\beta_3 = 3.4440$$

$$\boldsymbol{\alpha}_1 = (0.7054, 0.1857, -0.4890, -0.2122, -0.4147, -0.1465, 0, 0)$$

$$\boldsymbol{\alpha}_2 = (0.1686, 0.0179, 0, -0.1504, 0, 0, 0, -0.9740)$$

$$\boldsymbol{\alpha}_3 = (0.2009, 0.0215, -0.1325, 0, 0, 0, -0.9704, 0)$$

Similarly, the reliability of each component is calculated by the second-order SPA, which produces $R_1 = 1.0$, $R_2 = 0.9999$, and $R_3 = 0.9997$. The mean values of the three equivalent component responses $\mathbf{Z} = (Z_1, Z_2, Z_3)$ are then calculated by

$$\boldsymbol{\mu}_Z = \boldsymbol{\beta}^{\text{SPA}} = (\beta_i^{\text{SPA}})_{i=1,2,3} = \Phi^{-1}(R_i)_{i=1,2,3} = (4.5985, 3.7999, 3.4358)$$

The covariance matrix $\boldsymbol{\Sigma}_Z$ is

$$\boldsymbol{\Sigma}_Z = \begin{bmatrix} 1 & \rho_{12} & \rho_{13} \\ \rho_{21} & 1 & \rho_{23} \\ \rho_{31} & \rho_{32} & 1 \end{bmatrix} = \begin{bmatrix} 1 & 0.1542 & 0.2092 \\ 0.1542 & 1 & 0.0343 \\ 0.2092 & 0.0343 & 1 \end{bmatrix}$$

Thus, the system probability of failure is estimated to be $p_{sf} = 3.6983 \times 10^{-4}$.

When FORM is used, the covariance matrix remains the same, and the mean values of the three equivalent component responses are $\boldsymbol{\mu}_Z = (4.6396, 3.8122, 3.4440)$. Based on Eq. (38), the system probability of failure is $p_{sf} = 3.5714 \times 10^{-4}$. Similarly, the system probability of SORM is $p_{sf} = 3.6642 \times 10^{-4}$. The solution from MCS with a sample size of 1×10^7 serves as a benchmark for the accuracy comparison. All results are given in Table 3.4, which indicates that SOSPA is more accurate than FORM and SORM while the latter is more efficient than the former.

Table 3.4 Probability of system failure in Example 2

Method	p_{sf}	ε (%)	Total function calls
SOSPA	3.6983×10^{-4}	0.34	243
SORM	3.6642×10^{-4}	1.26	243
FORM	3.5714×10^{-4}	3.76	135
MCS	3.7110×10^{-4}	N/A	10^7

3.4.3 Example 3

This example has ten polynomial surface response functions used as a surrogate for a more computationally intensive numerical model of the various phenomena leading to failure [124, 125]. The system reliability is defined by

$$R_{sf} = \Pr(g_1(\mathbf{X}) \leq 0 \cap g_2(\mathbf{X}) \leq 0 \cap \dots \cap g_9(\mathbf{X}) \leq 0 \cap g_{10}(\mathbf{X}) \leq 0) \quad (56)$$

The limit-state functions $g_i(\cdot)$ are given below.

$$g_1(\mathbf{X}) = 1.16 - 0.3717X_2X_4 - 0.00931X_2X_{10} - 0.484X_3X_9 + 0.01343X_6X_{10} - 1 \quad (57)$$

$$g_2(\mathbf{X}) = 4.72 - 0.5X_4 - 0.19X_2X_3 - 0.0122X_4X_{10} + 0.009325X_6X_{10} + 0.000191X_{11}^2 - 4.01 \quad (58)$$

$$g_3(\mathbf{X}) = 28.98 + 3.818X_3 - 4.2X_1X_2 + 0.0207X_5X_{10} + 6.63X_6X_9 - 7.7X_7X_8 + 0.32X_9X_{10} - 32 \quad (59)$$

$$g_4(\mathbf{X}) = 33.86 + 2.95X_3 + 0.1792X_{10} - 5.057X_1X_2 - 11X_2X_8 - 0.0215X_5X_{10} - 9.98X_7X_8 - 22X_8X_9 - 32 \quad (60)$$

$$g_5(\mathbf{X}) = 46.36 - 9.9X_2 - 12.9X_1X_8 + 0.1107X_3X_{10} - 32 \quad (61)$$

$$g_6(\mathbf{X}) = 0.261 - 0.0159X_1X_2 - 0.188X_1X_8 - 0.019X_2X_7 + 0.0144X_3X_5 + 0.0008757X_5X_{10} - 0.32 \quad (62)$$

$$g_7(\mathbf{X}) = 0.214 + 0.00817X_5 - 0.131X_1X_8 - 0.0704X_1X_9 + 0.03099X_2X_6 - 0.018X_2X_7 + 0.0208X_3X_8 + 0.121X_3X_9 - 0.00364X_5X_6 + 0.0007715X_5X_{10} - 0.0005354X_6X_{10} + 0.00121X_8X_{11} - 0.32 \quad (63)$$

$$g_8(\mathbf{X}) = 0.74 - 0.61X_2 - 0.163X_3X_8 + 0.001232X_3X_{10} - 0.166X_7X_9 + 0.227X_2^2 - 32 \quad (64)$$

$$g_9(\mathbf{X}) = 10.58 - 0.674X_1X_2 - 1.95X_2X_8 + 0.02054X_3X_{10} - 0.0198X_4X_{10} + 0.028X_6X_{10} - 9.9 \quad (65)$$

$$g_{10}(\mathbf{X}) = 16.45 - 0.489X_3X_7 - 0.843X_5X_6 + 0.0432X_9X_{10} - 0.0556X_9X_{11} - 0.0003X_{11}^2 - 15.69 \quad (66)$$

There are eleven random variables which are B-pillar inner (X_1), B-pillar reinforcement (X_2), floor side inner (X_3), cross members (X_4), door beam (X_5), door belt line reinforcement (X_6), roof rail (X_7), B-pillar inner (X_8), floor side inner (X_9), barrier height (X_{10}), and barrier hitting position (X_{11}). All of them are normally distributed with parameters defined in the Table 3.5.

The reliability indexes of all components are at first calculated by FORM, which yields $\beta_1 = 9.3064$, $\beta_2 = 1.8772$, $\beta_3 = 4.0596$, $\beta_4 = 2.9767$, $\beta_5 = 1.2968$, $\beta_6 = 12.1197$, $\beta_7 = 15.5223$, $\beta_8 = 4.8357$, $\beta_9 = 3.7118$ and $\beta_{10} = 1.8782$. Therefore, for FORM, the mean values of ten equivalent component responses $\mathbf{Z} = (Z_1, Z_2, \dots, Z_{10})$ are

$$\boldsymbol{\mu}_z = (9.3064, 1.8772, 4.0596, 2.9767, 1.2968, 12.1197, 15.5223, 4.8357, 3.7118, 1.8782)$$

The 10-by-10 covariance matrix is given by

$$\Sigma_Z = \begin{bmatrix} 1 & -0.7651 & \cdots & 0.9021 & 0.5581 \\ -0.7651 & 1 & \cdots & -0.9285 & -0.7498 \\ \vdots & \vdots & \ddots & \vdots & \vdots \\ 0.9021 & -0.9285 & \cdots & 1 & 0.7093 \\ 0.5581 & -0.7498 & \cdots & 0.7093 & 1 \end{bmatrix}_{10 \times 10}$$

The system probability of failure from FORM method is $p_{sf} = 1 - R_S = 0.1390$.

When SOSPA method is used, the mean values of the ten equivalent component responses are given by

$$\mu_Z^{\text{SPA}} = (9.3286, 1.4495, 4.0629, 2.9759, 1.2983, 12.1274, 15.4725, 4.8079, 3.7234, 2.0335)$$

Table 3.5 Distribution of random variables

Random	Distribution
X_1 (mm)	N(0.500,0.030)
X_2 (mm)	N(1.310,0.030)
X_3 (mm)	N(0.500,0.030)
X_4 (mm)	N(1.395,0.030)
X_5 (mm)	N(0.875,0.030)
X_6 (mm)	N(1.200,0.030)
X_7 (mm)	N(0.400,0.030)
X_8 (GPa)	N(0.345,0.006)
X_9 (GPa)	N(0.192,0.006)
X_{10} (mm)	N(0.0,10.0)
X_{11} (mm)	N(0.0,10.0)

The probability of system probability from SOSPA is then given by $p_{sf} = 0.1777$. All results are given in Table 3.6, which also indicates that SOSPA is much more accurate than FORM and SORM while the latter is more efficient than the former. For this problem with 10 responses, the error from FORM and SORM are too large.

Table 3.6 Probability of system failure in Example 3

Method	P_{sf}	$\varepsilon(\%)$	Total function calls
SOSPA	0.1777	3.31	1572
SORM	0.1355	26.40	1572
FORM	0.1391	24.30	912
MCS	0.1838	N/A	10^7

3.4.4 Example 4

The final example involves an assembly system where a rectangular steel bar cantilevered to a steel channel with four identical tightly fitted bolts located at points A , B , C , and D as shown in Fig. 3.1. The rectangular bar is subjected to an external force F . All random variables are given in Table 3.7.

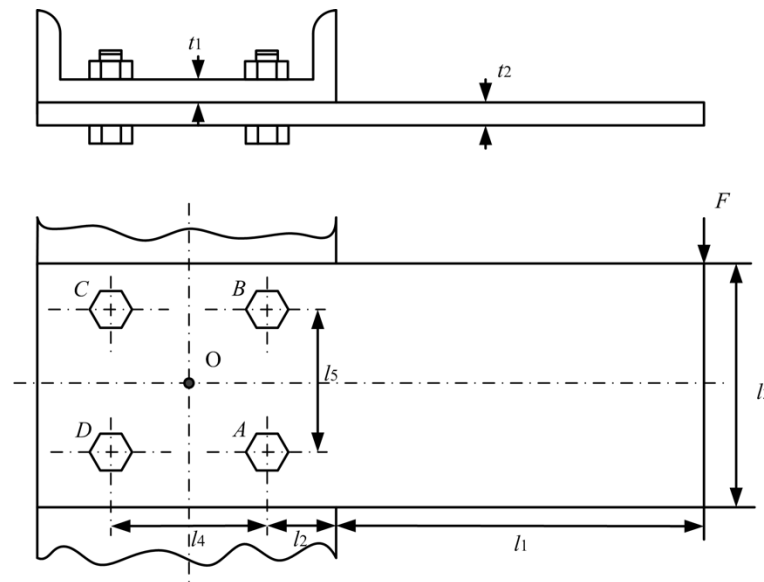


Figure 3.1 A cantilever bar

Table 3.7 Distribution of random variables

	Variables	Distribution
X_1	F (N)	$N(1.6 \times 10^4, 1.6 \times 10^3)$
X_2	S_1 (Pa)	$LN(300 \times 10^6, 57 \times 10^6)$
X_3	S_2 (Pa)	$LN(300 \times 10^6, 57 \times 10^6)$
X_4	τ_a (Pa)	$LN(310 \times 10^6, 59 \times 10^6)$
X_5	τ_b (Pa)	$LN(310 \times 10^6, 59 \times 10^6)$
X_6	τ_c (Pa)	$LN(310 \times 10^6, 59 \times 10^6)$
X_7	τ_d (Pa)	$LN(310 \times 10^6, 59 \times 10^6)$
X_8	t_1 (m)	$N(1.0 \times 10^{-2}, 2.0 \times 10^{-4})$
X_9	t_2 (m)	$N(1.0 \times 10^{-2}, 2.0 \times 10^{-4})$
X_{10}	d_a (m)	$N(1.6 \times 10^{-2}, 3.2 \times 10^{-4})$
X_{11}	d_b (m)	$N(1.6 \times 10^{-2}, 3.2 \times 10^{-4})$
X_{12}	d_c (m)	$N(1.6 \times 10^{-2}, 3.2 \times 10^{-4})$
X_{13}	d_d (m)	$N(1.6 \times 10^{-2}, 3.2 \times 10^{-4})$
X_{14}	l_1 (m)	$N(3.2 \times 10^{-1}, 6.4 \times 10^{-3})$
X_{15}	l_2 (m)	$N(5.0 \times 10^{-2}, 1.0 \times 10^{-3})$
X_{16}	l_3 (m)	$N(2.0 \times 10^{-1}, 4.0 \times 10^{-3})$
X_{17}	l_4 (m)	$N(1.5 \times 10^{-1}, 3.0 \times 10^{-3})$
X_{18}	l_5 (m)	$N(1.2 \times 10^{-2}, 2.4 \times 10^{-3})$
X_{19}	A_{sa} (m ²)	$N(1.44 \times 10^{-4}, 2.88 \times 10^{-6})$
X_{20}	A_{sb} (m ²)	$N(1.44 \times 10^{-4}, 2.88 \times 10^{-6})$
X_{21}	A_{sc} (m ²)	$N(1.44 \times 10^{-4}, 2.88 \times 10^{-6})$
X_{22}	A_{sd} (m ²)	$N(1.44 \times 10^{-4}, 2.88 \times 10^{-6})$

The centroid of the bolt group O is found by symmetry. The shear reaction V passes through O , and the moment reaction M is about O . They are given by $V = F$, $M = F(l_1 + l_2 + \frac{l_4}{2})$. The distance from the centroid to the center of each bolt is

$$r = 0.5 \sqrt{l_4^2 + l_5^2}$$

The primary shear load per bolt is $F' = \frac{V}{4}$. Since the secondary shear forces are equal, they become $F'' = \frac{Mr}{4r^2} = \frac{M}{4r}$. The resultants of the primary and secondary shear forces are obtained by using the parallelogram rule. The magnitudes are found to be

$$F_A = F_B = \sqrt{(F')^2 + (F'')^2 - 2F'F''\cos\theta_1}$$

$$F_C = F_D = \sqrt{(F')^2 + (F'')^2 - 2F'F''\cos\theta_2}$$

where $\theta_1 = \frac{pl}{2} + \arctan(\frac{l_4}{l_5})$, and $\theta_2 = \frac{pl}{2} - \arctan(\frac{l_4}{l_5})$.

The largest bearing stress is due to the pressing of the bolt against the channel web. The bearing area of the channel is $A_1 = t_1 d_a$. The maximum bearing stress of the channel should be smaller than its yield strength, which is given by

$$g_1(\mathbf{X}) = \frac{F_A}{A_1} - S_1 \quad (67)$$

Correspondingly, the limit-state function of the bar is defined by

$$g_2(\mathbf{X}) = \frac{F_A}{A_2} - S_2 \quad (68)$$

where $A_2 = t_2 d_a$

The critical bending stress in the bar occurs at the cross section $A-B$, where the bending moment is $M_1 = F(l_1 + l_2)$. The second moment of area of the section is

$$I = I_{bar} - 2(I_{holes} + \bar{d}^2 A) = \frac{t_2 l_2^3}{12} - 2 \left[\frac{t_2 d_a^3}{12} + \frac{l_5^2}{4} t_2 d_a \right]$$

The bending stress of the bar should be smaller than its yield strength, and this is given by

$$g_3(\mathbf{X}) = \frac{M_1}{I/c} - S_2 \quad (69)$$

where I/c is the section modulus for the bar, $c = l_3/2$.

Bolt A and B are critical because they carry the largest shear load F_A and F_B . The shear stress of the bolts should not be greater than the allowable shear stress. Thus, the limit-state functions of bolts A and B are defined by

$$g_4(\mathbf{X}) = \frac{F_A}{A_{sa}} - \tau_a \quad (70)$$

$$g_5(\mathbf{X}) = \frac{F_B}{A_{sb}} - \tau_b \quad (71)$$

where A_{sa} and A_{sb} are shear-stress areas.

Similarly, the limit-state functions of bolts C and D are defined by

$$g_6(\mathbf{X}) = \frac{F_C}{A_{sc}} - \tau_c \quad (72)$$

$$g_7(\mathbf{X}) = \frac{F_D}{A_{sd}} - \tau_d \quad (73)$$

where A_{sc} and A_{sd} are shear-stress areas.

There are seven limit-state functions. The system probabilities of failure and the function calls from all methods are provided in Table 3.8. The results show that SOSPA is the most accurate method because its error is only 0.593% compared with the MCS result and the errors of SORM and FORM are much larger. FORM is the most efficient method since its number of function calls is the least. SOSPA and SORM call the limit-state functions with the same time.

Table 3.8 Probability of system failure in Example 4

Method	p_{sf}	ε (%)	Total function calls
SOSPA	1.1672×10^{-3}	1.71	2599
SORM	1.0273×10^{-3}	13.50	2599
FORM	1.2292×10^{-3}	3.51	828
MCS	1.1875×10^{-3}	N/A	10^7

3.5 Summary

The proposed second order saddlepoint approximation (SOSPA) method is an alternative method for system reliability analysis. This method results in higher accuracy than the first order approximation method by combining the second order approximation and saddlepoint approximation. SOSPA accurately produces the marginal distributions of all component responses. This is achieved by employing the saddlepoint approximation after transforming the approximated second-order limit-state functions into linear combinations of noncentral chi-square variables. The dependences between component responses are considered with the only first approximation for the sake of efficiency. With the estimated marginal component distributions and component correlations, the joint distribution of all the component responses is formed by a multivariate normal distribution, which leads to a fast evaluation of the system reliability.

The accuracy of the proposed is largely determined by the accuracy of the approximated limit-state functions with second order Taylor expansion in the vicinity of the most probable points. The accuracy is also affected by the first order approximation for estimating correlations between component responses.

How to estimate component correlations more accurately by a second order approximation needs a further investigation. The other future work is to incorporate the system reliability analysis in reliability-based design optimization.

4. TIME-DEPENDENT SYSTEM RELIABILITY ANALYSIS WITH SECOND ORDER RELIABILITY METHOD

Hao Wu¹, Zhangli Hu², Xiaoping Du³

¹School of Mechanical Engineering, Purdue University, West Lafayette, IN, United States

²Department of Mechanical and Aerospace Engineering, Missouri University of Science and Technology, Rolla, MO, United States

³Department of Mechanical and Energy Engineering, Indiana University - Purdue University Indianapolis, IN, United States

Published in ASME. J. Mech., <https://doi.org/10.1115/1.4048732>

Authors' contribution: H.W. and X.D. designed the study. All authors contributed to the writing of the manuscript. H.W. detailed methodology and the code.

System reliability is quantified by the probability that a system performs its intended function in a period of time without failures. System reliability can be predicted if all the limit-state functions of the components of the system are available, and such a prediction is usually time consuming. This work develops a time-dependent system reliability method that is extended from the component time-dependent reliability method using the envelope method and second order reliability method. The proposed method is efficient and is intended for series systems with limit-state functions whose input variables include random variables and time. The component reliability is estimated by the second order component reliability method with an improve envelope approach, which produces a component reliability index. The covariance between component responses are estimated with the first order approximations, which are available from the second order approximations of the component reliability analysis. Then the joint distribution of all the component responses is approximated by a multivariate normal distribution with its mean vector being component reliability indexes and covariance being those between component responses. The proposed method is demonstrated and evaluated by three examples.

4.1 Background

System reliability is measured by the probability that the system performs its intended function in routine circumstances during a specified period of time [7]. It is necessary to predict system reliability accurately and efficiently in the early design stage since it can be used to estimate the lifecycle cost, determine maintenance policies, and optimize the system performance [57, 126]. A mechanical system consists of multiple components, and each component may also have multiple failure modes. In this work, we consider a failure mode as a component. If the limit-state function of a failure mode is invariant over time, its reliability and probability of failure are constant. However, the limit-state function may vary over time in many engineering problems, such as function generator mechanisms [127] and bridges under stochastic loading [128]. Then a time-dependent reliability method is required.

Suppose the limit-state function of the i -th failure mode is given by

$$Y_i = g_i(\mathbf{X}, t) \quad (1)$$

where Y_i is a component response, which is a function of time t ; $\mathbf{X} = (X_1, \dots, X_n)^T$ is the vector of independent input random variables. Then the time-dependent component reliability on a time interval $[t_0, t_s]$ is defined by

$$R(t_0, t_s) = \Pr(g(\mathbf{X}, t) \geq 0, \forall t \in [t_0, t_s]) \quad (2)$$

and the corresponding probability of failure is defined by

$$p_f(t_0, t_s) = \Pr(g(\mathbf{X}, t) < 0, \exists t \in [t_0, t_s]) \quad (3)$$

Eq. (3) indicates that if $g(\cdot) < 0$ at any instant of time on $[t_0, t_s]$, the component fails.

In this study, we focus on series system. For a series system, the entire series system fails if one failure mode occurs. For a time-dependent series system, the system fails if any failure mode occurs at any instant of time. The system reliability $R_s(t_0, t_s)$ and probability of system failure $p_{fs}(t_0, t_s)$ are given by

$$R_s(t_0, t_s) = \Pr\left(\bigcap_{i=1}^m g_i(\mathbf{X}, t_i) \geq 0, \forall t_i \in [t_0, t_s]\right) \quad (4)$$

and

$$p_{fs}(t_0, t_s) = \Pr\left(\bigcup_{i=1}^m g_i(\mathbf{X}, t_i) < 0, \exists t_i \in [t_0, t_s]\right) \quad (5)$$

where \cup and \cap stand for union and intersection, respectively.

Component reliability analysis is required for system reliability analysis. Methods of time-dependent component reliability analysis include three groups: Rice's formula based methods [46, 129-131], meta-model based methods [132-135], and methods which convert time-dependent into time-independent reliability. Rice's formula based methods are most commonly used [50]. For example, the PHI2 method [130] allows for time-variant reliability problems to be solved using classical time-invariant reliability method, the first order reliability method (FORM). Hu and Du then proposed the joint up-crossing rate method in estimating the time-dependent reliability [46]. Rice's formula-based methods are in general more efficient than others but may lead to large errors if up-crossings are strongly dependent.

Higher accuracy can be achieved by metamodeling methods. Hu and Du introduced a mixed efficient global optimization method employing the adaptive Kriging-Monte Carlo simulation (MCS) so that this high accuracy is achieved [134]. Wang and Wang developed a nested extreme response surface method by employing Kriging for reliability analysis with time-variant performance characteristics [135]. This group of methods may result in a high computational cost if the dimension of the problem is high.

Converting a time-dependent problem into a time-independent counterpart is possible by using the extreme value of the limit-state function. The methods include the envelope function method [136], extreme value response method [137], and the composite limit-state function method [138]. Still, obtaining accurate distribution of the extreme value in an efficient way is complicated. Hu and Du recently employed sequential efficient global optimization (EGO) to transform the time-dependent reliability problem into a time-independent problem with a second order method. The Hessian matrix is approximated by a quasi-Newton approach. It uses the gradients of the limit-state function at the points before the MPP search converges to the MPP. The method is efficient, but it may not accurately approximate the Hessian matrix since the points may not be on the surface of the envelope function [139].

Many studies have been conducted on time-dependent system reliability as well. For instance, Song and Der Kiureghian developed a joint first-passage probability method based on the conditional distribution analysis in estimating the reliability of systems subjected to stochastic excitation [140]. Radhika et al. investigated nonlinear vibrating systems under stochastic excitations by implementing the asymptotic extreme value theory and Monte Carlo simulation (MCS) [141]. Yu et al. employed the combination of the extreme value moment and improved

maximum entropy method to access the time-variant system reliability with temporal parameters [142]. Gong and Frangopol proposed a new efficient method for time-dependent reliability which is formulated as a large-scale series system consisting of time-independent response functions [143]. Hu and Mahadevan proposed a novel and efficient methodology for time-dependent system reliability by considering the system as an equivalent Gaussian random field [144]. Jiang and Wei introduced an improved time-variant reliability analysis method based on stochastic process discretization, which transformed the time-variant reliability problem into time-invariant series system problem [145].

Time-independent system reliability can be approximated by the multidimensional integration of the joint probability density function (PDF) of random variables once the marginal distributions and correlation coefficients of component states are obtained by the second and first order approximations [8]. Wu and Du proposed a method of predicting the time-independent system reliability by approximating the marginal distributions with the second order saddlepoint method (SOSPA) [14].

It is desirable to take advantages of methods for both time-dependent component reliability and time-independent system reliability. To this end, in this work we integrate the second order saddlepoint approximation [139] for both time-dependent component reliability and time-independent system reliability. The distinctive feature of our new method is the true second order approximation to component envelope functions with its accurate Hessian matrix calculation. The second derivatives of the envelope functions with respect to the input random variables are exactly evaluated from the second derivatives of the corresponding component limit-state functions with respect to the input random variables and time. The second feature is that the second order approximation is extended from component reliability analysis to system reliability analysis.

This paper is organized as follows: Section 2 reviews the first order reliability method for time dependent reliability analysis. Section 3 discusses the proposed method for time-dependent system reliability analysis. Section 4 presents three examples, and Section 5 provides conclusions and discusses possible future work.

4.2 Methodologies Review

4.2.1 Time-Dependent Component Reliability

The limit-state function of a component is given in Eq. (1), and its reliability is therefore a function of time (or timespan) as indicated in Eq. (2). The commonly used reliability method is FORM, which is reviewed below.

FORM is originally used for time-independent reliability analysis, and it can also be used for time-dependent reliability analysis. It converts a general non-Gaussian process response into an equivalent Gaussian process response. \mathbf{X} is at first transformed into standard normal variables \mathbf{U} . Then the most probable point (MPP) \mathbf{u}^* at t is identified by the following model:

$$\begin{cases} \min \sqrt{\mathbf{U}^T \mathbf{U}} \\ \text{s. t. } g(\mathbf{X}, t) = g(\mathbf{T}(\mathbf{U}), t) = 0 \end{cases} \quad (6)$$

where $\mathbf{T}(\cdot)$ is an operator of the transformation from \mathbf{U} to \mathbf{X} .

The limit-state function is linearized at $\mathbf{u}^*(t)$ by

$$\begin{aligned} g(\mathbf{T}(\mathbf{U}), t) &= g(\mathbf{u}^*, t) + \sum_{i=1}^N \left. \frac{\partial g}{\partial U_i} \right|_{\mathbf{u}^*} (U_i - u_i^*) \\ &= \nabla g(\mathbf{u}^*, t) (\mathbf{U} - \mathbf{u}^*) \end{aligned} \quad (7)$$

where $\nabla g(\mathbf{u}^*, t) = \left[\left. \frac{\partial g}{\partial U_1} \right|_{\mathbf{u}^*}, \dots, \left. \frac{\partial g}{\partial U_N} \right|_{\mathbf{u}^*} \right]$ is the gradient, and u_i^* is the i -th component of \mathbf{u}^* .

Then the probability of failure is computed by

$$\begin{aligned} p_f &= \Pr(g(\mathbf{X}, t) < 0, \exists t \in [t_0, t_s]) \\ &= \Pr(\beta(t) + \boldsymbol{\alpha}(t)\mathbf{U} < 0, \exists t \in [t_0, t_s]) \end{aligned} \quad (8)$$

where $\beta(t)$ is the time-dependent reliability index, given by

$$\beta(t) = \|\mathbf{u}^*\| \quad (9)$$

and $\boldsymbol{\alpha}(t)$ is the time-dependent unit gradient vector given by

$$\boldsymbol{\alpha}(t) = \frac{\nabla g(t)}{\|\nabla g(t)\|} = [\alpha_1(t), \alpha_2(t), \dots, \alpha_N(t)] \quad (10)$$

As Eq. (7) shows, the non-Gaussian process $g(\mathbf{X}, t)$ has been transformed into an equivalent Gaussian process represented as a sum of standard normal random variables. After this, many methodologies are available for solving for the probability of failure, such as the upcrossing rate method [46, 130] and MCS [45].

The time-dependent probability of failure can be evaluated by the extreme value of the limit-state function.

$$p_f(t_o, t_s) = \Pr(g(\mathbf{X}, t) < 0, \exists t \in [t_o, t_s]) = \Pr\left(\min_{t \in [t_o, t_s]} g(\mathbf{X}, t) < 0\right) \quad (11)$$

The extreme limit-state function is equivalent to the envelope function [136] or the composite limit-state function [138], and $\min_{t \in [t_o, t_s]} g(\mathbf{X}, t)$ is obtained by

$$G(\mathbf{X}) = \min_{t \in [t_o, t_s]} g(\mathbf{X}, t) = g(\mathbf{X}, \tilde{t}(\mathbf{X})) \quad (12)$$

where $G(\mathbf{X})$ is the global minimum value of $g(\mathbf{X}, t)$ with respect to t . $G(\mathbf{X})$ is time independent and only depends on \mathbf{X} . \tilde{t} is the time instant when the global minimal value of $G(\mathbf{X})$ occurs. \tilde{t} is the function of \mathbf{X} .

$$\tilde{t} = \left\{ \tilde{t} \mid \min_{t \in [t_o, t_s]} g(\mathbf{X}, t) \right\} \quad (13)$$

The envelope function $G(\mathbf{X})$ is a surface tangent to all the instantaneous limit-state functions at different time instants. If FORM is used for envelope function, its MPP is obtained by

$$\begin{cases} \min \sqrt{\mathbf{U}^T \mathbf{U}} \\ \text{s. t. } \min_{t \in [t_o, t_s]} g(\mathbf{T}(\mathbf{U}), t) = 0 \end{cases} \quad (14)$$

Eq. (14) is a double loop optimization problem. The inner loop is the global optimization with respect to time t while the outer loop is the MPP search with respect to \mathbf{U} . The double loop is decoupled into a sequential single-loop process.

The first cycle is FORM analysis, the MPP $\mathbf{u}_{(1)}^*$ at the initial time t_o by

$$\begin{cases} \min \sqrt{\mathbf{U}^T \mathbf{U}} \\ \text{s. t. } g(\mathbf{T}(\mathbf{U}), t_o) = 0 \end{cases} \quad (15)$$

Then the time is updated by global optimization at $\mathbf{u}_{(1)}^*$, and the new time is denoted by $\tilde{t}^{(1)}$, which is given by

$$\tilde{t}^{(1)} = \operatorname{argmin}_{t \in [t_o, t_s]} g\left(\mathbf{T}(\mathbf{u}_{(1)}^*), t\right) \quad (16)$$

In the next cycle, the new MPP $\mathbf{u}_{(2)}^*$ is located at the time instant $\tilde{t}^{(1)}$ using Eq. (16). And then the time is updated to $\tilde{t}^{(2)}$ by performing global optimization at $\mathbf{u}_{(2)}^*$.

$$\tilde{t}^{(2)} = \operatorname{argmin}_{t \in [t_o, t_s]} g\left(\mathbf{T}(\mathbf{u}_{(2)}^*), t\right) \quad (17)$$

The above process is repeated until convergence.

The Efficient Global Optimization (EGO) is employed to solve the time t [146]. EGO has been widely used in various areas because it can efficiently search for the global optimum [134, 147]. The task is to solve for the time so that $g(t) = g(\mathbf{T}(\mathbf{u}_{\text{MPP}}), t)$ is minimized. With a number of training points, the function is approximated by the following surrogate model:

$$\hat{y} = g(t) = g(\mathbf{T}(\mathbf{u}_{\text{MPP}}), t) = F(t)^T \gamma + Z(t) \quad (18)$$

where $F(t)^T \gamma$ is a deterministic term, $F(t)$ is a vector of regression functions, γ is a vector of regression coefficients, and $Z(t)$ is a stationary Gaussian process with zero mean and a covariance given by

$$\text{Cov}(Z(t_1), Z(t_2)) = \sigma_Z^2 R(t_1, t_2) \quad (19)$$

where σ_Z^2 is process variance, and $R(\cdot, \cdot)$ is the correlation function.

The output of the surrogate model is a Gaussian random variable following

$$\hat{y} = g(t) \sim N(\mu(t), \sigma^2(t)) \quad (20)$$

where $\mu(t)$ and $\sigma(t)$ are the mean and standard deviation of \hat{y} , respectively.

After building the initial model, the expected improvement (EI) metric is used to identify the new training point with the highest probability to produce a better extreme value of the response. The improvement is defined by

$$I = \max(y^* - y, 0) \quad (21)$$

where $y^* = \min_{i=1,2,\dots,k} g(t_i)$ is the current minimum response.

EI is computed by

$$\begin{aligned} \text{EI}(t) &= E[\max(y^* - y, 0)] \\ &= (y^* - \mu(t)) \Phi\left(\frac{y^* - \mu(t)}{\sigma(t)}\right) + \sigma(t) \phi\left(\frac{y^* - \mu(t)}{\sigma(t)}\right) \end{aligned} \quad (22)$$

where $\Phi(\cdot)$ and $\phi(\cdot)$ are the cumulative distribution function (CDF) and PDF of a standard normal variable, respectively.

The new training point t_{new} is identified as the time that minimizes the expected improvement.

$$t_{\text{new}} = \underset{t}{\text{argmin}} \text{EI}(t) \quad (23)$$

The convergence criterion of EGO is set to $\varepsilon_{\text{EI}} = |y^*| \times 2\%$. By combining sequential strategy with EGO, the MPP \mathbf{u}^* of extreme limit-state function $G(\mathbf{X})$ can be obtained efficiently by solving Eq. (14). The probability of failure with FORM is estimated by

$$p_f(t_o, t_s) = \Pr(g(\mathbf{X}, t) < 0, \exists t \in [t_o, t_s]) \quad (24)$$

$$= \Pr(G(\mathbf{X}) < 0) = \Phi(-\beta)$$

where $\beta = \|\mathbf{u}^*\|$ is the first order reliability index. In general, the envelope function can be highly nonlinear and FORM may not be accurate enough. Thus, a second order method is preferred, and it uses the envelope theorem to obtain the second order information of the extreme limit-state function. Then SOSPA is used to estimate the probability of failure.

4.3 Proposed Methods

4.3.1 Overview

The envelope function of a component (or limit-state function) is generally nonlinear as shown in Fig. 4.1. It is the reason we use a second order approximation for the envelope function. Specifically, we approximate the envelope function at its MPP with a quadratic function. As a result, we also need the gradient and the Hessian matrix of the envelope function at the MPP.

It is shown that the MPP of the envelope function is the worst-case MPP of the limit-state function on $[t_0, t_s]$ [139]. In other words, the MPP is the closest point between the origin and all the instantaneous limit-state functions on $[t_0, t_s]$. This is illustrated in Fig. 1. The MPP of the envelope function can be efficiently found using the sequential single loop method [139]. This MPP is also the MPP of the worst-case limit-state function; as a result, the gradient of the envelope function is equal to the gradient of the worst-case limit-state function [139].

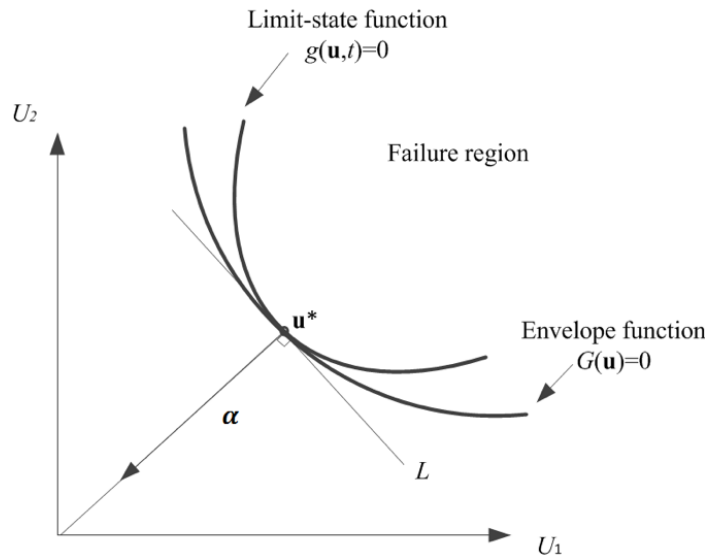


Figure 4.1 Relationship between the worst-case limit-state function and envelope function

The curvature of the envelope function, however, may not be the curvature of the worst-case limit-state function as shown in Fig. 1. This means that the Hessian matrix of the envelope function is in general not equal to that of the worst-case limit-state function. The Hessian matrix of the envelope function is approximated by the gradients of the instantaneous limit-state functions in [139], but the second derivative of the envelope function with respect to time is omitted. Hence the method in [139] may not always work. In this work, we derive analytical second derivatives of the envelope function with respect to both random input variables and time, and the Hessian matrix of the envelope function can then be obtained accurately.

The general procedure of finding the second order information of the envelope is summarized below. At first we employ the method in [139] to find the MPP of the envelope function using Eq. (14). Once we find the MPP, we know the gradient of the envelope function because it is equal to the gradient of the limit-state function at the MPP. Next we determine the Hessian matrix of the envelope function with Eq. (35). The Hessian matrix consists of second derivatives of the limit-state function with respect to random input variables \mathbf{X} and time t . The equations are derived in Sec. 3.2. When the MPP, gradient and Hessian matrix are available, we use the second order saddlepoint approximation to find the probability of component failure and then perform system reliability analysis. The method hereby is denoted by SOSPA.

4.3.2 Hessian Matrix of the Envelope Function

After the MPP of the envelope function is found, a quadratic envelope function is formulated as [14]

$$G(\mathbf{U}) = a + \mathbf{b}^T \mathbf{U} + \mathbf{U}^T \mathbf{C} \mathbf{U} \quad (25)$$

where

$$\begin{cases} a = \frac{1}{2} (\mathbf{u}^*)^T \mathbf{H} \mathbf{u}^* - \nabla G(\mathbf{u}^*)^T \mathbf{u}^* \\ \mathbf{b} = \nabla G(\mathbf{u}^*) - \mathbf{H} \mathbf{u}^* \\ \mathbf{C} = \frac{1}{2} \mathbf{H} = \text{diag}(\tilde{c}_1, \tilde{c}_2, \dots, \tilde{c}_N) \end{cases} \quad (26)$$

$\nabla G(\mathbf{u}^*) = \left(\left. \frac{\partial G}{\partial u_1} \right|_{\mathbf{u}^*}, \dots, \left. \frac{\partial G}{\partial u_n} \right|_{\mathbf{u}^*} \right)^T$ is the gradient of the envelope function. \mathbf{H} is the Hessian matrix, which is given by

$$\mathbf{H} = \begin{bmatrix} \frac{\partial^2 G}{\partial U_1^2} & \cdots & \frac{\partial^2 G}{\partial U_1 \partial U_n} \\ \vdots & \ddots & \vdots \\ \frac{\partial^2 G}{\partial U_n \partial U_1} & \cdots & \frac{\partial^2 G}{\partial U_n^2} \end{bmatrix}_{\mathbf{u}^*} \quad (27)$$

The envelope function $G(\mathbf{X}) = 0$ at \mathbf{u}^* is given by

$$G(\mathbf{U}) = \min_{t \in [t_o, t_s]} g(\mathbf{U}, t) = g(\mathbf{U}, \tilde{t})|_{\mathbf{u}^*} \quad (28)$$

\tilde{t} is the worst-case time instant, and it is found by

$$\dot{g}(\mathbf{U}, t) = 0 \quad (29)$$

where \dot{g} is the derivative of g with respect to t .

The first derivative of $G(\mathbf{U})$ with respect to a random input variable at \mathbf{u}^* is

$$\frac{\partial G}{\partial U_i} = \frac{\partial g}{\partial U_i} + \frac{\partial g}{\partial \tilde{t}} \frac{\partial \tilde{t}}{\partial U_i} \quad (30)$$

As $\dot{g}(\mathbf{U}, t) = 0$, Eq. (30) becomes

$$\frac{\partial G}{\partial U_i} = \frac{\partial g}{\partial U_i} \quad (31)$$

Eq. (31) indicates that the envelope function and the limit-state function have the same gradient at \mathbf{u}^* . Then, the second derivative of $G(\mathbf{U})$ with respect random input random variables at \mathbf{u}^* is

$$\begin{aligned} \frac{\partial^2 G}{\partial U_i \partial U_j} &= \frac{\partial}{\partial U_j} \left(\frac{\partial G}{\partial U_i} \right) = \frac{\partial}{\partial U_j} \left(\frac{\partial g}{\partial U_i} \right) \\ &= \frac{\partial^2 g}{\partial U_i \partial U_j} + \frac{\partial^2 g}{\partial U_i \partial t} \frac{\partial t}{\partial U_j} \end{aligned} \quad (32)$$

We then take the derivative of Eq. (29) with respect to U_j , and it is given by

$$\frac{\partial \dot{g}}{\partial U_j} + \frac{\partial \dot{g}}{\partial t} \frac{\partial t}{\partial U_j} = 0 \quad (33)$$

$$\frac{\partial t}{\partial U_j} = - \frac{\partial \dot{g} / \partial U_j}{\partial \dot{g} / \partial t} \quad (34)$$

Plugging Eqs. (29) and (34) into Eq. (32) yields the Hessian matrix \mathbf{H} at \mathbf{u}^* and \tilde{t} .

$$\left. \frac{\partial^2 G}{\partial U_i \partial U_j} \right|_{\mathbf{u}^*, \tilde{t}} = \left. \frac{\partial^2 g}{\partial U_i \partial U_j} \right|_{\mathbf{u}^*, \tilde{t}} - \left. \frac{\partial^2 g}{\partial U_i \partial t} \frac{\partial^2 g}{\partial U_j \partial t} / \frac{\partial^2 g}{\partial t^2} \right|_{\mathbf{u}^*, \tilde{t}} \quad (35)$$

The finite difference method can be used to calculate the Hessian matrix of the envelope function.

Next, the second order saddlepoint approximation is employed to estimate the probability of failure. Saddlepoint approximation has several excellent features. It yields an accurate probability estimation, especially in the tail area of a distribution [148, 149].

The cumulant generating function (CGF) of $G(\mathbf{U})$ is given by

$$K(s) = -\beta s + \frac{1}{2} s^2 - \frac{1}{2} \sum_{i=1}^{n-1} \log(1 - 2sk_i) \quad (36)$$

where $k_i = \tilde{c}_i$

The derivatives of CGF are

$$K'(s) = -\beta + s + \sum_{i=1}^{n-1} \frac{k_i}{1 - 2sk_i} \quad (37)$$

$$K''(s) = 1 + \sum_{i=1}^{n-1} \frac{k_i^2}{(1 - 2sk_i)^2} \quad (38)$$

The saddlepoint s_s is obtained by solving the following equation:

$$K'(t) = -\beta + s + \sum_{i=1}^{n-1} \frac{k_i}{1 - 2sk_i} = 0 \quad (39)$$

Then the probability of failure is evaluated by

$$\begin{aligned} p_f(t_o, t_s) &= \Pr(g(\mathbf{X}, t) < 0, \exists t \in [t_o, t_s]) \\ &= \Phi(w) + \phi(w) \left(\frac{1}{w} - \frac{1}{v} \right) \end{aligned} \quad (40)$$

where

$$w = \text{sgn}(s_s) \{2[-K(s_s)]\}^{\frac{1}{2}} \quad (41)$$

$$v = s_s [K''(s_s)]^{\frac{1}{2}} \quad (42)$$

in which $\text{sgn}(s_s) = +1, -1$, or 0 , depending on whether s_s is positive, negative, or zero.

The detailed steps of time-dependent component reliability analysis using SOSPA are summarized below.

Step 1: Set $k = 1$. Use the initial time instant as the initial extreme value time $\tilde{t}^{(0)} = t_0$ and use a unit vector as the initial MPP $\mathbf{u}_{(1)}^* = \mathbf{u}_0$.

Step 2: Search for the MPP at time instant $\tilde{t}^{(k-1)}$ and obtain MPP $\mathbf{u}_{(k)}^*$ in the k -th cycle by solving

$$\begin{cases} \min \sqrt{\mathbf{U}^T \mathbf{U}} \\ \text{s. t. } g(\mathbf{T}(\mathbf{U}), \tilde{t}^{(k-1)}) = 0 \end{cases}$$

Step 3: Determine the optimal time $\tilde{t}^{(k)}$ and the corresponding minimum value $g_{\min}^{(k)}$ by implementing EGO method with $\mathbf{u}_{(k)}^*$.

Step 4: Check convergence. The convergence criterion is defined as

$$\varepsilon = \left| g_{\min}^{(k)} \right| \leq \varepsilon_{tol}$$

If $\varepsilon \leq \varepsilon_{tol}$, terminate the iteration. Otherwise, set $k = k + 1$ and return to Step 2.

Step 5: Determine the gradient ∇G and Hessian matrix \mathbf{H} of the envelope function at $\mathbf{u}_{(k)}^*$ and $\tilde{t}^{(k)}$.

Step 6: Calculate p_f using SOSPA.

Note that the proposed method does not work when the extreme value of the limit-state function occurs at the beginning time instant t_o or end time instant t_s , where Eq. (29) is invalid.

4.3.3 System Reliability with SOSPA

In this section, we discuss how to extend SOSPA for time dependent component reliability to time dependent system reliability analysis.

System reliability can be estimated by integrating the joint PDF of all responses in the safe region. To use SOSPA, we consider the PDF of component responses directly. The system state is determined by component states predicted from component limit-state functions $Y_i = g_i(\mathbf{X}, t)$ ($i = 1, 2, \dots, m$).

Given all the limit-state functions with time, the series system reliability is then determined by the

$$R_S = \Pr \left(\bigcap_{i=1}^m Y_i = g_i(\mathbf{X}, t) > 0, \forall t \in [t_0, t_s] \right) \quad (43)$$

Eq. (43) enable us to consider component reliability and dependencies since it needs the joint PDF $f_{\mathbf{Y}}(\mathbf{y})$ of $\mathbf{Y} = (Y_1, Y_2, \dots, Y_m)$. We approximate the joint PDF $f_{\mathbf{Y}}(\mathbf{y})$ by a multivariate normal

distribution. If we only consider the first order terms of the extreme limit-state function Eq. (25), it becomes

$$G_i(\mathbf{U}) = -\nabla G(\mathbf{u}_i^*)^T \mathbf{u}_i^* + \nabla G(\mathbf{u}_i^*)^T \mathbf{U} \quad (44)$$

If we divide both sides of Eq. (44) by the magnitude of the gradient, we obtain

$$\frac{G_i(\mathbf{U})}{\|\nabla G(\mathbf{u}_i^*)\|} = -\frac{\nabla G_i(\mathbf{u}_i^*)^T}{\|\nabla G(\mathbf{u}_i^*)\|} \mathbf{u}_i^* + \frac{\nabla G_i(\mathbf{u}_i^*)^T}{\|\nabla G(\mathbf{u}_i^*)\|} \mathbf{U} \quad (45)$$

or

$$\frac{G_i(\mathbf{U})}{\|\nabla G(\mathbf{u}_i^*)\|} = -\boldsymbol{\alpha}_i^T \mathbf{u}_i^* + \boldsymbol{\alpha}_i^T \mathbf{U} \quad (46)$$

where $\boldsymbol{\alpha}_i$ is the unit vector of $\nabla G_i(\mathbf{u}_i^*)$. At the MPP, the reliability index is given by

$$\mathbf{u}_i^* = -\beta_i \boldsymbol{\alpha}_i \quad (47)$$

Then event of the safe component $G_i(\mathbf{U}) > 0$ is equivalent to the event $\beta_i + \boldsymbol{\alpha}_i^T \mathbf{U} > 0$. We then define a new variable

$$Z_i = \beta_i + \boldsymbol{\alpha}_i^T \mathbf{U} \quad (48)$$

Z_i is an equivalent component response. It is obvious that Z_i follows a normal distribution. As a result, all the equivalent component responses follow a multivariate normal distribution if the envelope functions of all the components are linearized at their MPPs. The system reliability is then approximated by

$$R_S = \Pr\left(\bigcap_{i=1}^m -Z_i(\mathbf{U}) < 0\right) \quad (49)$$

$\mathbf{Z} = (Z_1, Z_2, \dots, Z_m)^T$ follows a multivariate normal distribution denoted by $N(\boldsymbol{\mu}_Z, \boldsymbol{\Sigma}_Z)$, where $\boldsymbol{\mu}_Z$ is the mean vector and $\boldsymbol{\Sigma}_Z$ is the covariance matrix. $-\mathbf{Z}$ also follows a multivariate normal distribution $N(-\boldsymbol{\mu}_Z, \boldsymbol{\Sigma}_Z)$. System reliability thus becomes the CDF $\Phi_m(\mathbf{0}; -\boldsymbol{\mu}_Z, \boldsymbol{\Sigma}_Z)$ of $-\mathbf{Z}$ at $\mathbf{0}$; namely

$$R_S = \Phi_m(\mathbf{0}; -\boldsymbol{\mu}_Z, \boldsymbol{\Sigma}_Z) = \int_{-\infty}^0 \dots \int_{-\infty}^0 f_Z(\mathbf{z}) d\mathbf{z} \quad (50)$$

where $f_Z(\mathbf{z})$ is the joint PDF of $-\mathbf{Z}$, given by

$$f_Z(\mathbf{z}) = \frac{1}{\sqrt{(2\pi)^m |\boldsymbol{\Sigma}_Z|}} \exp\left(-\frac{(\mathbf{z} - \mathbf{u}_Z)^T \boldsymbol{\Sigma}_Z^{-1} (\mathbf{z} - \mathbf{u}_Z)}{2}\right) \quad (51)$$

The accuracy of the mean vector $\boldsymbol{\mu}_Z$ and covariance matrix $\boldsymbol{\Sigma}_Z$ determines the accuracy of the multivariate normal integration in Eq. (51). To maintain high accuracy, we use SOSPA to determine $\boldsymbol{\mu}_Z$. The marginal CDF of Z_i at 0, which is the component reliability is given by

$$R_{SPA_i} = \Pr(Z_i > 0) \quad (52)$$

Then the associated reliability index is determined by

$$\beta_{SPA_i} = \Phi^{-1}(R_{SPA_i}) \quad (53)$$

and β_{SPA_i} is an equivalent reliability index. Since β_{SPA} is estimated with higher accuracy in the estimated reliability, we use it to replace β in Eq. (48). The mean vector of the multivariable distribution of \mathbf{Z} becomes

$$\mathbf{u}_Z = (\beta_{SPA_1}, \dots, \beta_{SPA_m}) \quad (54)$$

The above treatment ensures that the component reliability or the marginal distributions of component responses are accurately estimated by the second order approximation. For higher efficiency, we use FORM or Eq. (48) to estimate the covariance matrix $\boldsymbol{\Sigma}_Z$ [119]. Let the components of $\boldsymbol{\Sigma}_Z$ be ρ_{ij} ($i \neq j$, $i, j = 1, 2, \dots, m$), which is given by

$$\rho_{ij} = \boldsymbol{\alpha}_i^T \boldsymbol{\alpha}_j \quad (55)$$

Then $\boldsymbol{\Sigma}_Z$ is given by

$$\boldsymbol{\Sigma}_Z = \begin{bmatrix} 1 & \cdots & \rho_{1m} \\ \vdots & \ddots & \vdots \\ \rho_{m1} & \cdots & 1 \end{bmatrix}_{m \times m} \quad (56)$$

With \mathbf{u}_Z and $\boldsymbol{\Sigma}_Z$ available, the system reliability R_s can be easily calculated by integrating the joint PDF in Eq. (51) from $(-\infty, \dots, -\infty)$ to $(0, \dots, 0)$ and the time dependent probability of system failure is

$$p_{fs} = 1 - R_s \quad (57)$$

Many methods such as the first order multi-normal approximation (FOMN) [150] and Alan Genz method [151-153] are developed to integrate $f_Z(\mathbf{z})$ in Eq. (51). The proposed method provides a new way to estimate the time dependent system reliability with nonlinear limit-state functions. The dependencies between component responses are automatically accommodated in the system covariance matrix, and component marginal CDFs can be obtained accurately using SOSPA. The procedure of the system reliability analysis is briefly summarized below. The flowchart of this procedure is given in Fig. 4.2.

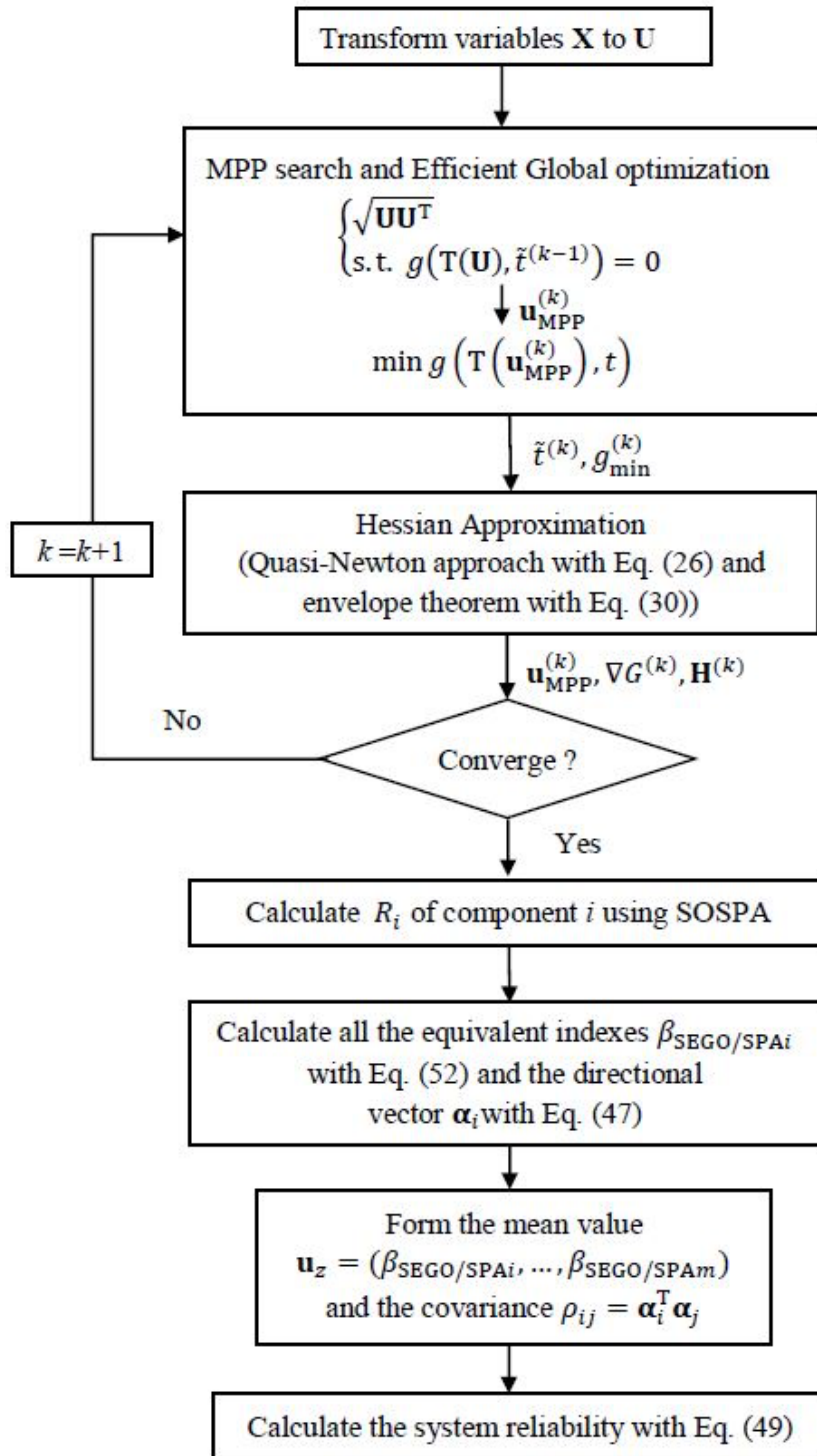


Figure 4.2 Flowchart of time-dependent system reliability

Step 1: Transform random variables \mathbf{X} into \mathbf{U} in the standard normal space.

Execute Step 2 and 4 for all components in the system.

Step 2: Search for MPPs \mathbf{u}^* , obtain the optimal time \tilde{t} of the component limit-state function with the efficient global optimization method.

Step 3: Determine the gradient ∇G and Hessian matrix \mathbf{H} of the envelope function.

Step 4: Calculate the probability of component failure and use SOSPA to find the mean vector of equivalent component responses.

Execute Steps 5 and 6 for system reliability analysis.

Step 5: Use the MPPs and reliability indexes of all components to find the covariance matrix of component responses.

Step 6: Form the multivariate normal PDF and integrate it to obtain time dependent system reliability.

4.3.4 Extension to the Problems with Input Random Process

When the limit-state function involves random processes, it becomes $Y = g(\mathbf{X}, \mathbf{L}(t), t)$, where $\mathbf{L}(t)$ is a vector of random processes. Series expansion methods, such as the Karhunen–Loeve series expansion, the orthogonal series expansion, and the expansion optimal linear estimation method (EOLE) [154], can be used to convert them into independent random variables, and then the proposed method can still work. Take EOLE as an example for a Gaussian random process $L(t)$. The time interval $[t_0, t_s]$ is evenly discretized into N points, and the $N \times N$ autocorrelation coefficient matrix $\mathbf{\Sigma} = [\rho(t_i, t_j)]$, $i = 1, 2, \dots, N, j = 1, 2, \dots, N$ is obtained. Then the EOLE expansion is given by

$$L(\mathbf{U}, t) \approx \mu(t) + \sigma(t) \sum_{j=1}^r \frac{U_k}{\sqrt{\lambda_j}} \boldsymbol{\phi}_j^T \boldsymbol{\Sigma}(:, t), k = 1, 2, \dots, r \quad (58)$$

where $\mu(t)$ and $\sigma(t)$ are mean and standard deviation of $\mathbf{L}(t)$, respectively. $U_k, k = 1, 2, \dots, r$, are independent standard normal variables, $\boldsymbol{\lambda} = (\lambda_1, \lambda_2, \dots, \lambda_r)^T$ is the eigenvalue vector, and $\boldsymbol{\phi}_1, \boldsymbol{\phi}_2, \dots, \boldsymbol{\phi}_r$ are the corresponding eigenvectors obtained from autocorrelation coefficient matrix $\mathbf{\Sigma}$. Note that r is determined as the smallest integer that meets the following criterion:

$$\frac{\sum_{j=1}^r \lambda_j}{\sum_{j=1}^N \lambda_j} \geq \eta \quad (59)$$

where η is a hyperparameter determining the accuracy of the expansion. It takes a value close to, but not larger than 1. The smaller is η , the less accurate is the expansion. If $\eta = 1$, the expansion is exact. Normally, η is set to 0.9999.

4.3.5 Parallel Systems

The above results can be extended to parallel systems. For a parallel system, the probability of failure can be computed by

$$p_{fs} = \Pr\left(\bigcup_{i=1}^m Y_i = g_i(\mathbf{X}, t) < 0, \exists t \in [t_0, t_s], i = 1, 2, \dots, m\right) \quad (60)$$

Let $G_i(\mathbf{X}, t) = -g_i(\mathbf{X}, t)$, then

$$p_{fs} = \Pr\left(\bigcap_{i=1}^m Y_i = G_i(\mathbf{X}, t) > 0, \exists t \in [t_0, t_s], i = 1, 2, \dots, m\right) \quad (61)$$

Eq. (61) evaluates the probability of an intersection of m events as Eq. (43) does for a series system. Hence the proposed method can be used to calculate Eq. (61), which leads to the system reliability $R_S = 1 - p_{fs}$.

4.4 Examples

In this section, three examples are presented to test SOSPA for system reliability analysis. Example 1 is a mathematical problem which is used to demonstrate the details of the proposed method. Examples 2 and 3 are engineering problems. The accuracy is measured by the percentage error with respect to a solution from MCS. The error is calculated by

$$\varepsilon = \frac{|p_{fs} - p_{fs}^{\text{MCS}}|}{p_{fs}^{\text{MCS}}} \times 100\% \quad (62)$$

where p_{fs} is the result from SOSPA or FORM, and p_{fs}^{MCS} is the result from MCS.

4.4.1 Example 1: A Math Problem

A series system consists of two components with random basic variables $\mathbf{X} = (X_1, X_2)$. X_i ($i = 1, 2$) is normally distributed with parameter $\mu_i = 3.5$ and $\sigma_i = 0.3$. The two limit-state functions are given by

$$g_1(\mathbf{X}, t) = X_1^2 X_2 - 5X_1 t + (X_2 + 1)t^2 - 8.2 \quad (63)$$

$$g_2(\mathbf{X}, t) = (\cos(5^\circ) X_1 + \sin(5^\circ) X_2)^2 (-\sin(5^\circ) X_1 + \cos(5^\circ) X_2) - 5(\cos(5^\circ) X_1 + \sin(5^\circ) X_2)t + ((-\sin(5^\circ) X_1 + \cos(5^\circ) X_2 + 1)t^2 - 3.9) \quad (64)$$

where t varies within $[155]$.

Fig. 4.3 shows the parabolic curve of the envelope function of $g_1(\mathbf{X}, t)$ formed by the instantaneous limit-state surface at different time instants within the interval $[155]$. The contours of the analytical envelope functions of G_1 and G_2 are plotted in Fig. 4.4. The shaded area represents the system failure region.

To explain clearly how the SOSPA method works, we only show the details for $g_1(\mathbf{X}, t)$. First, the MPP of the envelope function at \tilde{t} is obtained using sequential EGO. The iteration history is shown in Table 4.1. Once the iteration is convergent, the MPP is found at $(-1.0714, -3.1172)^T$.

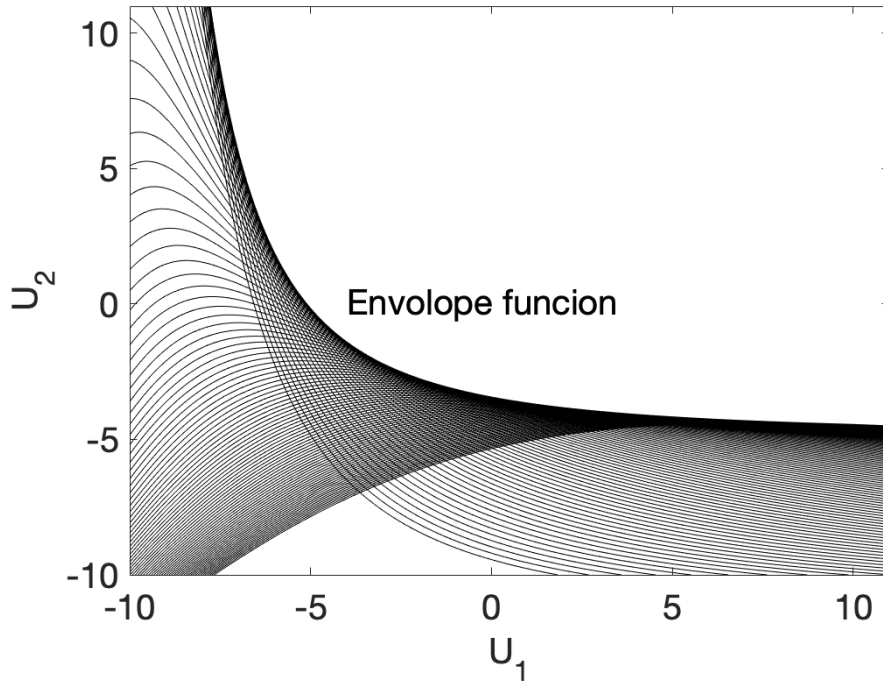


Figure 4.3 Envelope function formed by instantaneous limit-state surfaces

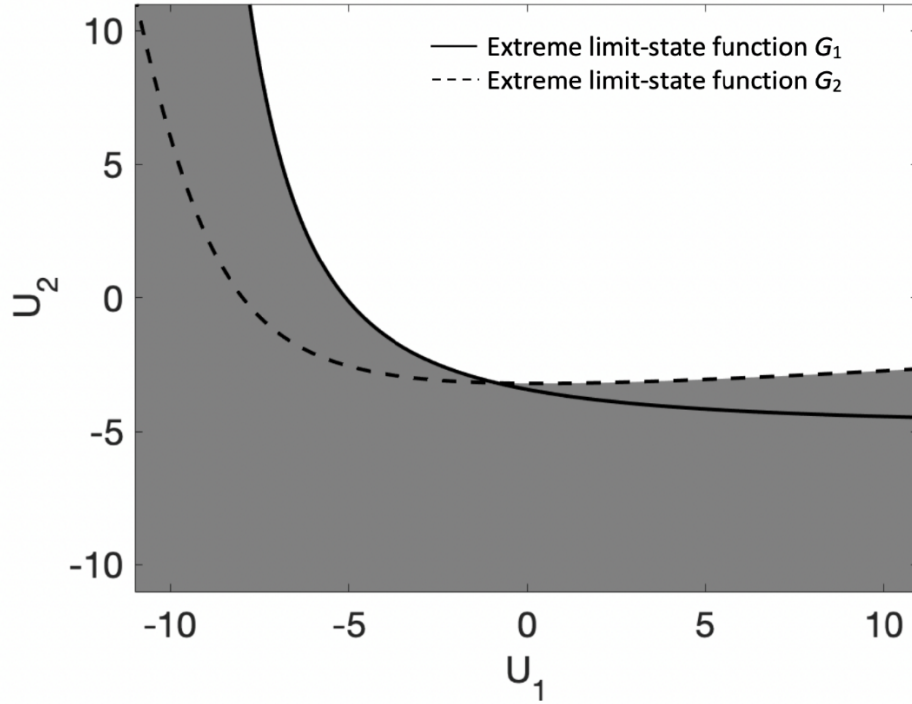


Figure 4.4 System extreme limit-state function

The probabilities of failure for g_1 and g_2 from SOSPA are $p_{f1} = 6.0040 \times 10^{-4}$ and $p_{f2} = 7.2248 \times 10^{-4}$. The mean values of the two equivalent component responses $\mathbf{Z} = (Z_1, Z_2)^T$ are then given by $\mathbf{u}_z = \boldsymbol{\beta}_{\text{SOSPA}} = (-3.2387, -3.1855)^T$. The unit directional vectors of the two limit-state functions are $\boldsymbol{\alpha}_1 = (0.3254, 0.9456)^T$ and $\boldsymbol{\alpha}_2 = (0.0098, 1.0)^T$. Thus, the correlation coefficient between g_1 and g_2 is $\rho_{12} = \boldsymbol{\alpha}_1^T \boldsymbol{\alpha}_2 = 0.9487$, and the covariance matrix is obtained as follow.

$$\boldsymbol{\Sigma}_z = \begin{bmatrix} 1 & \rho_{12} \\ \rho_{21} & 1 \end{bmatrix} = \begin{bmatrix} 1 & 0.9487 \\ 0.9487 & 1 \end{bmatrix}$$

The probability of system failure from SOSPA is $p_{fs} = 1 - R_s = 9.4747 \times 10^{-4}$. When FORM is used, the covariance is the same as $\boldsymbol{\Sigma}_z$, and the mean values of the two equivalent component responses are below

$$\mathbf{u}_z = \boldsymbol{\beta}_{\text{FORM}} = (-3.2963, -3.2079)^T$$

The probability of system failure from FORM is $p_{fs} = 8.3738 \times 10^{-4}$. The MCS solution with a sample size of 10^6 is also obtained. For MCS, the time interval is evenly discretized into 100 points. The total number of function calls is therefore 2×10^8 . The results are shown in Table

4.2 where the errors calculated by Eq. (62) are given in brackets. Table 4.2 shows that SOSPA is much more accurate than FORM which produces a large error due to the nonlinearity of the envelope functions. However, the total function calls of FORM and SOSPA are 365 and 410, respectively, showing FORM is more efficient.

Table 4.1 Iteration history of MPP search for g_1

Iterations	\mathbf{u}^*	$\tilde{\epsilon}$
1	$(-6.1450, -1.7052)^T$	1.4735
2	$(-2.1526, -2.9252)^T$	1.9689
3	$(-1.3877, -3.0305)^T$	2.1483
4	$(-1.1631, -3.0878)^T$	2.2063
5	$(-1.0941, -3.1096)^T$	2.2251
6	$(-1.0714, -3.1172)^T$	2.2314

Table 4.2 Probability of system failure in Example 1

Methods	SOSPA	FORM	MCS
p_{f1}	6.0040×10^{-4} (2.81%)	4.8989×10^{-4} (16.10%)	5.840×10^{-4}
p_{f2}	7.2248×10^{-4} (3.28%)	6.6864×10^{-4} (10.50%)	7.470×10^{-4}
p_{fs}	9.4747×10^{-4} (0.89%)	8.3738×10^{-4} (12.40%)	9.560×10^{-4}
N_{calls} of g_1	127	112	10^8
N_{calls} of g_2	283	253	10^8
Total	410	365	2×10^8

4.4.2 Example 2: A Roof Truss Structure

A roof truss problem is modified as our second example shown in Fig. 4.5 The top boom and all the compression bars are made of concrete while the bottom boom and all the tension bars are made of steel. The bars bear a nonstationary Gaussian process whose autocorrelation coefficient function is given by

$$\rho(t_1, t_2) = \exp \left[- \left(\frac{t_1 - t_2}{6} \right)^2 \right] \quad (65)$$

A_c and E_c are the cross-sectional area and elastic modulus of the concrete bars, respectively. A_s and E_s are the cross-sectional area and elastic modulus of the steel bars, respectively. All parameters are independent and are listed in Table 4.3.

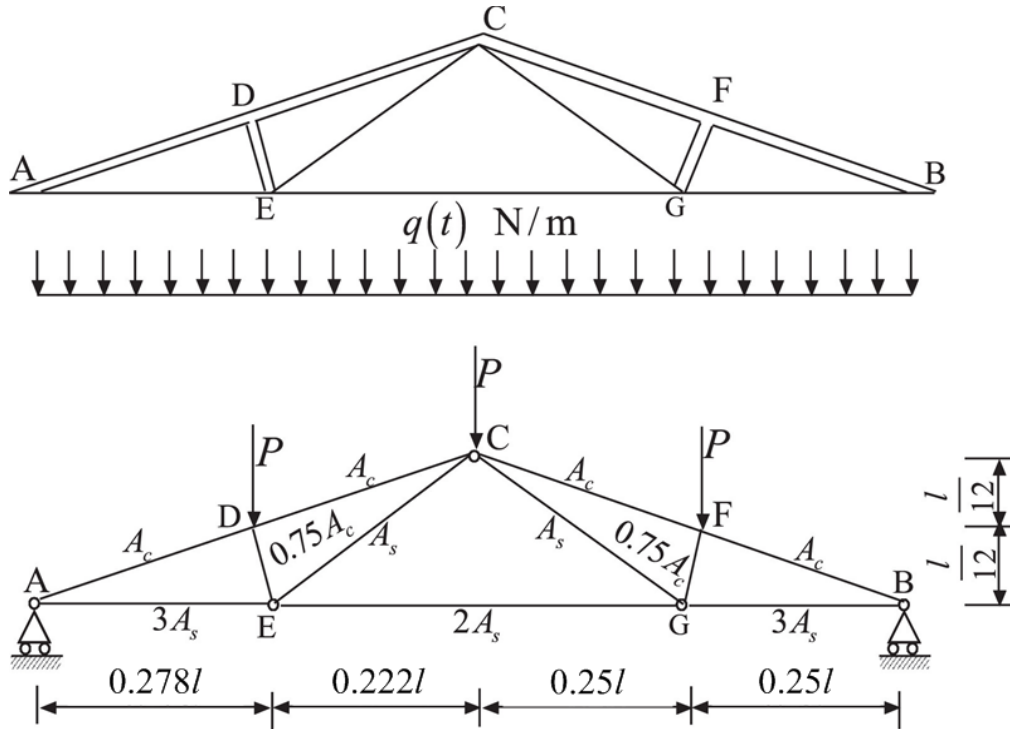


Figure 4.5 A roof truss

The perpendicular deflection of the roof peak node is calculated by

$$\Delta C = \frac{ql^2}{2} \left(\frac{3.81}{A_c E_c} + \frac{1.13}{A_s E_s} \right) \quad (66)$$

A failure occurs when the perpendicular deflection ΔC exceeds 1.6 cm at any instant of time period $[0,10]$. The limit-state function is then defined by

$$g_1(\mathbf{X}, t) = 0.016 - \frac{ql^2}{2} \left(\frac{3.81}{A_C E_C} + \frac{1.13}{A_S E_S} \right) \quad (67)$$

The second failure mode is that the internal force of one bar exceeds its ultimate stress. The internal force of the bar is $1.185ql$, and the ultimate strength of the bar is $f_c A_C$, where f_c is the compressive stress of the bar. The second limit-state function is then given by

$$g_2(\mathbf{X}, t) = f_c A_C - 1.185ql \quad (68)$$

The third failure occurs when the internal force of another bar $0.75ql$ exceeds its ultimate stress $f_s A_S$, where f_s is the tensile strength of the bar. Therefore, the third limit-state function is formulated by

$$g_3(\mathbf{X}, t) = f_s A_S - 0.75ql \quad (69)$$

Table 4.3 Distribution of random variables

Variabl e (Unit)	Mean	Standard deviation	Distribution
q (N/m)	$14000(0.2 \sin(0.25t) + 0.8)$	500	Nonstationary Gaussian process
L (m)	12	0.12	Normal
A_S (m ²)	9.0×10^{-4}	9.0×10^{-5}	Normal
A_C (m ²)	5×10^{-2}	5×10^{-3}	Normal
E_S (N/m ²)	2×10^{11}	2×10^{10}	Lognormal
E_C (N/m ²)	3×10^{10}	3×10^9	Lognormal
f_S (N/m ²)	3.35×10^8	6.7×10^7	Normal
f_C (N/m ²)	1.34×10^7	2.68×10^6	Normal

The time period $[0,10]$ years is evenly discretized into $N = 50$ points. With Eq. (65), the 50×50 autocorrelation coefficient matrix Σ of random process q is obtained. The most significant five eigenvalues of Σ are 35.54, 11.90, 2.24, 0.28, and 0.03. We use EOLE to generate the series expansion of $q(t)$ and only keep the first five orders.

SOSPA produces mean vector of the equivalent component responses:

$$\boldsymbol{\mu}_z = (-2.6681, -3.4056, -2.7416)^T$$

and the covariance matrix is as follows:

$$\boldsymbol{\Sigma}_z = \begin{bmatrix} 1 & \rho_{12} & \rho_{13} \\ \rho_{21} & 1 & \rho_{23} \\ \rho_{31} & \rho_{32} & 1 \end{bmatrix} = \begin{bmatrix} 1 & 0.1564 & 0.2824 \\ 0.1564 & 1 & 0.0375 \\ 0.2824 & 0.0375 & 1 \end{bmatrix}$$

The probability of system failure from SOSPA is $p_{fs} = 7.1017 \times 10^{-3}$.

FORM and MCS are also used, and the sample size of MCS for each component is 5×10^8 . The results from three methods are given in Table 4, showing that SOSPA has the higher accuracy than FORM with less efficiency.

Table 4.4 Probability of system failure in Example 2

Methods	SOSPA	FORM	MCS
p_{f1}	3.8140×10^{-3} (3.74%)	3.4370×10^{-3} (13.35%)	3.9623×10^{-3}
p_{f2}	3.3010×10^{-4} (2.16%)	3.0768×10^{-4} (8.81%)	3.3740×10^{-4}
p_{f3}	3.0569×10^{-3} (2.41%)	2.8297×10^{-3} (9.66%)	3.1324×10^{-3}
p_{fs}	7.1017×10^{-3} (2.78%)	6.4885×10^{-3} (11.20%)	7.3049×10^{-3}
N_{calls} of g_1	306	188	5×10^8
N_{calls} of g_1	599	363	5×10^8
N_{calls} of g_1	592	538	5×10^8
Total	1797	1089	1.5×10^9

4.4.3 Example 3: A Function Generator Mechanism System

Fig. 4.6 shows a function generator mechanism system, which can achieve a desire motion. This system consists of two function generator mechanisms [10].

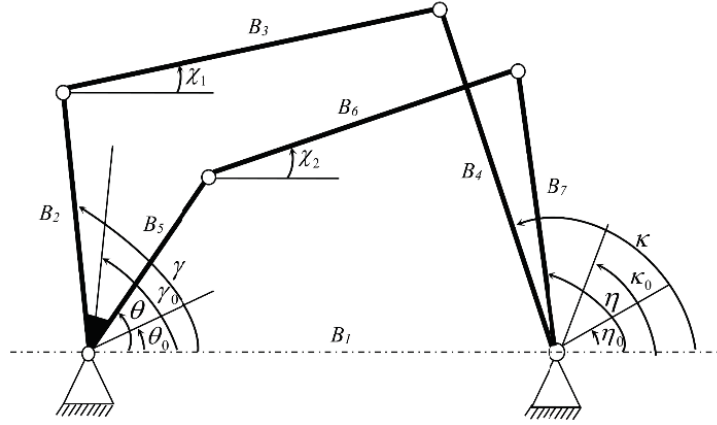


Figure 4.6 A Function Generator Mechanism System

Mechanism 1 is a four-bar linkage mechanism with links B_1 , B_2 , B_3 , and B_4 , and it generates a sine function. Its motion error is the difference between the actual motion output and the required motion output. It is defined as

$$\varepsilon_1(\mathbf{X}_1, \gamma) = \kappa_a(\mathbf{X}_1, \gamma) - \kappa_d(\gamma) \quad (70)$$

where $\mathbf{X}_1 = (B_1, B_2, B_3, B_4)$ and links B_2 and B_5 are welded together. The two input angles satisfy

$$\gamma = 62^\circ + \theta \quad (71)$$

From the mechanism analysis, $\kappa_a(\mathbf{X}_1, \gamma)$ and $\kappa_d(\gamma)$ can be obtained by

$$\kappa_a(\mathbf{X}_1, \gamma) = 2 \arctan \left(\frac{-E_1 \pm \sqrt{E_1^2 + D_1^2 - F_1^2}}{F_1 - D_1} \right) \quad (72)$$

and

$$\kappa_d(\gamma) = 60^\circ + 60^\circ \sin \left(\frac{3}{4}(\gamma - 97^\circ) \right) \quad (73)$$

where $D_1 = 2B_4(B_1 - B_2 \cos \gamma)$, $E_1 = -2B_2B_4 \sin \gamma$, and $F_1 = B_1^2 + B_2^2 + B_4^2 - B_3^2 - 2B_1B_2 \cos \gamma$.

Mechanism 2 is the other four-bar linkage mechanism with links B_1 , B_5 , B_6 , and B_7 , and it generates a logarithm function. The motion error is given by

$$\varepsilon_2(\mathbf{X}_2, \theta) = \eta_a(\mathbf{X}_2, \theta) - \eta_d(\theta) \quad (74)$$

where $\mathbf{X}_2 = (B_1, B_5, B_6, B_7)$.

$$\eta_a(\mathbf{X}_2, \theta) = 2 \arctan \left(\frac{-E_2 \pm \sqrt{E_2^2 + D_2^2 - F_2^2}}{F_2 - D_2} \right) \quad (75)$$

$$\eta_d(\theta) = 60^\circ \log_{10} \frac{[(\theta + 15^\circ)/60^\circ]}{\log_{10} 2} \quad (76)$$

where $D_2 = 2B_7(B_1 - B_5 \cos\theta)$, $E_2 = -2B_5B_7 \sin\theta$, and $F_2 = B_1^2 + B_5^2 + B_7^2 - B_6^2 - 2B_1B_5 \cos\theta$.

Mechanism 1 is considered reliable if $\{e_2 < \varepsilon_1(\mathbf{X}_1, \gamma) < e_1\}$, where e_1 and e_2 are allowable motion errors with $e_1 = 1.4$ and $e_2 = -0.8$. When the motion error is positive, the limit-state function is defined by

$$g_1(\mathbf{X}_1, \gamma) = e_1 - \varepsilon_1(\mathbf{X}_1, \gamma) \quad (77)$$

As for the negative motion error, the limit-state function is given by

$$g_2(\mathbf{X}_1, \gamma) = \varepsilon_1(\mathbf{X}_1, \gamma) - e_2 \quad (78)$$

Similarly, the limit-state functions of mechanism 2 are as follows:

$$g_3(\mathbf{X}_2, \theta) = e_3 - \varepsilon_2(\mathbf{X}_2, \theta) \quad (79)$$

$$g_4(\mathbf{X}_2, \theta) = \varepsilon_2(\mathbf{X}_2, \theta) - e_4 \quad (80)$$

in which $e_3 = 1.0$ and $e_4 = -2.4$. The random variables are given in Table 4.5. The mechanism system performs its intended functions over an interval of $[\theta_0, \theta_s] = [45^\circ, 95^\circ]$. The system is a series system with four components (limit-state functions).

Table 4.5 Parameters in Example 3

Variable (Unit)	Mean	Standard deviation	Distribution
B_1 (mm)	100	0.3	Normal
B_2 (mm)	55.5	0.05	Normal
B_3 (mm)	144.1	0.05	Normal
B_4 (mm)	72.5	0.05	Normal
B_5 (mm)	79.5	0.05	Normal
B_6 (mm)	203	0.05	Normal
B_7 (mm)	150.8	0.05	Normal

Table 4.6 shows the results. It indicates that the accuracy of SOSPA is in general better than FORM. However, both methods produce almost identical results for p_{f2} and p_{f4} . The reason is that the extreme values of two corresponding limit-state functions occur at the beginning of the time period (at 45°). Thus, the Hessian matrices of the two envelope functions are not accurate, and SOSPA is not accurate for p_{f2} and p_{f4} . Since the two probabilities of component failure are much smaller than the other two probabilities, their effect on the probability of system failure is insignificant.

Table 4.6 Probability of system failure in Example 3

Methods	SOSPA	FORM	MCS
p_{f1}	6.8663×10^{-3} (1.12%)	5.6273×10^{-3} (18.94%)	6.9440×10^{-3}
p_{f2}	6.1088×10^{-5} (4.55%)	6.1088×10^{-5} (4.55%)	6.430×10^{-5}
p_{f3}	2.5156×10^{-3} (0.17%)	2.0006×10^{-3} (19.20%)	2.520×10^{-3}
p_{f4}	4.3845×10^{-4} (11.80%)	4.3845×10^{-4} (11.80%)	4.970×10^{-4}
p_{fs}	7.5580×10^{-3} (1.11%)	6.2230×10^{-3} (18.60%)	7.6430×10^{-3}
N_{calls} of g_1	179	124	10^8
N_{calls} of g_2	398	288	10^8
N_{calls} of g_3	320	210	10^8
N_{calls} of g_4	479	369	10^8
Total	1376	991	4×10^8

4.5 Summary

The proposed time dependent system reliability method predicts system reliability with a second order approximation. It is therefore in general more accurate than the first order

approximation method. But it is less efficient than the latter method due to the need of second derivatives.

The new method converts a time dependent problem into a time independent problem by using the envelope function or the extreme value of a limit-state function over the time span under consideration. The most probable point (MPP) of the envelope function is found with the help of efficient global optimization. Then the envelope function is approximated at the MPP with its gradient and Hessian matrix. The reliability of each component is calculated by the second order saddlepoint approximation, and the dependencies between component responses are considered with the first approximation for the sake of efficiency. Once the estimated marginal component distributions and component correlations are available, the joint distribution of all the component responses is formed by a multivariate normal distribution, which leads to a fast evaluation of the system reliability.

The proposed envelope method works well if the envelope function is convex. The global MPP of the envelope function may not be found if the envelope function has multiple MPPs. For this case, the MPP search may start from different instants of time, and then the worst-case MPP is used. The proposed method does not work for a special case where the extreme value of a limit-state function occurs at the beginning or end of the period of time under consideration, and the reason is that the derivations of the Hessian matrix of the envelope function are for the case where the extreme value occurs inside the period of time.

Out future work will address the above two issues. The proposed method can also be further extended to time and space dependent problems where random processes and random fields are also involved.

5. ENVELOPE METHOD FOR TIME- AND SPACE-DEPENDENT RELIABILITY PREDICTION

Hao Wu¹, Xiaoping Du²

¹School of Mechanical Engineering, Purdue University, West Lafayette, IN, United States

²Department of Mechanical and Energy Engineering, Indiana University - Purdue University Indianapolis, IN, United States

Published in ASME. ASME J. Risk Uncertainty Part B, doi: <https://doi.org/10.1115/1.4054171>

Authors' contribution: H.W. and X.D. designed the study and contributed to the writing of the manuscript. H.W. detailed methodology and the code.

Reliability can be predicted by a limit-state function, which may vary with time and space. This work extends the envelope method for a time-dependent limit-state function to a time- and space-dependent limit-state function. The proposed method uses the envelope function of time- and space-dependent limit-state function. It at first searches for the most probable point (MPP) of the envelope function using the sequential efficient global optimization in the domain of the space and time under consideration. Then the envelope function is approximated by a quadratic function at the MPP, for which analytic gradient and Hessian matrix of the envelope function are derived. Subsequently, the second-order saddlepoint approximation method is employed to estimate the probability of failure. Three examples demonstrate the effectiveness of the proposed method. The method can efficiently produce an accurate reliability prediction when the MPP is within the domain of the space and time under consideration.

5.1 Background

Reliability is the probability that a product or component performs its intended function under a specific condition. Reliability can be predicted by a physics-based approach if the state of a component can be predicted by a physical model, which is called a limit-state function. A physics-based reliability problem may be time- and space-independent, time-dependent, space-dependent, or time- and space-dependent.

A time- and space-independent reliability problem involves limit-state functions that do not vary with respect to time and space, and its inputs might involve random variables or random fields at a specific point in space. Many methods are available for this problem. Monte Carlo simulation (MCS) is one method. It is accurate when the sample size is sufficiently large, but it is computationally expensive [156, 157]. When failure probabilities are small in reliability analysis of engineering systems, subset simulation is an alternative method [27]. Importance sampling methods could be used to reduce the computational cost because they generate more samples in the failure region [4].

The first-order reliability method (FORM) [8, 158] is much more efficient because it linearizes the limit-state function. FORM can produce satisfactory accuracy for many engineering applications, but it is less accurate for highly nonlinear limit-state functions. The second-order reliability method (SORM) [13, 15] can produce higher accuracy than FORM due to the second-order approximation but is less efficient than FORM. The accuracy of SORM may be further improved by the second-order saddlepoint approximation (SOSPA) since the saddlepoint approximation may yield a more accurate probability estimation, especially in the tail area of distribution [14, 16, 159]. Reliability can also be predicted by regressions, such as the Gaussian process method [37, 87, 160, 161] and the support vector machines method [31, 162, 163].

The limit-state function may vary over time, which results in a time-dependent reliability problem. The input of the limit-state function may involve time and random processes. Rice's formula-based methods are commonly used [46, 130, 132, 164]. They are in general more efficient than other methods but may lead to large errors if up-crossing events are strongly dependent [21]. Regression methods can also be used and may achieve higher accuracy if the surrogate model is well trained [29, 165-167]. Converting a time-dependent problem into a time-independent counterpart is possible by using the extreme value of the limit-state function [32, 126, 137, 168]. The methods include the envelope function method [168], extreme value response method [137], and the composite limit-state function method [126],

The most general problems are those with time- and space-dependent limit-state functions, which may take input of stochastic processes, random fields, and tempo-spatial variables [31-36]. Hu and Mahadevan developed a surrogate modeling approach for reliability analysis of a multidisciplinary system [169]. Shi et al. presented a method for the moment estimation of the extreme response using two strategies [170]. One strategy is combining the sparse grid technique

and the fourth-moment method while the other one is combining the dimensional reduction with the maximum entropy method. Shi and Lu proposed an active learning Kriging method [53]. Wei and Du combined FORM and SORM for the time- and space-dependent reliability analysis [54, 171]. Despite the progress, there is still a need to improve the accuracy and efficiency of time- and space-dependent reliability prediction.

The proposed method is an extension of the time-dependent methodology in Ref. [168]. This method converts a time- and space-dependent problem into a time- and space-independent problem by using the envelope function or the extreme value of a limit-state function over the time and the space span. The MPP of the envelope function is found by combining the sequential efficient global optimization (EGO) with FORM. Then the quadratic envelope function is approximated at the MPP with its gradient and Hessian matrix. Then the probability of failure is estimated by the second-order saddlepoint approximation method.

The rest of the paper is organized as follows. Section 2 reviews FORM for time- and space-dependent reliability. Section 3 discusses the proposed method. Section 4 presents three examples, and Section 5 provides the conclusions and future work.

5.2 Review Fundamental Methodologies

5.2.1 Problem Statement

In this work, we consider a limit-state function given by

$$y = g(\mathbf{X}, \mathbf{z}) \quad (1)$$

in which $\mathbf{X} = [X_1, \dots, X_n]^T$ are n input random variables. The time variable is $z_1 \in [\underline{z}_1, \bar{z}_1]$, and the spatial variables are z_k with the following ranges: $z_k \in [\underline{z}_k, \bar{z}_k]$, ($k = 2, \dots, m$). Then, $\mathbf{z} = [z_1, z_2, \dots, z_m]^T$ is a vector of the temporal/spatial variables bounded on $\mathbf{\Omega} = [\underline{z}_k, \bar{z}_k]$.

The reliability over the temporal and spatial domain is defined by

$$R = \Pr\{g(\mathbf{X}, \mathbf{z}) > 0, \forall \mathbf{z} \in \mathbf{\Omega}\} \quad (2)$$

where \forall means “for all”. The associated probability of failure is given by

$$p_f = \Pr\{g(\mathbf{X}, \mathbf{z}) \leq 0, \exists \mathbf{z} \in \mathbf{\Omega}\} \quad (3)$$

where \exists means “there exists at least one”. Note that the spatio-temporal domain in Eq. (1) is rectangular. In reality, the domain may be non-rectangular. This study focuses on only a rectangular domain.

5.2.2 First Order Reliability Method (FORM)

FORM is the commonly used reliability method. It is originally intended for time- and space-independent reliability analysis. In this work, we at first review the time- and space-independent reliability problem with the FORM method, then the discussion furtherly can be extended to the time- and space-dependent reliability problem.

5.2.3 Time- and Space-independent Reliability Problem

The time- and space-independent reliability is defined by

$$R = \Pr\{y = g(\mathbf{X}) > 0\} \quad (4)$$

where y is response and \mathbf{X} is a random vector. FORM at first searches for the most probable point (MPP) in the standard normal space. At first, random variables \mathbf{X} are transformed into standard and independent normal variables \mathbf{U} [38]. Then, the minimum distance from the origin to the limit-state surface $g(\mathbf{X}) = 0$ is identified. The distance is the reliability index β . The minimum distance point is called the MPP. The model for searching for the MPP is given by

$$\begin{cases} \min \sqrt{\mathbf{u}^T \mathbf{u}} \\ \text{s. t. } g(\mathbf{X}) = g(\mathbf{T}(\mathbf{u})) = 0 \end{cases} \quad (5)$$

where $\mathbf{T}(\cdot)$ is an operator of the transformation from \mathbf{U} to \mathbf{X} .

$$\beta = \|\mathbf{u}\| = \sqrt{u_1^2 + u_2^2 + \dots + u_n^2} \quad (6)$$

The solution from Eq. (5) is the MPP \mathbf{u}_{MPP} .

Lastly, the reliability is calculated by

$$R = \Pr\{y = g(\mathbf{X}) > 0\} \approx \Phi(\beta) = \Phi(\|\mathbf{u}_{\text{MPP}}\|) \quad (7)$$

where $\Phi(\cdot)$ is the cumulative distribution function (CDF) of the standard normal distribution.

5.2.4 Time-Dependent Reliability Problem

When it comes to the limit-state function that varies over time, FORM can still be used to find the MPP. The MPP \mathbf{u}_{MPP} at the time instant z_1 is identified by the following model:

$$\begin{cases} \min \|\mathbf{u}\| \\ \text{s. t. } g(\mathbf{X}, z_1) = g(\mathbf{T}(\mathbf{u}), z_1) = 0 \end{cases} \quad (8)$$

The limit-state function is linearized at $\mathbf{u}_{\text{MPP}}(z_1)$ by

$$g(\mathbf{T}(\mathbf{u}), z_1) \approx g(\mathbf{u}_{\text{MPP}}, z_1) + \sum_{i=1}^N \left. \frac{\partial g}{\partial U_i} \right|_{\mathbf{u}_{\text{MPP}}} (U_i - u_{\text{MPP}i}) = \nabla g \times (\mathbf{U} - \mathbf{u}_{\text{MPP}}) \quad (9)$$

where $\nabla g = \left[\left. \frac{\partial g}{\partial U_1} \right|_{\mathbf{u}_{\text{MPP}}}, \dots, \left. \frac{\partial g}{\partial U_n} \right|_{\mathbf{u}_{\text{MPP}}} \right]$ is the gradient, and the probability of failure is

computed by

$$p_f = \Pr(g(\mathbf{X}, z_1) \leq 0, z_1 \in [z_1, \bar{z}_1]) \approx \Pr(\beta(z_1) + \boldsymbol{\alpha}(z_1)\mathbf{U} \leq 0, z_1 \in [z_1, \bar{z}_1]) \quad (10)$$

where $\beta(z_1)$ is the time-dependent reliability index, given by

$$\beta(z_1) = \|\mathbf{u}_{\text{MPP}}\| \quad (11)$$

and $\boldsymbol{\alpha}(z_1)$ is the time-dependent unit gradient vector given by

$$\boldsymbol{\alpha}(z_1) = \frac{\nabla g(z_1)}{\|\nabla g(z_1)\|} = [\alpha_1(z_1), \alpha_2(z_1), \dots, \alpha_n(z_1)] \quad (12)$$

As indicated in Eq. (9), the limit-state function $g(\mathbf{X}, z_1)$ is approximated as a linear combination of standard normal random variables. Many methodologies are available for solving for the probability of failures, such as Rice's formula-based methods and metamodeling-based methods.

5.3 Envelope Method for Time- and Space-dependent Problem

The envelope function is tangent to all the instantaneous limit-state functions with respect to time and space. The envelope function of a limit-state function is in general nonlinear and can be approximated as a quadratic function at its MPP by the second-order approximation method.

It is known that the MPP of the envelope function is the worst-case MPP of the limit-state function [37]. In other words, the MPP is the closest point between the origin and all the instantaneous limit-state functions. The MPP of the envelope function can be efficiently found by the sequential single-loop method [37]. Consequently, the gradient of the envelope function is

consistent with the gradient of the worst-case limit-state functions at MPP [37]. However, as the curvature of the envelope function may not be the curvature of the worst-case limit-state function, the analytical Hessian matrix of the envelope function is derived. In this paper, we extend our work in a more general situation. The second derivative of the envelope function with respect to random variables and multiple temporal/spatial variables is analytically derived. As a result, the Hessian matrix of the envelope function can be accurately obtained.

Different from the existing method [37], the new method also covers problems where a single call of a limit-state function returns a complete response with respect to time and space. Hence the method can be used for the following two cases.

Case 1: The input includes a realization of random variables \mathbf{X} , as well as a time instance/spatial location \mathbf{z} , and the output is a single response. This case requires calling the limit-state function repeatedly so that the worst-case response can be found.

Case 2: The input includes a realization of random variables \mathbf{X} and the temporal/spatial domain Ω of \mathbf{z} . Calling the limit-function returns a complete time- and space-dependent response with respect to \mathbf{z} in Ω . In this case, the output is a hypersurface of the response $y(\mathbf{z})$. For example, if we call a computational fluid dynamics (CFD) simulation, we obtain the 4-D pressure and velocity fields with respect to time and space. Since we know $y(\mathbf{z})$, the minimum value $\min_{\mathbf{z} \in \Omega} y(\mathbf{z})$ is also known.

In Sec. 3.1, we focus our discussions on Case 1 for limit-state function $y = g(\mathbf{X}, \mathbf{z})$. Since Case 2 is much easier than Case 1, we briefly discuss it at the end of Sec. 3.1. We then extend the method into a general problem with input random fields in Sec. 3.2.

5.3.1 Problems with Random Variables, and Temporal/Spatial Parameters

We now discuss Case 1 with the limit-state function is given in Eq. (1). For this case we need to search for the worst-case MPP.

The time- and space-dependent probability of failure in the time span $[\underline{z}_1, \bar{z}_1]$ and the space span $[\underline{z}_k, \bar{z}_k]$ can be evaluated by the extreme value of the limit-state function.

$$p_f = \Pr(g(\mathbf{X}, \mathbf{z}) < 0, \exists \mathbf{z} \in \Omega) = \Pr\left(\min_{\mathbf{z} \in \Omega} g(\mathbf{X}, \mathbf{z}) < 0\right) \quad (13)$$

Eq. (13) indicates that a failure occurs if the minimum response is negative. The function of the extreme response is equivalent to the envelope function or the composite limit-state function [29], which is given by

$$G(\mathbf{X}) = \min_{\mathbf{z} \in \Omega} g(\mathbf{X}, \mathbf{z}) = g(\mathbf{X}, \tilde{\mathbf{z}}) \quad (14)$$

where the envelope function $G(\mathbf{X})$ is the global minimum of $g(\mathbf{X}, \mathbf{z})$ with respect to \mathbf{z} , and the global minimum occurs at $\tilde{\mathbf{z}}$.

If FORM is used to linearize $G(\mathbf{X})$, the MPP is obtained by

$$\begin{cases} \min \sqrt{\mathbf{u}^T \mathbf{u}} \\ \text{s. t. } \min_{\mathbf{z} \in \Omega} g(\mathbf{T}(\mathbf{u}), \mathbf{z}) = 0 \end{cases} \quad (15)$$

Eq. (15) requires a double loop optimization process because minimization appears in both the objective and constraint functions. The inner loop is for the minimum value of $g(\mathbf{T}(\mathbf{u}), \mathbf{z})$ relative to \mathbf{z} while the outer loop is the MPP search relative to \mathbf{u} . In this work, we decouple the double loop into sequential single loops.

The first loop is FORM analysis, the MPP $\mathbf{u}_{\text{MPP}}^{(1)}$ at the initial $\tilde{\mathbf{z}}^{(0)} = [z_1^0, z_2^0, \dots, z_m^0]$ is obtained by

$$\begin{cases} \min \sqrt{\mathbf{u}^T \mathbf{u}} \\ \text{s. t. } g(\mathbf{T}(\mathbf{u}), \mathbf{z}_0) = 0 \end{cases} \quad (16)$$

Then \mathbf{z} is determined by fixing the random variables on its realization $\mathbf{u}_{\text{MPP}}^{(1)}$, and \mathbf{z} is denoted by $\tilde{\mathbf{z}}^{(1)}$, which is given by

$$\tilde{\mathbf{z}}^{(1)} = \underset{\mathbf{z} \in \Omega}{\operatorname{argmin}} g(\mathbf{T}(\mathbf{u}_{\text{MPP}}^{(1)}), \mathbf{z}) \quad (17)$$

In the next loop, the new MPP $\mathbf{u}_{\text{MPP}}^{(2)}$ is located at point $\tilde{\mathbf{z}}^{(1)}$ using Eq. (16). And then \mathbf{z} is updated to $\tilde{\mathbf{z}}^{(2)}$.

$$\tilde{\mathbf{z}}^{(2)} = \underset{\mathbf{z} \in \Omega}{\operatorname{argmin}} g(\mathbf{T}(\mathbf{u}_{\text{MPP}}^{(2)}), \mathbf{z}) \quad (18)$$

The above process is repeated until convergence, and the MPP is found. It is the worst-case MPP of the limit-state function with respect to \mathbf{z} .

The global minimum value of $G(\mathbf{X})$ occurs at $\tilde{\mathbf{z}}^{(1)} = [\tilde{z}_1^{(1)}, \tilde{z}_2^{(1)}, \dots, \tilde{z}_m^{(1)}]$, which is given by

$$\tilde{\mathbf{z}}^{(1)} = \underset{\mathbf{z} \in \Omega}{\operatorname{argmin}} g(\mathbf{T}(\mathbf{u}_{\text{MPP}}), \mathbf{z}) \quad (19)$$

Note that finding the optimal point is still in the sequential loops. There are many methods to solve the optimal point $\tilde{\mathbf{z}}^{(1)}$ corresponding to the global minimum value of $G(\mathbf{X})$. The first partial derivative of the limit-state function with respect to z_k at MPP is as below:

$$\begin{cases} \frac{\partial g(T(\mathbf{u}_{\text{MPP}}), z_1, z_2, \dots, z_m)}{\partial z_1} = 0 \\ \vdots \\ \frac{\partial g(T(\mathbf{u}_{\text{MPP}}), z_1, z_2, \dots, z_m)}{\partial z_m} = 0 \end{cases} \quad (20)$$

The optimal point $\tilde{\mathbf{z}}^{(1)} = [\tilde{z}_1^{(1)}, \tilde{z}_2^{(1)}, \dots, \tilde{z}_m^{(1)}]$ can be obtained by solving Eq. (20).

We use efficient global optimization (EGO) to find the MPP. EGO has been widely used in various areas because it can efficiently search for the global optimum [39]. Suppose we have called the limit-state function at several initial training points of \mathbf{z}^{in} and the number of initial training points is n_{in} , which denote by as follows

$$\mathbf{z}^{in} = \begin{bmatrix} z_1^1 & \dots & z_m^1 \\ \vdots & \ddots & \vdots \\ z_1^{n_{in}} & \dots & z_m^{n_{in}} \end{bmatrix}$$

and the associated responses are $\mathbf{y}^{in} = [g(T(\mathbf{u}^*), \mathbf{z}^1), g(T(\mathbf{u}^*), \mathbf{z}^2), \dots, g(T(\mathbf{u}^*), \mathbf{z}^{n_{in}})]^T$. An initial function is fitted from $(\mathbf{z}^{in}, \mathbf{y}^{in})$ by the following surrogate model [39]:

$$\hat{y} = g(\mathbf{z}) = g(T(\mathbf{u}^*), \mathbf{z}) = F(\mathbf{z})^T \boldsymbol{\gamma} + e(\mathbf{z}) \quad (21)$$

where $F(\mathbf{z})^T \boldsymbol{\gamma}$ is a deterministic term, $e(\mathbf{z})$ is a vector of regression functions, $\boldsymbol{\gamma}$ is a vector of regression coefficients, and $e(\mathbf{z})$ is a stationary Gaussian process with zero mean and a covariance given by

$$\text{Cov}(e(\mathbf{z}_1), e(\mathbf{z}_2)) = \sigma_e^2 R(\mathbf{z}_1, \mathbf{z}_2) \quad (22)$$

where σ_e^2 is process variance, and $R(\cdot, \cdot)$ is the correlation function.

The output of the surrogate model is a Gaussian random variable following

$$\hat{y} = g(\mathbf{z}) \sim N(\mu(\mathbf{z}), \sigma^2(\mathbf{z})) \quad (23)$$

where $\mu(\mathbf{z})$ and $\sigma(\mathbf{z})$ are the mean and standard deviation of \hat{y} , respectively.

The initial model is likely not accurate. The expected improvement (EI) metric [39] is used to identify new training points that will be added to refine the model. The improvement is defined by

$$I = \max(y^* - y, 0) \quad (24)$$

where $y^* = \min_{i=1,2,\dots,n_{in}} g(\mathbf{z}^i)$ is the minimum from the sampling training points.

EI is computed by

$$\text{EI}(\mathbf{z}) = \text{E}[\max(y^* - y, 0)] = (y^* - \mu(\mathbf{z}))\Phi\left(\frac{y^* - \mu(\mathbf{z})}{\sigma(\mathbf{z})}\right) + \sigma(\mathbf{z})\phi\left(\frac{y^* - \mu(\mathbf{z})}{\sigma(\mathbf{z})}\right) \quad (25)$$

where $\phi(\cdot)$ is the probability density function (PDF).

A new training point \mathbf{z}_{new} is identified by minimizing the expected improvement.

$$\mathbf{z}_{new} = \underset{\mathbf{z}}{\text{argmin}} \text{EI}(\mathbf{z}) \quad (26)$$

By combining sequential strategy with EGO, \mathbf{u}_{MPP} of envelope function $G(\mathbf{X})$ can be obtained efficiently by solving Eq. (15). The probability of failure with FORM is estimated by

$$p_f = \Pr(g(\mathbf{X}, \mathbf{z}) < 0, \exists \mathbf{z} \in \Omega) \approx \Pr(G(\mathbf{X}) < 0) = \Phi(-\beta) \quad (27)$$

where $\beta = \|\mathbf{u}_{MPP}\|$ is the first-order reliability index.

In general, the envelope function is nonlinear, and FORM may not be accurate enough. Thus, a second-order method is preferred, and it uses the envelope theorem to obtain the second-order information of the extreme limit-state function. Then SOSPA is used to estimate the probability of failure.

The envelope function is generally nonlinear, and we therefore approximate it as a quadratic function, instead of a linear function in FORM. As a result, we need the gradient ∇G and Hessian matrix \mathbf{H} at the MPP of the envelope function. The quadratic function is formed as follows [12]:

$$G(\mathbf{U}) = a + \mathbf{b}^T \mathbf{U} + \mathbf{U}^T \mathbf{C} \mathbf{U} \quad (28)$$

where

$$\begin{cases} a = \frac{1}{2} (\mathbf{u}_{MPP})^T \mathbf{H} \mathbf{u}_{MPP} - \nabla G(\mathbf{u}_{MPP})^T \mathbf{u}_{MPP} \\ \mathbf{b} = \nabla G(\mathbf{u}_{MPP}) - \mathbf{H} \mathbf{u}_{MPP} = (\tilde{b}_1, \tilde{b}_2, \dots, \tilde{b}_n) \\ \mathbf{C} = \frac{1}{2} \mathbf{H} = \text{diag}(\tilde{c}_1, \tilde{c}_2, \dots, \tilde{c}_n) \end{cases} \quad (29)$$

$\nabla G(\mathbf{u}^*) = \left[\frac{\partial G}{\partial U_1} \Big|_{\mathbf{u}_{MPP}}, \dots, \frac{\partial G}{\partial U_n} \Big|_{\mathbf{u}_{MPP}} \right]^T$ is the gradient of the envelope function. \mathbf{H} is the Hessian

matrix shown below.

$$\mathbf{H} = \begin{bmatrix} \frac{\partial^2 G}{\partial U_1^2} & \cdots & \frac{\partial^2 G}{\partial U_1 \partial U_n} \\ \vdots & \ddots & \vdots \\ \frac{\partial^2 G}{\partial U_n \partial U_1} & \cdots & \frac{\partial^2 G}{\partial U_n^2} \end{bmatrix}_{\mathbf{u}_{MPP}} \quad (30)$$

The envelope function $G(\mathbf{X})$ at \mathbf{u}_{MPP} is given by

$$G(\mathbf{U}) = \min_{\mathbf{z} \in \Omega} g(\mathbf{U}, \mathbf{z}) = g(\mathbf{U}, \tilde{\mathbf{z}})|_{\mathbf{u}_{\text{MPP}}} \quad (31)$$

where $\tilde{\mathbf{z}} = [\tilde{z}_1, \dots, \tilde{z}_m]$ is the optimal point where the global minimum value of function $g(\mathbf{U}, \mathbf{z})$ occurs, and it is found by

$$\frac{\partial g(\mathbf{U}, \mathbf{z})}{\partial z_1} = \frac{\partial g(\mathbf{U}, \mathbf{z})}{\partial z_2} = \dots = \frac{\partial g(\mathbf{U}, \mathbf{z})}{\partial z_m} = 0 \quad (32)$$

The envelope function satisfies the following equation:

$$\begin{cases} \dot{g}(\mathbf{U}, \tilde{z}_1, z_2, \dots, z_m) = 0 \\ \vdots \\ \dot{g}(\mathbf{U}, z_1, z_2, \dots, \tilde{z}_m) = 0 \end{cases} \quad (33)$$

where \dot{g} is the derivative of g with respect to z_i .

Next, the first derivative of $G(\mathbf{U})$ with respect to a random input variable U_i at \mathbf{u}_{MPP} is

$$\frac{\partial G}{\partial U_i} = \frac{\partial g}{\partial U_i} + \frac{\partial g}{\partial \tilde{z}_1} \frac{\partial \tilde{z}_1}{\partial U_i} + \frac{\partial g}{\partial \tilde{z}_2} \frac{\partial \tilde{z}_2}{\partial U_i} + \dots + \frac{\partial g}{\partial \tilde{z}_m} \frac{\partial \tilde{z}_m}{\partial U_i} \quad (34)$$

By plugging Eq. (33) into Eq. (34), it becomes

$$\frac{\partial G}{\partial U_i} = \frac{\partial g}{\partial U_i} \quad (35)$$

Eq. (35) indicates that the gradient of the envelope function ∇G is equal to the gradient of the limit-state function ∇g at the MPP. Subsequently, the second derivative of $G(\mathbf{U})$ with respect to the input random variables U_j at \mathbf{u}^* is

$$\frac{\partial^2 G}{\partial U_i \partial U_j} = \frac{\partial}{\partial U_j} \left(\frac{\partial G}{\partial U_i} \right) = \frac{\partial}{\partial U_j} \left(\frac{\partial g}{\partial U_i} \right) = \frac{\partial^2 g}{\partial U_i \partial U_j} + \frac{\partial^2 g}{\partial U_i \partial \tilde{z}_1} \frac{\partial \tilde{z}_1}{\partial U_j} + \dots + \frac{\partial^2 g}{\partial U_i \partial \tilde{z}_m} \frac{\partial \tilde{z}_m}{\partial U_j} \quad (36)$$

Take the derivative of Eq. (32) with respect to U_j , and it is given by

$$\frac{\partial \dot{g}}{\partial U_j} + \frac{\partial \dot{g}}{\partial \tilde{z}_k} \frac{\partial \tilde{z}_k}{\partial U_j} = 0 \quad (37)$$

$$\frac{\partial \tilde{z}_k}{\partial U_j} = - \frac{\partial \dot{g} / \partial \tilde{z}_k}{\partial \dot{g} / \partial U_j} = - \frac{\partial^2 g}{\partial \tilde{z}_k \partial U_j} / \frac{\partial^2 g}{\partial \tilde{z}_k^2} \quad (38)$$

The Hessian matrix \mathbf{H} with respect to random variables and multiple temporal/spatial variables is obtained by plugging Eq. (38) into Eq. (36) at $\mathbf{u}_{\text{MPP}}, \tilde{z}_k$.

$$\frac{\partial^2 G}{\partial U_i \partial U_j} \Big|_{\mathbf{u}^*, \tilde{z}_k} = \frac{\partial^2 g}{\partial U_i \partial U_j} - \sum_{k=1}^m \frac{\partial^2 g}{\partial U_i \partial \tilde{z}_k} \frac{\partial^2 g}{\partial U_j \partial \tilde{z}_k} / \frac{\partial^2 g}{\partial \tilde{z}_k^2} \quad (39)$$

The forward finite difference method with step size $\delta = \max(|u|/1000, \epsilon)$ and $\epsilon = 10^{-4}$ is employed to calculate the derivations in Eq. (39).

Once the envelope function is approximated by a quadratic function, we use the second order saddlepoint approximation to estimate the probability of failure. The reason we use saddlepoint approximation is due to its high accuracy in the tail area of a distribution; a failure usually occurs in a tail area.

Eq. (28) can be written as the sum of quadratic functions of different standard normal variables

$$G(\mathbf{U}) = \sum_{i=1}^n Q_i(\tilde{\mathbf{U}}) = \sum_{i=1}^n (\tilde{a}_i + \tilde{b}_i \tilde{U}_i + \tilde{c}_i \tilde{U}_i^2) \quad (40)$$

The cumulant generating function (CGF) of $G(\mathbf{U})$ is given by

$$K_Q(t_s) = \sum_{i=1}^n K_{Q_i}(t_s) \quad (41)$$

After the CGF $K_Q(t_s)$ is obtained, it is straightforward to find the PDF of the limit-state function, and this needs to solve the saddlepoint t_s , which is found by solving the following equation:

$$K_Q'(t_s) = 0 \quad (42)$$

where $K_Q'(t_s)$ is the first derivative of $K_Q(t_s)$. The details of the implementation of SOSPA refer to Ref. [14]. According to Lugannani and Rice's formula,

Then the probability of failure is evaluated by

$$p_f \approx \Pr(G(\mathbf{U}) < 0) = \Phi(w) + \phi(w) \left(\frac{1}{w} - \frac{1}{v} \right) \quad (43)$$

where

$$w = \text{sgn}(t_s) \{2[-K_Q(t_s)]\}^{\frac{1}{2}} \quad (44)$$

$$v = t_s [K_Q''(t_s)]^{\frac{1}{2}} \quad (45)$$

in which $\text{sgn}(t_s) = +1, -1$, or 0 , depending on whether t_s is positive, negative, or zero. $K_Q''(t_s)$ is the second derivative of $K_Q(t_s)$ concerning t_s . Since the above method uses SOSPA and envelope theorem, we denote this method as SOSPA/ENV.

Case 2: Calling the limit-function returns a complete time- and space-dependent response

In this case, the output is a hypersurface of the response $y(\mathbf{z})$. The complete response $y(\mathbf{z})$ is available, so the minimum value $\min_{\mathbf{z} \in \Omega} y(\mathbf{z})$ is also known. We do not need to use the sequential single loops in case 1. Thus, the MPP in Eq. (15) can be obtained from the following model:

$$\begin{cases} \min \sqrt{\mathbf{u}^T \mathbf{u}} \\ \text{s. t. } \min_{\mathbf{z} \in \Omega} y(\mathbf{z}) = 0 \end{cases} \quad (46)$$

where $\min_{\mathbf{z} \in \Omega} y(\mathbf{z})$ is a function of \mathbf{u} and is obtained by calling the limit-state function once at \mathbf{u} , where \mathbf{u} is the vector of independent normal variables transformed from \mathbf{X} . We just need a single-loop MPP search, which is more efficient than the sequential loop approach.

The model in Eq. (46) may have multiple MPPs [40]. The accuracy of the reliability prediction may be poor if only one MPP is used and if other MPPs also have significant contributions. There are three strategies to deal with multiple MPPs. The first strategy is to repeat the standard MPP search with different starting points and find different solutions if they exist. The second strategy is to use an optimization algorithm that can find multiple local optima. The methods include genetic algorithm [40] and particle swarm optimization [41]. The third strategy is to employ methodologies specifically designed for multiple MPP search [29,42]. Although there is no guarantee to find all possible MPPs, these strategies can significantly increase the chance of finding multiple MPPs [29,40-42]. Once all potential MPPs are identified, the corresponding limit-state surfaces are linearized at these points as

$$Q_i(\mathbf{U}) = -\nabla G(\mathbf{u}_{\text{MPP}i})^T \mathbf{u}_{\text{MPP}i} + \nabla G(\mathbf{u}_{\text{MPP}i}) \mathbf{U} \quad (47)$$

where $i = 1, 2, \dots, m$, in which m is the number of MPPs. The reliability is calculated as the reliability of a series system.

$$R = \Pr \left(\bigcap_{i=1}^m Q_i(\mathbf{U}) > 0 \right) = \Pr \left(\bigcap_{i=1}^m -\nabla G(\mathbf{u}_{\text{MPP}i})^T \mathbf{u}_{\text{MPP}i} + \nabla G(\mathbf{u}_{\text{MPP}i}) \mathbf{U} > 0 \right) \quad (48)$$

Since $Q_i(\mathbf{U})$ follows a normal distribution, all the responses at their MPPs follow a multivariate normal distribution, whose joint probability density is integrated in the safe region, resulting the reliability. The second order method is used for higher accuracy. The method still uses a multivariate normal distribution, whose mean vector is obtained by the second order saddlepoint approximation and whose covariance matrix is estimated by the first order approximation [12].

5.3.2 Problems with Random Variables, Random Fields, and Temporal/Spatial Parameters

We have discussed limit-state functions with random variables \mathbf{X} and temporal/spatial variables \mathbf{z} . In this subsection, we discuss how to extend the method to limit-state functions with random variable \mathbf{X} , random fields $\mathcal{F}(\mathbf{z})$ and temporal/spatial variables \mathbf{z} . A limit-state function is given by $y(\mathbf{z}) = \mathbf{g}(\mathbf{X}, \mathcal{F}(\mathbf{z}), \mathbf{z})$. The time- and space-dependent probability of failure is calculated by

$$p_f = \Pr(g(\mathbf{X}, \mathcal{F}(\mathbf{z}), \mathbf{z}) < 0, \exists \mathbf{z} \in \Omega) = \Pr\left(\min_{\mathbf{z} \in \Omega} y(\mathbf{z}) < 0\right) \quad (49)$$

Eq. (49) indicates that failure happens when the minimum value of the limit-state function $g(\mathbf{X}, \mathcal{F}(\mathbf{z}), \mathbf{z})$ is negative. There are still two cases: a single call of a limit-state function does not return a time- and space-dependent response and a single call of a limit-state function returns a complete response with respect to time and space.

Case 1 requires calling the limit-state function repeatedly to obtain the worst-case response in Ω . We need to convert random fields into time- and space-dependent random fields so that the proposed method can be used. The expansion optimal linear estimation method (EOLE) [40] can be used to convert the random fields $\mathcal{F}(\mathbf{z})$ into independent standard Gaussian random variables $\boldsymbol{\xi} = (\xi_1, \xi_2, \dots, \xi_r)$, where r is the dimension of $\boldsymbol{\xi}$. Take a two-dimensional random field $\mathcal{F}(\mathbf{z})$, where $\mathbf{z} = (z_1, z_2)$, as an example. z_1 and z_2 are discretized into n_{z_1} and n_{z_2} points, respectively. The autocorrelation coefficient matrix is given by

$$\boldsymbol{\Sigma} = [\rho(\mathbf{z}_i, \mathbf{z}_j)]_{n_{z_1}n_{z_2} \times n_{z_1}n_{z_2}} \quad (50)$$

where $\rho(\mathbf{z}_i, \mathbf{z}_j)$ is the correlation between two points \mathbf{z}_i ($i = 1, 2, \dots, n_{z_1}n_{z_2}$) and \mathbf{z}_j ($j = 1, 2, \dots, n_{z_1}n_{z_2}$) in the domain of $\mathcal{F}(\mathbf{z})$. Then $\mathcal{F}(\mathbf{z})$ is expanded by

$$\mathcal{F}(\boldsymbol{\xi}, \mathbf{z}) \approx \mu(\mathbf{z}) + \sigma(\mathbf{z}) \sum_{k=1}^r \frac{\xi_k}{\sqrt{\lambda_k}} \boldsymbol{\phi}_k^T \boldsymbol{\Sigma}(:, \mathbf{z}), k = 1, 2, \dots, r \quad (51)$$

where $\mu(\mathbf{z})$ is the mean of $\mathcal{F}(\mathbf{z})$, and $\sigma(\mathbf{z})$ is the standard deviation of $\mathcal{F}(\mathbf{z})$. ξ_k ($k = 1, 2, \dots, r$) are independent standard normal variables, $\boldsymbol{\lambda} = (\lambda_1, \lambda_2, \dots, \lambda_r)$ is the eigenvalue vector, and $\boldsymbol{\phi}_1, \boldsymbol{\phi}_2, \dots, \boldsymbol{\phi}_r$ are eigenvectors of $\boldsymbol{\Sigma}$. Note that r is determined as the smallest integer that meets the following criterion:

$$\frac{\sum_{j=1}^r \lambda_k}{\sum_{j=1}^{n_{z_1}n_{z_2}} \lambda_k} \geq \eta \quad (52)$$

where η is a hyperparameter determining the accuracy of the expansion. It takes a value close to, but not larger than 1. The smaller is η , the less accurate is the expansion. If $\eta = 1$, the expansion is exact at the points of discretization. Normally, η is set to 0.9999.

Then the limit-state function becomes $y = g(\tilde{\mathbf{X}}, \mathbf{z})$, where $\tilde{\mathbf{X}} = (\mathbf{X}, \boldsymbol{\xi})$. It is a function given in Eq. (1) and the proposed method in Sec. 3.1 of case 1 can be used.

For Case 2, a single call of a limit-state function returns a complete response with respect to time and space. After random fields are expanded with respect to random variables, the problem becomes the one discussed in Sec. 3.1 for Case 2. The same method in Sec. 3.1 can then be used.

5.3.3 Implementation

The detailed steps of solving time- and space-dependent reliability problems using SOSPA are summarized below.

Step 1: Transform random variables \mathbf{X} into \mathbf{U} in the standard normal space.

Step 2: Set $k = 1$. Generate a random point $\mathbf{z} \in \Omega$ as the initial optimal point $\tilde{\mathbf{z}}^{(0)}$ and use a unit vector as the initial MPP $\mathbf{u}_{\text{MPP}}^{(1)} = \mathbf{u}_0$.

Step 3: Perform the MPP search at the point $\tilde{\mathbf{z}}^{(k-1)}$, and obtain the MPP $\mathbf{u}_{\text{MPP}}^{(k)}$ and the corresponding $\beta^{(k)}$ by solving the following optimization model:

$$\begin{cases} \min \sqrt{\mathbf{u}^T \mathbf{u}} \\ \text{s. t. } g(\mathbf{T}(\mathbf{u}), \tilde{\mathbf{z}}^{(k-1)}) = 0 \end{cases}$$

Step 4: Determine the optimal point $\tilde{\mathbf{z}}^{(k)}$ implementing EGO method at $\mathbf{u}_{\text{MPP}}^{(k)}$. The optimal point $\tilde{\mathbf{z}}^{(k)}$ makes the limit-state function minimized. The initial number of training points to determine the time and spatial parameters is $n_{in}=2$.

$$\tilde{\mathbf{z}}^{(k)} = \underset{\mathbf{z} \in \Omega}{\operatorname{argmin}} g\left(\mathbf{T}\left(\mathbf{u}_{\text{MPP}}^{(k)}\right), \mathbf{z}\right)$$

Step 5: Repeat step 3 and step 4 until convergence. The convergence criterion is defined as

$$|\beta^{(k)} - \beta^{(k-1)}| \leq \varepsilon$$

The tolerance ε can take a small positive value, for example, 10^{-4} . If $|\beta^{(k)} - \beta^{(k-1)}| \leq 10^{-4}$, terminate the iteration. Otherwise, set $k = k + 1$, and return to step 3. Note that the method of a single-loop MPP search can be used if calling the limit-state function returns a complete time- and space-dependent response

Step 6: Calculate the gradient ∇G and Hessian matrix \mathbf{H} of the envelope function.

Step 7: Calculate the probability of failure using SOSPA/ENV from the above information $\mathbf{u}_{\text{MPP}}^{(k)}$, gradient ∇G , and Hessian matrix \mathbf{H} .

5.4 Examples

In this section, three examples are used to demonstrate the proposed method. Example 1 is a mathematical problem that is used to show the details of the proposed method. The remaining examples are engineering problems. MCS is employed to provide accurate solutions for the accuracy comparison. SOSPA/ENV is compared with the FORM-based envelope method (FORM/ENV). The errors of SOSPA/ENV and FORM/ENV are calculated by

$$\varepsilon = \frac{|p_f - p_f^{\text{MCS}}|}{p_f^{\text{MCS}}} \times 100\% \quad (53)$$

where p_f is the result from SOSPA/ENV or FORM/ENV, and p_f^{MCS} is the result from MCS. We also use the number of function calls as a measure of efficiency.

5.4.1 Example 1: A Math Problem

This example is a math problem, which belongs to Case 1 without any random field input. The limit-state function $g(\mathbf{X}, s, t)$ regarding random variables and explicit temporal/spatial parameter is defined by

$$g(\mathbf{X}, s, t) = X_1^2 X_2 - 5X_1 t + (X_2 + 1)t^2 - 2X_2 s + X_1 s^2 - 8 \quad (54)$$

where $\mathbf{X} = (X_1, X_2)$, X_i ($i = 1, 2$) are normally distributed with parameters $\mu_i = 3.5$ and $\sigma_i = 0.25$. The temporal parameter is $t \in [0, 5]$ and the spatial parameter is $s \in [-1, 1]$. Therefore, $\mathbf{z} = (s, t)$, and $\Omega = \{[0, 5] \times [-1, 1]\}$. X_1 and X_2 are independent.

We can easily plot the envelope function for this problem since an analytic envelope function $G(\mathbf{X})$ is available for this problem. From the partial derivatives of the limit-state function with respective to t and s

$$\begin{cases} \frac{\partial g(\mathbf{X}, s, t)}{\partial t} = 0 \\ \frac{\partial g(\mathbf{X}, s, t)}{\partial s} = 0 \end{cases} \quad (55)$$

we have

$$\begin{cases} t = \frac{5X_1}{2(X_2 + 1)} \\ s = \frac{X_2}{X_1} \end{cases} \quad (56)$$

Plugging Eq. (56) into Eq. (54) yields the envelope function.

$$G(\mathbf{X}) = X_1^2 X_2 - \frac{25X_1^2}{4(X_2 + 1)} - \frac{X_2^2}{X_1} - 8 \quad (57)$$

The envelope function at the limit state $G(\mathbf{X}) = 0$ is plotted in Fig. 5.1, and the failure region is colored grey. The figure shows that the envelope function is nonlinear.

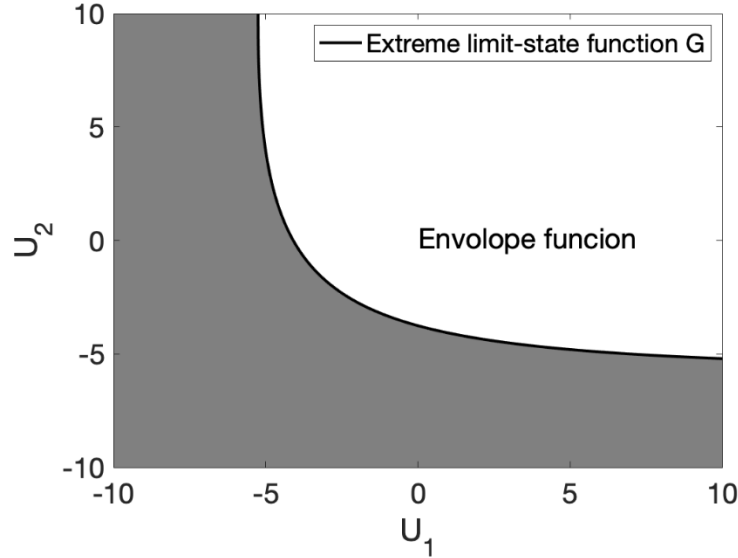


Figure 5.1 The envelope function

Even though the envelope function has an explicit function, we treat it as a black box by following the numerical procedure discussed in Sec. 3. SOSPA/ENV searches for the worst-case MPP with the sequential EGO. Table 5.1 shows the iteration history of the MPP search. The worst-case MPP is found at $\mathbf{u}_{\text{MPP}} = (-2.1702, -2.6185)$ with $\tilde{t} = 1.8150$ and $\tilde{s} = 0.8763$. Fig. 5.2 displays the convergence history of first-order reliability index β . With FORM/ENV, the probability of failure is $p_f = 3.3575 \times 10^{-4}$.

Once the worst-case MPP is available, the gradient and Hessian matrix are computed at the MPP. The latter is given by

$$\nabla^2 G(\mathbf{u}_{\text{MPP}}) = \begin{bmatrix} 0.1200 & 0.5542 \\ 0.5542 & -0.1494 \end{bmatrix}$$

Table 5.1 Iteration history of searching for the worst-case MPP

Iterations	\mathbf{u}^*	\tilde{t}	\tilde{s}
1	(-7.4573, -2.0392)	0.9157	1.2272
2	(-3.9028, -1.4544)	1.2886	1.0077
3	(-3.1172, -2.0203)	1.4821	0.8722
4	(-2.7126, -2.3219)	1.5695	0.8059
5	(-2.5333, -2.4574)	1.7458	0.9219
6	(-2.3025, -2.5225)	1.7859	0.8956
7	(-2.2254, -2.5784)	1.8030	0.8843
8	(-2.1928, -2.6021)	1.8101	0.8795
9	(-2.1928, -2.6120)	1.8131	0.8776
10	(-2.1735, -2.6161)	1.8143	0.8767
11	(-2.1712, -2.6178)	1.8148	0.8764
12	(-2.1702, -2.6185)	1.8150	0.8763

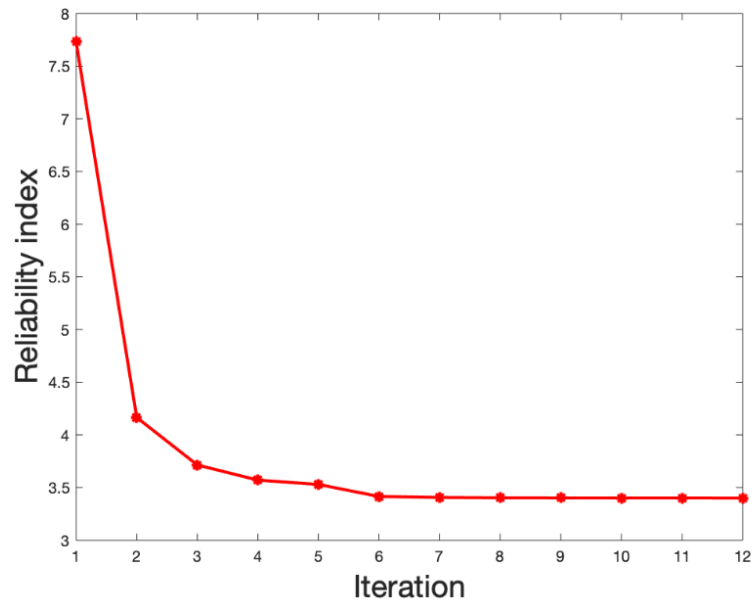


Figure 5.2 Convergence history of reliability index β

Then SOSPA/ENV produces $p_f = 4.9022 \times 10^{-4}$. The number of simulations for MCS is $N_C = 10^7$. The time and space intervals are discretized evenly into 20 points, yielding 400 points. Accordingly, the number of function calls of MCS is 4×10^9 .

All the results are shown in Table 5.2. SOSPA/ENV is much more accurate than FORM/ENV as the error of the former is 3.5% while that of the latter is 33.9%. SOSPA/ENV, however, is less efficient than FORM/ENV.

Table 5.2 Results of Example 1

Method	Probability of failure	Error	Number of function calls
MCS	5.080×10^{-4}	-	4×10^9
FORM/ENV	3.3575×10^{-4}	33.9%	314
SOSPA/ENV	4.9022×10^{-4}	3.5%	333

5.4.2 Example 2: A Truss Structure

A truss structure is shown in Fig. 5.3. This example belongs to Case 1 without any random field input. The inputs of this truss structure are random variables, temporal parameter t and spatial parameter h . Each bar of the system has its cross-sectional area A_i and the modulus of elasticity E_i , $i = 1,2,3$. The coefficient of thermal expansion of all bars is $\alpha = 12 \times 10^{-6} \text{C}^{-1}$. The temperature change is related to the installation height of the truss structure and is given by $\Delta T = T e^{-0.01(\Delta h^2 + 2\Delta h + 1)^2}$, where $\Delta h \in [2,5]$ m is the difference of two different installation heights. A downward force $P = P_0(0.9 + 0.1\cos(0.2t))$ is applied at joint A , where $t \in [0,10]$ years. The domain Ω of $\mathbf{z} = [\Delta h, t]$ is $\{[2,5] \times [0,10]\}$. All the random variables are given in Table 5.3.

The perpendicular displacement of joint A is calculated by

$$\Delta\delta = \frac{A}{B} \quad (58)$$

where

$$\begin{aligned} A = & L_{AD}(PA_1E_1L_{AC}\cos\theta_1^2 + PA_2E_2L_{AB}\cos\theta_2^2 + A_1A_3E_1E_3L_{AC}T\alpha\cos\theta_1^2 \\ & + A_2A_3E_2E_3L_{AB}T\alpha\cos\theta_2^2 + A_1A_2E_1E_2T\alpha(L_{AB}\sin\theta_1\cos\theta_2^2 + L_{AC}\sin\theta_2\cos\theta_1^2 \\ & + L_{AC}\sin\theta_1\cos\theta_2\cos\theta_1 + L_{AB}\sin\theta_2\cos\theta_2\cos\theta_1)) \end{aligned}$$

$$B = A_1 A_3 E_1 E_3 L_{AC} \cos \theta_1^2 + A_2 A_3 E_2 E_3 L_{AB} \cos \theta_2^2 + A_1 A_2 E_1 E_2 L_{AD} (\sin \theta_2^2 \cos \theta_1^2 + \sin \theta_1^2 \cos \theta_2^2 + 2 \sin \theta_1 \sin \theta_2 \cos \theta_1 \cos \theta_2)$$

$$\theta_1 = \arctan \left(\frac{L_{AD}}{\sqrt{L_{AB}^2 - L_{AD}^2}} \right)$$

$$\theta_2 = \arctan \left(\frac{L_{AD}}{\sqrt{L_{AC}^2 - L_{AD}^2}} \right)$$

A failure occurs when $\Delta\delta > 0.65$ mm. Thus, the limit-state function is defined by

$$g(\mathbf{X}, s, t) = 0.65 - \Delta\delta \quad (59)$$

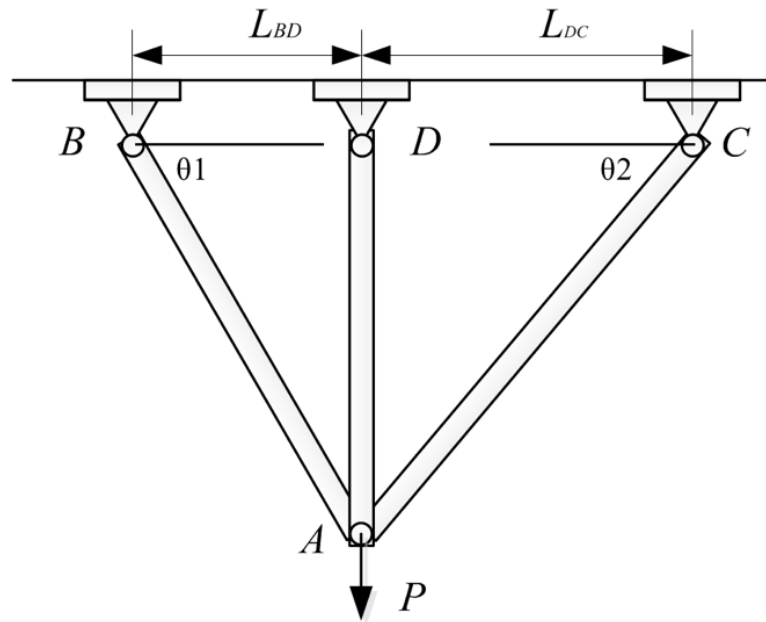


Figure 5.3 A truss structure

10^7 samples are used for MCS and the domain of $\mathbf{Z} = (\Delta h, t)$ is discretized evenly into $10 \times 10 = 100$ points. FORM/ENV and SOSPA/ENV are used to calculate the probability of failure. Table 5.4 shows the results. Even though FORM/ENV is more efficient than SOSPA/ENV, it produces a large error. SOSPA/ENV achieves higher accuracy than FORM/ENV although it needs more function calls.

Table 5.3 Random variables of Example 3

Variable (Unit)	Mean	Standard deviation	Distribution
$A_1(\text{mm}^2)$	60	0.6	Normal
$A_2(\text{mm}^2)$	60	0.6	Normal
$A_3(\text{mm}^2)$	60	0.6	Normal
$E_1(\text{GPa})$	200	20	Lognormal
$E_2(\text{GPa})$	200	20	Lognormal
$E_3(\text{GPa})$	200	20	Lognormal
$P_0(\text{KN})$	40	6	Normal
$L_{AB}(\text{mm})$	200	2	Normal
$L_{AD}(\text{mm})$	231	2.31	Normal
$L_{AC}(\text{mm})$	283	2.83	Normal
$T(^{\circ}\text{C})$	35	7	Lognormal

Table 5.4 Results of Example 3

Method	Probability of failure	Error (%)	Number of function calls
MCS	3.0270×10^{-4}	-	10^9
FORM/ENV	2.7654×10^{-4}	8.64%	189
SOSPA/ENV	2.9958×10^{-4}	1.03%	305

5.4.3 Example 3: An Electron Accelerator

Fig. 5.4 shows an electron accelerator that accelerates electrons. The inputs of this example are random variable L and random field $V(w, h, t)$, calling the limit-state function return a complete time-and space-dependent responses by sampling the random field $V(w, h, t)$. This problem belongs to Case 2 with an input random field, and it therefore requires single-loop MPP search. The device is placed horizontally. Electrons are emitted from the electrode and then enter the

electric field E in the accelerator, and finally fly out. The initial velocity of the electrons is a non-stationary Gaussian random field $V_0(w, h, t)$, whose mean is $\mu_{V_0} = 10^5 e^{-0.001(w^2+h^2+(t-6)^2)}$ m/s and standard deviation is $\sigma_{V_0} = 10000$ m/s. The spatial variable $w \in [-0.05, 0.05]$ m is the width of the electrode, and $h \in [-0.05, 0.05]$ m is the height of the electrode. The temporal variable is $t \in [0, 10]$ s. The autocorrelation coefficient function of the Gaussian field is given by

$$\rho_{V_0}(w_1, h_1, t_1; w_2, h_2, t_2) = \exp \left[- \left(\frac{w_1 - w_2}{5} \right)^2 - \left(\frac{h_1 - h_2}{5} \right)^2 - \left(\frac{t_1 - t_2}{10} \right)^2 \right] \quad (60)$$

The length of the accelerator L is normally distributed with $N(1, 0.01^2)$ m. The electric field $E(w, h)$ is a two-dimensional stationary Gaussian random field, whose mean μ_E and standard deviation σ_E are 10 N/C and 1 N/C, respectively. Its autocorrelation coefficient function is given by

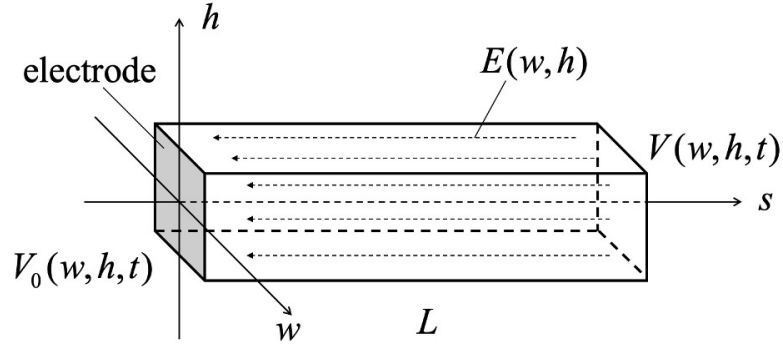


Figure 5.4 An electron accelerator

$$\rho_E(w_1, h_1; w_2, h_2) = \exp \left[- \left(\frac{w_1 - w_2}{5} \right)^2 - \left(\frac{h_1 - h_2}{5} \right)^2 \right] \quad (61)$$

If the acceleration time and the interaction among the electrons are negligible, the velocity $V(w, h, t)$ of the electrons after acceleration is

$$V(w, h, t) = \sqrt{\frac{2qE(w, h)L}{m} + V_0^2(w, h, t)} \quad (62)$$

where $q = 1.6 \times 10^{-19}$ C and $m = 9.109 \times 10^{-31}$ kg are the electric quantity and mass of an electron, respectively. The target velocity is $V_t = 1.4519 \times 10^6$ m/s. The domain Ω of $\mathbf{z} = [w, h, t]$ is $\{[-0.05, 0.05] \times [-0.05, 0.05] \times [0, 10]\}$. The limit-state function is defined by

$$g(\mathbf{X}, V(w, h, t)) = V(w, h, t) - V_t \quad (63)$$

in which a failure occurs if the velocity after acceleration is smaller than the target velocity.

The EOLE method is used to generate the series expansion of the nonstationary Gaussian field $V_0(w, h, t)$. w, h , and t are evenly discretized into 10 points, so there are a total of 1000 discretization points. The 1000×1000 autocorrelation coefficient matrix Σ_{V_0} of the random field is obtained. The three most significant eigenvalues of Σ_{V_0} are 841, 146, and 12, and therefore $V_0(w, h, t)$ can be expanded with three standard independent normal variables $\xi_k, k = 1, 2, 3$. Similarly, we use EOLE to generate the series expansion of $E(w, h)$ and keep only the first two orders. With 1000 discretization expansion points of $V(w, h, t)$, the minimal value of $g_{\min}(w, h, t)$ can be found. Then the traditional FORM method is employed to find the worst-case MPP $\mathbf{u}_{\text{MPP}} = (-2.2726, -0.0164, -0.0038, 0.0014, -2.2726, -0.0050)$ and the reliability index $\beta = 3.2140$. Then FORM/ENV produces $p_f = 6.5558 \times 10^{-4}$ with only 28 function calls which leading tremendous efficiency improvement instead of using sequential loops to find the worst-case MPP. SOSPA/ENV produces $p_f = 7.8862 \times 10^{-4}$ with 87 function calls. MCS uses 10^7 samples of all random variables at each of the 1000 discretization points of the temporal/spatial variables. The results are provided in Table 5.5. By using the sing-loop MPP search method, the function calls of both FORM/ENV and SOSPA/ENV methods are reduced tremendously. SOSPA/ENV is more accurate than FORM/ENV but less efficient.

Table 5.5 Results of Example 2

Method	Probability of failure	Error (%)	Number of function calls
MCS	$8,1360 \times 10^{-4}$	-	10^7
FORM/ENV	6.5558×10^{-4}	19.4%	28
SOSPA/ENV	7.8862×10^{-4}	3.1%	87

5.5 Summary

In this work, the envelope method for time-dependent reliability is extended to time- and space-dependent reliability analysis for limit-state functions with input of random variables, random fields, and temporal and spatial parameters. The envelope function is obtained with respect to temporal/spatial variables. Then the time- and space-dependent problem is converted into a time-

and space-independent counterpart, and the second order saddlepoint approximation method is used to estimate the reliability. Equations of the second derivatives of the envelope function are derived for the second order approximation. The major computational cost is the MPP search and second derivative calculations. In this case, efficient global optimization is used for the MPP search, and other global optimization methods can also be used. The first and second derivatives are evaluated by the finite difference method. The results show that the proposed method is much more accurate than the first-order approximation method since the envelope function is in general nonlinear. The new method, however, is less efficient than the first-order approximation method because it requires second derivatives of the envelope function.

The new method shares the same drawbacks as the MPP-based reliability methods. Its accuracy may become poor if the envelope function has multiple MPPs. If the MPP occurs on the boundary of the time and space domain, a large error may be produced. How to address these problems needs further investigation.

6. ENVELOPE METHOD FOR TIME- AND SPACE-DEPENDENT RELIABILITY- BASED DESIGN

Hao Wu¹, Xiaoping Du²

¹School of Mechanical Engineering, Purdue University, West Lafayette, IN, United States

²Department of Mechanical and Energy Engineering, Indiana University - Purdue University
Indianapolis, IN, United States

Published in Proceedings of the ASME 2022 International Design Engineering Technical
Conferences and Computers and Information in Engineering Conference

Authors' contribution: H.W. and X.D. designed the study and contributed to the writing of
the manuscript. H.W. detailed methodology and the code.

Deterministic optimization may lead to unreliable design results if significant uncertainty exists. Including reliability constraints in reliability-based design optimization (RBDO) can solve such a problem. It is difficult to use current RBDO methods to deal with time- and space-dependent reliability when responses vary randomly with respect to time and space. This study employs an envelope method for time- and space-dependent reliability for the optimal design. To achieve high accuracy, we propose an inverse envelope method that converts a time- and space-dependent limit-state function into a time- and space-independent counterpart, and then the second-order saddlepoint approximation is used to estimate the probability of failure. The strategy is to find an equivalent most probable point for a given permitted probability of failure for each of the reliability constraint. To achieve high efficiency, the new method uses a sequential optimization process to decouple the double-loop structure of RBDO. The overall optimization is performed with a sequence of cycles consisting of deterministic optimization and reliability analysis. The constraints of the deterministic optimization are formulated using the equivalent most probable points. The accuracy and efficiency are demonstrated with four examples, including one mathematical problem and three engineering problems.

6.1 Background

Engineers always encounter uncertainty in material properties, component dimensions, manufacturing processes, and operational environments [1,2] in all stages of product design and development. RBDO is a typical methodology to manage uncertainty by identifying optimal design variables and ensuring satisfied reliability in the design stage [3-5].

RBDO minimizes a cost-type objective while maintaining reliability constraints. If responses are static, meaning that they are time and space invariant, we have static RBDO method, for which there are many mature methodologies, such as double-loop methods [6,7], single loop single variable approaches [8], sequential optimization method [4,9], and safety-factor approaches [10,11]. Some examples follow. Tu and Choi use a performance measure approach to main robustness and efficiency for evaluating reliability constraints [7]. Liang and Mourelatos proposed a computationally efficient RBDO approach using a single loop process where the search of the optimum design variables and the reliability analysis is performed simultaneously [8]. Wu demonstrated that the safety-factor based RBDO approach is efficient and robust with a new concept of the sequential loop procedure [11]. By generalizing Wu's method to accommodate any continuous distributions, Du and Chen performed RBDO by sequential optimization and reliability analysis so that the search of design variables and reliability analysis are executed with a series of cycles of deterministic optimization and reliability analysis [4]. This reduces the computational time. Yin and Du developed a modified RBDO approach to mechanical component design so that the traditional safety factor design can be used without optimization and complex reliability analysis [10].

Many responses are also time-dependent due to time-varying stochastic operation conditions and system aging [12]. For instance, the function generator mechanism [13] involves time-dependent motion output. Static RBDO methods are not able to handle time-dependent problems. They were extended to time-dependent RBDO, and new time-dependent RBDO methods have been investigated. Several examples are given. In [14], a nested extreme response surface approach accurately carries out time-dependent reliability analysis and determines the optimal designs with efficacy. The sequential optimization and reliability analysis are extended to time-dependent problems with both stationary stochastic process loads and random loads, and it effectively solves design optimization with dependent reliability constraints [15]. The equivalent most probable point method is proposed to transform the original time-variant RBDO problem into an equivalent time-

invariant RBDO problem formulated by performance measure approach [16]. The time-dependent concurrent reliability-based design optimization methods are developed to improve the confidence of design results with reduced experimental cost and increased computational efficiency [17]. In [18], a sequential Kriging modeling approach is introduced to deal with the reliability constraint for time variant RBDO involving stochastic processes.

Although the time-dependent RBDO methods have been developed, the most general problems should be addressed where the limit-state functions may take input of stochastic processes, random fields, and tempo-spatial variables. It is still a challenge to address the time- and space-dependent RBDO as the research about this work is limited. Currently some time- and space-dependent reliability analysis methods have been proposed. Hu and Mahadevan developed a surrogate modeling approach for reliability analysis of a multidisciplinary system [19]. Shi et al. presented a method for the moment estimation of the extreme response using two strategies. One strategy is combining the sparse grid technique and the fourth-moment method while the other one is combining the dimensional reduction with the maximum entropy method [20]. Shi and Lu proposed an active learning Kriging method for dealing with dynamic reliability analysis for structure with temporal and spatial multi-parameter [21]. Wei and Du combined the first-order reliability method (FORM) and second-order reliability method (SORM) for the time- and space-dependent reliability analysis [22,23]. Yu and Wang developed a general decoupling approach with a simulation-based method addressing reliability assessment for time and space-variant system reliability-based design optimization [24]. Motivating by the above method, we integrate the time- and space-dependent reliability analysis method into RBDO.

This paper proposes a decoupling method for time- and space-variant RBDO using the envelope method. The time- and space-dependent RBDO start with the deterministic optimization, then the optimization results are passed to do the time- and space-dependent reliability analysis to satisfy the probability constraint. In the reliability analysis process, the envelope method converts a time- and space-dependent problem into a time- and space-independent counterpart. Subsequently, the MPP, gradient and Hessian matrix are available, the second-order saddle point approximation method can be used to estimate the reliability. The deterministic optimization and reliability analysis are performed cycle by cycle until the optimal design points are found.

The remainder of the paper is organized as follows. Section 2 gives a brief introduction of sequential RBDO. Section 3 introduces a time- and space-dependent RBDO model with the envelope method. Section 4 presents four examples, followed by conclusions in Section 5.

6.2 Problem Statement

In this section we give the problem that this study addresses. We also review the sequential RBDO, based on which the new method is developed.

6.2.1 Problem Statement

This study addresses the most general RBDO which includes time- and space-dependent reliability. The RBDO model is defined as

$$\begin{cases} \min_{\mathbf{d}, \mu_X} & f(\mathbf{d}) \\ \text{s. t.} & \Pr\{y_i = g_i(\mathbf{d}, \mathbf{X}, \mathbf{z}) \leq 0, \exists \mathbf{z} \in \Omega\} \leq \tilde{p}_{fi} \\ & i = 1, 2, \dots, n_g \\ & \mathbf{d}^L \leq \mathbf{d} \leq \mathbf{d}^U \end{cases} \quad (1)$$

where $f(\mathbf{d})$ is the objective function, and \mathbf{d} is the vector of design variables with their lower and upper bounds \mathbf{d}^L and \mathbf{d}^U , respectively. $\Pr\{y_i = g_i(\mathbf{d}, \mathbf{X}, \mathbf{z}) \leq 0, \exists \mathbf{z} \in \Omega\}$ is the probability of failure for i -th response y_i . The associated reliability constraint is that the probability of failure should be smaller than or equal to the allowable probability of failure \tilde{p}_{fi} or $1 - \tilde{R}_i$, where $[R_i]$ is desired reliability. n_g is the number of constraints. In the constraint, the limit-state function is defined by

$$y_i = g_i(\mathbf{d}, \mathbf{X}, \mathbf{z}) \quad (2)$$

in which $\mathbf{X} = [X_1, \dots, X_n]^T$ are input random variables. The time given by $z_1 \in [\underline{z}_1, \bar{z}_1]$, and the spatial variables are z_k with the following ranges: $z_k \in [\underline{z}_k, \bar{z}_k]$, ($k = 2, \dots, m$). Then, $\mathbf{z} = [z_1, z_2, \dots, z_m]^T$ is a vector of the temporal and spatial variables bounded on $\Omega = [\underline{z}_k, \bar{z}_k]$. Note that Ω is a rectangular domain.

Accordingly, the probability of failure for a general response y is defined by

$$p_f = \Pr\{y = g(\mathbf{d}, \mathbf{X}, \mathbf{z}) \leq 0, \exists \mathbf{z} \in \Omega\} \quad (3)$$

where \exists means “there exists at least one”.

Solving the time- and space-dependent RBDO is time-consuming since evaluating p_f in Eq. (3) is computationally expensive and p_f should be evaluated repeatedly during the optimization.

6.2.2 Review of Sequential RBD

Sequential RBDO methods in general are more efficient than double-loop methods. It decouples the optimization loop and reliability analysis loop and performs the two loops sequentially. Usually, the first-order reliability method (FORM) is used for reliability analysis. FORM searches for the Most Probable Most (MPP), from which the probability of failure is easily calculated.

The optimal design point is first found from the deterministic optimization loop and then FORM is performed to search for the MPP at this optimal point in the reliability analysis loop. The MPP is then used to modify a reliability constraint for the next deterministic optimization, which is followed by the next reliability analysis. This process repeats until iterative convergence.

The deterministic optimization is formulated by

$$\begin{cases} \min_{\mathbf{d}} & f(\mathbf{d}) \\ \text{s. t.} & g_i(\mathbf{d}, T(\mathbf{u}_x), \mathbf{z}) \leq 0, i = 1, 2, \dots, n_g \end{cases} \quad (4)$$

where \mathbf{u}_x is the MPP in the standard normal space for the i -th reliability constraint from the reliability analysis. $T(\cdot)$ is the transformation operator for transforming random variables \mathbf{X} to independent and standard normal variables \mathbf{U} . The result of the optimization is the optimal design point $\tilde{\mathbf{d}}$.

After the deterministic optimization, the reliability analysis or the MPP search is performed at $\tilde{\mathbf{d}}$ for each constraint. The MPP is obtained through an optimization problem given by

$$\begin{cases} \min_{\mu_x} & g_i(\mathbf{d}, T(\mathbf{u}_x), \mathbf{z}) \\ \text{s. t.} & \|\mathbf{u}_x\| = \beta_i \end{cases} \quad (5)$$

where β_i is the desired reliability index. It is calculated by $\beta_i = -\Phi^{-1}(\tilde{p}_{fi})$, and $\Phi^{-1}(\cdot)$ is inverse cumulative density function.

The final solution can be found after a few cycles of deterministic optimization and reliability analysis. As a result, the efficiency is higher than solving the original RBDO model directly. Since FORM may not be accurate for highly nonlinear limit-state functions, several studies employ the second-order reliability method (SORM) with lower efficiency.

6.3 Sequential RBDO with the Envelope Method

6.3.1 Overview

This work aims to include time- and space-dependent reliability constraints in optimization. To achieve high accuracy, we use second-order saddlepoint approximation to calculate the reliability. To achieve high efficiency, we use sequential RBDO. In the original sequential RBDO, the MPP is directly related to the permitted probability of failure by $\tilde{p}_{fi} = \Phi(-\|\mathbf{u}_{XMPP}\|)$. In the present study, the MPP is not directly related to the permitted time- and space-dependent probability of failure, and the relationship is unknown and nonlinear. The challenge is to find an equivalent MPP $\tilde{\mathbf{u}}_{XMPP}$, which satisfies

$$\Pr\{g_i(\mathbf{d}, T(\tilde{\mathbf{u}}_{XMPP}), \mathbf{z}) \leq 0, \exists \mathbf{z} \in \Omega\} = \tilde{p}_{fi} \quad (6)$$

The model of searching for the equivalent MPP becomes

$$\begin{cases} \min g_i(\mathbf{d}, T(\mathbf{u}_X), \mathbf{z}) \\ \text{s. t. } \|\mathbf{u}_X\| = \beta^k \\ p_{fi} = \Pr\{g_i(\mathbf{d}, T(\mathbf{u}_X), \mathbf{z}) \leq 0, \exists \mathbf{z} \in \Omega\} = \tilde{p}_{fi} \end{cases} \quad (7)$$

The model gives the solution $\mathbf{u}_X = \tilde{\mathbf{u}}_{XMPP}$.

The envelope method can be used for reliability analysis when the equivalent MPP $\tilde{\mathbf{u}}_{XMPP}$ is available from Eq. (7). To solve Eq. (7), we at first search for the MPP using FORM at the optimal point of \mathbf{z} parameter that minimizes $g_i(\cdot)$, and then the probability of failure p_{fi} is calculated using the envelop method, and the flowchart of reliability analysis with envelope method is shown in Figure 6.1. We update β^k iteratively until $p_{fi} = \tilde{p}_{fi}$. The sequential RBDO with the envelope method involves cycles of deterministic optimization and equivalent MPP search (reliability analysis).

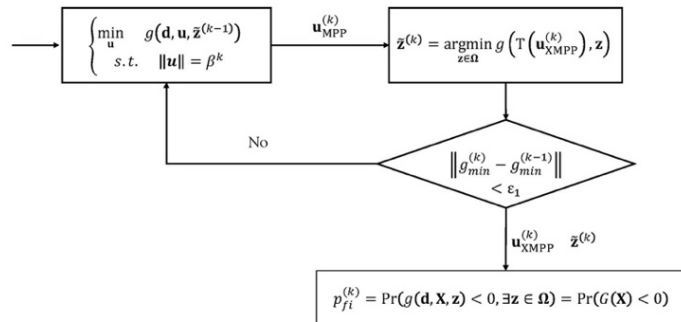


Figure 6.1 Search for equivalent MPP with the envelope method

6.3.2 Time- and Space-dependent Reliability Analysis

This subsection discusses the time- and space-dependent reliability using the envelope method. We have already developed an envelope method, but the envelope method in this study is different from the existing method. The existing method calculates the probability of failure directly given the limit state. The new method is for an inverse problem: given the probability of failure, find the equivalent MPP. The new method is more difficult.

We use the envelope method for two case encounters in engineering applications.

Case 1: Calling the limit-state function one time returns only one response at a specific time instant and spatial point, or a point of $\mathbf{z} \in \Omega$. As a result, solving for the equivalent MPP in Eq. (5) needs a double-loop procedure. This double procedure will be discussed in Section 3.2.1.

Case 2: Calling the limit-state function one time returns all responses at all specific time instants and spatial points, or all points of $\mathbf{z} \in \Omega$. For instance, if we call a computational fluid dynamics (CFD) simulation, we obtain all 4-D pressure and velocity fields with respect to time and space. For this case, solving for the equivalent MPP in Eq. (5) needs only a single loop.

Since Case 1 is much more difficult than Case 2. We focus our discussions primarily on Case 1. The probability of failure can be evaluated by the extreme value of the limit-state function.

$$\begin{aligned} p_f &= \Pr(g(\mathbf{d}, T(\mathbf{u}), \mathbf{z}) \leq 0, \exists \mathbf{z} \in \Omega) \\ &= \Pr\left(\min_{\mathbf{z} \in \Omega} g(\mathbf{d}, T(\mathbf{u}), \mathbf{z}) \leq 0\right) \end{aligned} \quad (8)$$

Eq. (8) indicates that a failure occurs if the minimum response is negative. The function of the extreme response is equivalent to the envelope function

$$G(\mathbf{X}) = \min_{\mathbf{z} \in \Omega} g(\mathbf{d}, T(\mathbf{u}), \mathbf{z}) = g(\mathbf{d}, T(\mathbf{u}), \tilde{\mathbf{z}}) \quad (9)$$

where $G(\mathbf{X})$ is the envelope function and it is the global minimum of $g(\mathbf{d}, T(\mathbf{u}), \tilde{\mathbf{z}})$. $G(\mathbf{X})$ is time- and space-independent and only depends on \mathbf{X} .

6.3.2.1 Search for the Equivalent MPP Using FORM

There are two constraints in Eq. (7) and directly solving the model in Eq. (7) is too computationally expensive as it involves a double loop procedure. In this work, an alternative sequential procedure is proposed to find the worst-case MPP.

At first, the MPP search is performed by giving the initial reliability index β at $\tilde{\mathbf{z}}^{(0)} = [z_1^0, z_2^0, \dots, z_m^0]$ with the following model

$$\begin{cases} \min_{\mathbf{u}} & g(\mathbf{d}, T(\mathbf{u}), \mathbf{z}) \\ \text{s. t.} & \|\mathbf{u}\| = \beta \end{cases} \quad (10)$$

Eq. (10) produces the MPP $\mathbf{u}_{\text{MPP}}^{(1)}$. The next analysis is to find the optimal time and space parameter $\tilde{\mathbf{z}}^{(1)}$ by fixing the random variables on its realization $\mathbf{u}_{\text{XMPP}}^{(1)}$. The next optimal $\tilde{\mathbf{z}}^{(1)}$ can be obtained by another optimization $\tilde{\mathbf{z}}^{(1)} = \underset{\mathbf{z} \in \Omega}{\text{argmin}} g(\mathbf{d}, T(\mathbf{u}_{\text{MPP}}^{(1)}), \mathbf{z})$. The details of solving $\tilde{\mathbf{z}}^{(1)}$ is illustrated in Subsection 3.2.3. The process repeats until numerical convergence. The sequential procedure of the MPP search produces the worst-case MPP \mathbf{u}_{XMPP} and the optimal $\tilde{\mathbf{z}}$. When the worst-case MPP is found, the probability of failure with FORM is estimated by $p_f = \Pr(g(\mathbf{d}, T(\mathbf{u}), \mathbf{z}) < 0, \exists \mathbf{z} \in \Omega) = \Phi(-\|\mathbf{u}_{\text{XMPP}}\|)$. However, FORM may not be accurate enough. As a result, we use the second-order reliability method to achieve higher accuracy.

6.3.2.2 The Envelope Method

To have higher accuracy, we use the SORM and envelope method. Generally, the envelope function is nonlinear, and it is tangent to all the instantaneous limit-state functions. It can be approximated by the second-order approximation method as a quadratic function at the MPP. As indicated by Ref. [14], the MPP of the envelope function is the worst-case MPP of the limit-state function. We also need the gradient ∇G and Hessian matrix \mathbf{H} at the MPP, of the envelope function. The quadratic function is formed as follows:

$$G(\mathbf{U}) = a + \mathbf{b}^T \mathbf{U} + \mathbf{U}^T \mathbf{C} \mathbf{U} \quad (11)$$

where

$$\begin{cases} a = \frac{1}{2} (\mathbf{u}_{\text{XMPP}})^T \mathbf{H} \mathbf{u}_{\text{XMPP}} - \nabla G(\mathbf{u}_{\text{XMPP}})^T \mathbf{u}_{\text{XMPP}} \\ \mathbf{b} = \nabla G(\mathbf{u}_{\text{XMPP}}) - \mathbf{H} \mathbf{u}_{\text{XMPP}} = (\tilde{b}_1, \tilde{b}_2, \dots, \tilde{b}_n) \\ \mathbf{C} = \frac{1}{2} \mathbf{H} = \text{diag}(\tilde{c}_1, \tilde{c}_2, \dots, \tilde{c}_n) \end{cases} \quad (12)$$

$\nabla G(\mathbf{u}_{\text{XMPP}}) = \left[\left. \frac{\partial G}{\partial U_1} \right|_{\mathbf{u}_{\text{XMPP}}}, \dots, \left. \frac{\partial G}{\partial U_n} \right|_{\mathbf{u}_{\text{XMPP}}} \right]^T$ is the gradient of the envelope function. \mathbf{H} is the

Hessian matrix and is given by

$$\mathbf{H} = \begin{bmatrix} \frac{\partial^2 G}{\partial U_1^2} & \cdots & \frac{\partial^2 G}{\partial U_1 \partial U_n} \\ \vdots & \ddots & \vdots \\ \frac{\partial^2 G}{\partial U_n \partial U_1} & \cdots & \frac{\partial^2 G}{\partial U_n^2} \end{bmatrix}_{\mathbf{u}_{\text{XMPP}}} \quad (13)$$

The envelope function $G(\mathbf{X})$ at \mathbf{u}_{XMPP} is given by

$$G(\mathbf{U}) = \min_{\mathbf{z} \in \Omega} g(\mathbf{d}, \mathbf{U}, \mathbf{z}) = g(\mathbf{U}, \tilde{\mathbf{z}})|_{\mathbf{u}_{\text{XMPP}}} \quad (14)$$

where $\tilde{\mathbf{z}} = [\tilde{z}_1, \dots, \tilde{z}_m]$ is the optimal point where the global minimum of function $g(\mathbf{d}, \mathbf{U}, \mathbf{z})$ occurs. For an easier demonstration without loss of generality, we use a two-parameter case $\tilde{\mathbf{z}} = [\tilde{z}_1, \tilde{z}_2]$ as an example to derive the envelope function's Hessian matrix and gradient. The envelope function satisfies the following equations:

$$\begin{cases} \dot{g}(\mathbf{d}, \mathbf{U}, \tilde{z}_1, z_2) = 0 \\ \dot{g}(\mathbf{d}, \mathbf{U}, z_1, \tilde{z}_2) = 0 \end{cases} \quad (15)$$

where \dot{g} is the derivative of g with respect to z_i .

The first derivative of $G(\mathbf{U})$ at \mathbf{u}_{XMPP} is

$$\frac{\partial G}{\partial U_i} = \frac{\partial g}{\partial U_i} + \frac{\partial g}{\partial \tilde{z}_1} \frac{\partial \tilde{z}_1}{\partial U_i} + \frac{\partial g}{\partial \tilde{z}_2} \frac{\partial \tilde{z}_2}{\partial U_i} \quad (16)$$

Plugging Eq. (15) into Eq. (16) yields

$$\frac{\partial G}{\partial U_i} = \frac{\partial g}{\partial U_i} \quad (17)$$

The gradient of the envelope function ∇G is equal to the gradient of the limit-state function ∇g at the MPP. Subsequently, the second derivative of $G(\mathbf{U})$ with respect to the input random variables U_j at \mathbf{u}_{XMPP} is

$$\begin{aligned} \frac{\partial^2 G}{\partial U_i \partial U_j} &= \frac{\partial}{\partial U_j} \left(\frac{\partial G}{\partial U_i} \right) = \frac{\partial}{\partial U_j} \left(\frac{\partial g}{\partial U_i} \right) \\ &= \frac{\partial^2 g}{\partial U_i \partial U_j} + \frac{\partial^2 g}{\partial U_i \partial \tilde{z}_1} \frac{\partial \tilde{z}_1}{\partial U_j} + \frac{\partial^2 g}{\partial U_i \partial \tilde{z}_2} \frac{\partial \tilde{z}_2}{\partial U_j} \end{aligned} \quad (18)$$

Taking the derivative of Eq. (15) with respect to U_j yields

$$\frac{\partial \dot{g}}{\partial U_j} + \frac{\partial \dot{g}}{\partial \tilde{z}_1} \frac{\partial \tilde{z}_1}{\partial U_j} = 0 \quad (19)$$

Rearrange the equation, we have

$$\frac{\partial \tilde{z}_1}{\partial U_j} = -\frac{\partial \dot{g}}{\partial U_j} / \frac{\partial \dot{g}}{\partial \tilde{z}_1} = -\frac{\partial^2 g}{\partial \tilde{z}_1 \partial U_j} / \frac{\partial^2 g}{\partial \tilde{z}_1^2} \quad (20)$$

Similarly,

$$\frac{\partial \tilde{z}_2}{\partial U_j} = -\frac{\partial \dot{g}}{\partial U_j} / \frac{\partial \dot{g}}{\partial \tilde{z}_2} = -\frac{\partial^2 g}{\partial \tilde{z}_2 \partial U_j} / \frac{\partial^2 g}{\partial \tilde{z}_2^2} \quad (21)$$

By plugging Eq. (20) and Eq. (21) into Eq. (18), we obtain the Hessian matrix at \mathbf{u}_X and \tilde{z}_i .

$$\frac{\partial^2 G}{\partial U_i \partial U_j} \Big|_{\mathbf{u}^*, \tilde{z}_k} = \frac{\partial^2 g}{\partial U_i \partial U_j} - \sum_{k=1}^2 \frac{\partial^2 g}{\partial U_i \partial \tilde{z}_k} \frac{\partial^2 g}{\partial U_j \partial \tilde{z}_k} / \frac{\partial^2 g}{\partial \tilde{z}_k^2} \quad (22)$$

We use the forward finite difference method with step size $\delta = \max(|u|/1000, \epsilon)$, where $\epsilon = 10^{-4}$, to calculate the derivations in Eq. (22).

The worst-case MPP \mathbf{u}_{XMPP} , gradient ∇G , and the Hessian matrix are now available. The second-order saddlepoint approximation (SOSPA) is then used to estimate the probability of failure p_{fi} after the envelope function is approximated as a quadratic function. SOSPA in general is more accurate than FORM because it yields an accurate probability estimation especially in the tail area of distribution. The details of the implementation of SOSPA are given in Ref [27]. If p_{fi} is not equal to \tilde{p}_{fi} , we should update the reliability index β_i [28], and the MPP search is executed again using Eq. (10). The process is repeated until $p_{fi} = \tilde{p}_{fi}$. When the probability of failure is equal to the required probability of failure, it will produce the equivalent MPP $\tilde{\mathbf{u}}_{\text{XMPP}}$. The detail procedure is given as follows.

Step 1: Set the initial reliability index $\beta^{(1)}$. $\beta^{(1)} = -\Phi^{-1}([p_{fi}])$, and $k=1$. Set the initial optimal point $\mathbf{z}^{(0)}$ and an initial MPP $\mathbf{u}_{\text{MPP}}^{(1)} = \mathbf{u}_0$.

Step 2: Search for the inverse MPP using Eq. (10) at $\tilde{\mathbf{z}}^{(k-1)}$, and obtain the MPP $\mathbf{u}_{\text{MPP}}^{(k)}$ by solving the following optimization model:

$$\begin{cases} \min_{\mathbf{u}} & g(\mathbf{d}, T(\mathbf{u}), \mathbf{z}) \\ \text{s. t.} & \|\mathbf{u}\| = \beta^{(k)} \end{cases} \quad (23)$$

Step 3: Determine the optimal point $\tilde{\mathbf{z}}^{(k)}$ at $\mathbf{u}_{\text{XMPP}}^{(k)}$. The optimal point $\tilde{\mathbf{z}}^{(k)}$ minimizes the limit-state function.

$$\tilde{\mathbf{z}}^{(k)} = \underset{\mathbf{z} \in \Omega}{\operatorname{argmin}} g(\mathbf{d}, T(\mathbf{u}_{\text{XMPP}}^{(k)}), \mathbf{z}) \quad (24)$$

(The optimization method we use in this study is Global Efficient Optimization or EGO [25].)

Step 4: Check the iterative convergence criterion.

$$g_{\min}^{(k)} - g_{\min}^{(k-1)} \leq \varepsilon_1 \quad (25)$$

The tolerance ε_1 takes a small positive value, for example, 10^{-4} . If $g_{\min}^{(k)} - g_{\min}^{(k-1)} \leq \varepsilon_1$, terminate the iteration. Otherwise, set $k = k + 1$, and return to step 2.

Step 5: Calculate the gradient ∇G and Hessian matrix \mathbf{H} of the envelope function at $\mathbf{u}_{\text{XMPP}}^{(k)}$. Calculate the probability of failure $p_{fi}^{(k)}$ using SOSPA from the above information $\mathbf{u}_{\text{XMPP}}^{(k)}$, gradient ∇G , and Hessian matrix \mathbf{H} .

Step 6: Check the iterative convergent criterion.

$$\varepsilon = \left| \frac{p_{fi}^{(k)} - [p_{fi}]}{[p_{fi}]} \right| \leq \varepsilon_2 \quad (26)$$

where ε_2 is a user-defined threshold.

If the iterative convergence is reached, return the equivalent MPP $\tilde{\mathbf{u}}_{\text{XMPP}}$ and stop. Otherwise, update the reliability index $\beta^{(k+1)}$ and return to Step 2.

6.3.2.3 Find the Optimal $\tilde{\mathbf{z}}$

The global minimum value of $g(\mathbf{d}, T(\mathbf{u}_{\text{XMPP}}), \mathbf{z})$ occurs at $\tilde{\mathbf{z}} = [\tilde{z}_1, \tilde{z}_2]$, which is given by

$$\tilde{\mathbf{z}} = \underset{\mathbf{z} \in \Omega}{\operatorname{argmin}} g(\mathbf{d}, T(\mathbf{u}_{\text{XMPP}}), \mathbf{z}) \quad (27)$$

Finding the optimal point still needs sequential loops. The first partial derivatives of the limit-state function with respect to z_i at MPP are obtained as follows:

$$\begin{cases} \frac{\partial g(\mathbf{d}, T(\mathbf{u}_{\text{MPP}}), z_1, z_2)}{\partial z_1} = 0 \\ \frac{\partial g(\mathbf{d}, T(\mathbf{u}_{\text{MPP}}), z_1, z_2)}{\partial z_2} = 0 \end{cases} \quad (28)$$

The optimal point $\tilde{\mathbf{z}} = [\tilde{z}_1, \tilde{z}_2]$ can be obtained by solving Eq. (28). For an explicit and simple limit-state function, the solution of the derivative equations can be obtained analytically. For an implicit and complicated limit state function, EGO can be used. EGO has been widely used in various areas because it can efficiently search for the global optimum [25].

EGO generates the training points of the input $\mathbf{z}^{in} = [z_1^{(i)}, z_2^{(i)}]_{i=1,2,\dots,h} = [\mathbf{z}^{(i)}]_{i=1,2,\dots,h}$, where h is the number of initial training points, and the training points of the output dataset are $\mathbf{y}^{in} = [g(T(\mathbf{u}_{\text{XMPP}}), \mathbf{z}^{(i)})]_{i=1,2,\dots,h}$. Once the training dataset $(\mathbf{z}^{in}, \mathbf{y}^{in})$ is ready, the next step is to train the initial model using the Gaussian process regression. The initial surrogate model is $\hat{y} = g(\mathbf{z}) = g(T(\mathbf{u}_{\text{XMPP}}), \mathbf{z}) = F(\mathbf{z})^T \boldsymbol{\gamma} + e(\mathbf{z})$, where $F(\mathbf{z})^T \boldsymbol{\gamma}$ is a deterministic term, $e(\mathbf{z})$ is a vector of regression functions, $\boldsymbol{\gamma}$ is a vector of regression coefficients, and $e(\mathbf{z})$ is a stationary Gaussian process with zero mean and covariance is $\text{Cov}(e(\mathbf{z}_i), e(\mathbf{z}_j)) = \sigma_e^2 C(\mathbf{z}_i, \mathbf{z}_j)$, where σ_e^2 is process variance, and $C(\cdot, \cdot)$ is the correlation function [26]. The initial model may not be accurate; hence new training points are then added one by one so that the model is continuously refined. EGO select a new training point \mathbf{z}_{new} using the expected improvement (EI) metric defined by

$$\mathbf{z}_{new} = \underset{\mathbf{z}}{\text{argmin}} \text{EI}(\mathbf{z}) \quad (29)$$

where EI is computed by

$$\begin{aligned} \text{EI}(\mathbf{z}) &= \text{E}[\max(y^* - y, 0)] \\ &= (y^* - \mu(\mathbf{z})) \Phi\left(\frac{y^* - \mu(\mathbf{z})}{\sigma(\mathbf{z})}\right) + \sigma(\mathbf{z}) \phi\left(\frac{y^* - \mu(\mathbf{z})}{\sigma(\mathbf{z})}\right) \end{aligned} \quad (30)$$

where $y^* = \min_{i=1,2,\dots,k} g(\mathbf{z}^i)$, $\mu(\mathbf{z})$ and $\sigma(\mathbf{z})$ are the mean and standard deviation of \hat{y} , respectively, and $\phi(\cdot)$ is the probability density function (PDF).

6.3.3 Extension to Case 2

We now discuss Case 2 where we have a complete time- and space-dependent responses with respect to \mathbf{z} in Ω from a single call of the limit-state function. This case has the most general limit-state function $y(\mathbf{z}) = g(\mathbf{X}, \mathcal{F}(\mathbf{z}), \mathbf{z})$. The probability of failure is calculated by

$$p_f = \Pr(g(\mathbf{X}, \mathcal{F}(\mathbf{z}), \mathbf{z}) \leq 0, \exists \mathbf{z} \in \Omega) = \Pr\left(\min_{\mathbf{z} \in \Omega} y(\mathbf{z}) \leq 0\right) \quad (31)$$

Eq. (31) indicates that failure happens when the minimum value of the limit-state function $g(\mathbf{X}, \mathcal{F}(\mathbf{z}), \mathbf{z})$ is negative. Since calling the limit-function returns a complete hypersurface of the response $y(\mathbf{z})$ with respect to time and space, the minimum value $\min_{\mathbf{z} \in \Omega} y(\mathbf{z})$ is known. Thus, the MPP can be obtained from the following model:

$$\begin{cases} \min \sqrt{\mathbf{u}^T \mathbf{u}} \\ \text{s. t. } \min_{\mathbf{z} \in \Omega} y(\mathbf{z}) = 0 \end{cases} \quad (32)$$

where $\min_{\mathbf{z} \in \Omega} y(\mathbf{z})$ is a function of \mathbf{u} and is obtained by calling the limit-state once at \mathbf{u} . Therefore, a single single-loop MPP is needed. This is more efficient than the sequential loop approach. The expansion optimal linear estimation method (EOLE) [29] is used to expand the random field response with respect to independent standard Gaussian random variables $\boldsymbol{\xi} = (\xi_1, \xi_2, \dots, \xi_r)$, where r is the dimension of $\boldsymbol{\xi}$. Then, the limit-state function becomes $y = g(\tilde{\mathbf{X}}, \mathbf{z})$, where $\tilde{\mathbf{X}} = (\mathbf{X}, \boldsymbol{\xi})$. Thus, the proposed method can still work. Take EOLE as an example for a two-dimensional random field $\mathcal{F}(\mathbf{z})$ with $\mathbf{z} \in (z_1, z_2)$. z_1 and z_2 are discretized into $n_{z_1} n_{z_2}$ points, and the autocorrelation coefficient matrix is given by

$$\boldsymbol{\Sigma} = [\rho(\mathbf{z}_i, \mathbf{z}_j)]_{n_{z_1} n_{z_2} \times n_{z_1} n_{z_2}} \quad (33)$$

where $\rho(\mathbf{z}_i, \mathbf{z}_j)$ is the correlation between two points \mathbf{z}_i ($i = 1, 2, \dots, n_{z_1} n_{z_2}$) and \mathbf{z}_j ($j = 1, 2, \dots, n_{z_1} n_{z_2}$) in the domain of $\mathcal{F}(\mathbf{z})$.

Then the EOLE expansion is given by

$$\mathcal{F}(\boldsymbol{\xi}, \mathbf{z}) \approx \mu(\mathbf{z}) + \sigma(\mathbf{z}) \sum_{k=1}^r \frac{\xi_k}{\sqrt{\lambda_k}} \boldsymbol{\Phi}_k^T \boldsymbol{\Sigma}(:, \mathbf{z}), k = 1, 2, \dots, r \quad (34)$$

where $\mu(\mathbf{z})$ is the mean of $\mathcal{F}(\mathbf{z})$, and $\sigma(\mathbf{z})$ is the standard deviation of $\mathcal{F}(\mathbf{z})$. ξ_k ($k = 1, 2, \dots, r$) are independent standard normal variables, $\boldsymbol{\lambda} = (\lambda_1, \lambda_2, \dots, \lambda_r)$ is the eigenvalue vector, and

$\boldsymbol{\phi}_1, \boldsymbol{\phi}_2, \dots, \boldsymbol{\phi}_r$ are the corresponding eigenvectors obtained from autocorrelation coefficient matrix $\boldsymbol{\Sigma}$. Note that r is determined as the smallest integer that meets the following criterion:

$$\frac{\sum_{j=1}^r \lambda_k}{\sum_{j=1}^{n_{z_1} n_{z_2}} \lambda_k} \geq \eta \quad (35)$$

where η is a hyperparameter determining the accuracy of the expansion. It takes a value close to, but not larger than 1. The smaller is η , the less accurate is the expansion. If $\eta = 1$, the expansion is exact at the points of discretization. η could be set to 0.9~0.99.

6.3.4 Procedure of Sequential RBDO with Envelope Method

After discussing all the details, we now summarize the procedure of the proposed method. The steps are summarized below. The flowchart of the SORA with envelop method is provided in Fig. 6.2.

Step 1: Initialize parameters.

Step 2: Perform deterministic optimization. For $k = 1$, solve deterministic optimization at means of a random variable. For $k > 1$, perform the following deterministic optimization using the MPP $\mathbf{u}_{i, \text{XMPP}}^{(k-1)}$ obtained from the $(k - 1)$ -th cycle. The solution is $\mathbf{d}^{(k)}$.

$$\begin{cases} \min_{\mathbf{d}, \boldsymbol{\mu}_X} & f(\mathbf{d}) \\ \text{s. t.} & g_i(\mathbf{d}, \mathbf{T}(\mathbf{u}_{i, \text{XMPP}}^{(k-1)}), \mathbf{z}) \leq 0, i = 1, 2, \dots, n \\ & \mathbf{d}^L \leq \mathbf{d} \leq \mathbf{d}^U \end{cases} \quad (36)$$

Step 3: Perform time- and space-dependent reliability analysis at $\mathbf{d}^{(k)}$ for each constraint. At first, search for the equivalent MPP given $\beta^{(k)}$. Obtain the $\mathbf{u}_{i, \text{XMPP}}^{(k)}$, gradient $\nabla G(\mathbf{u}_{i, \text{XMPP}}^{(k)})$, and Hessian matrix $\mathbf{H}_{\mathbf{u}_{i, \text{XMPP}}^{(k)}}$. Note that if the inputs of limit-state function are random variables and random fields, the method in section 3.3 is used to find the $\mathbf{u}_{i, \text{XMPP}}^{(k)}$. Next, calculate the probability of failure $p_{fi}^{(k)}$ using SOSPA.

Step 4: Check the iterative convergent criterion by

$$\varepsilon = \left| \frac{p_{fi}^{(k)} - [P_{fi}]}{[P_{fi}]} \right| \leq \varepsilon_2 \quad (37)$$

If numerical convergence is reached, the optimal solution is found at $\mathbf{d}^{(k)}$, and the process stops. Otherwise update the reliability index $\beta^{(k+1)}$ by

$$\mathbf{u}_{iXMPP}^{(k+1)} = \beta^{(k+1)} \frac{\nabla g(\mathbf{u}_{iXMPP}^{(k)})}{\|\mathbf{u}_{iXMPP}^{(k)}\|} \quad (38)$$

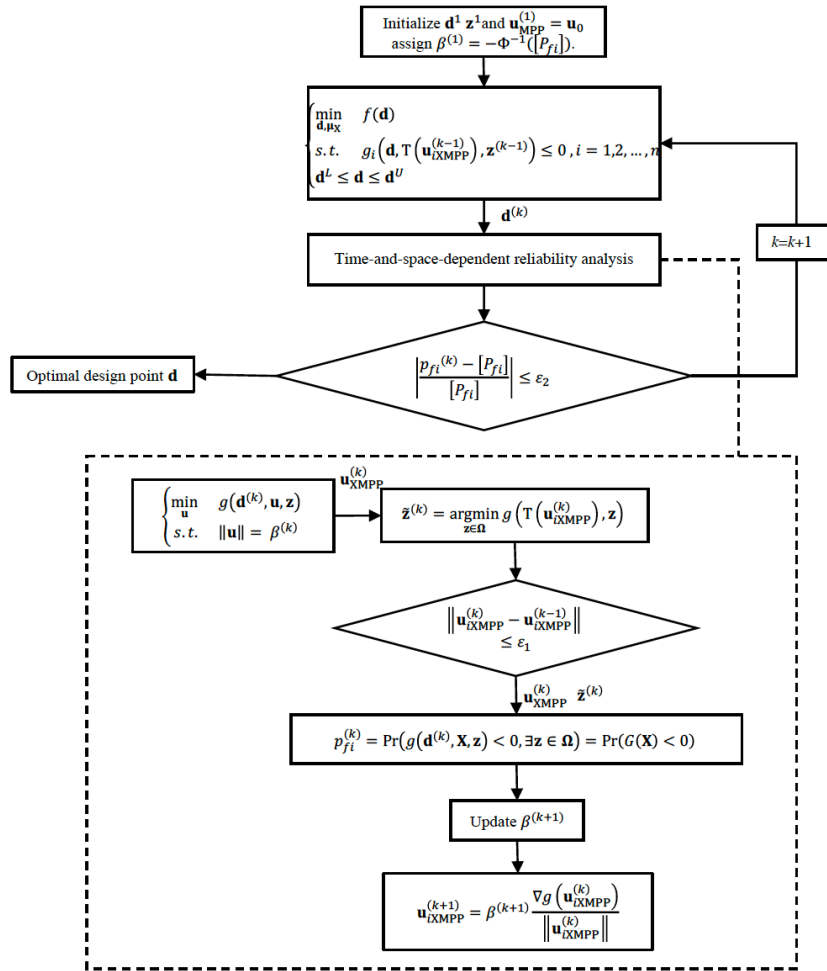


Figure 6.2 Sequential RBDO with the envelope method

6.4 Examples

A mathematical example is provided to show the feasibility of the proposed method. Three engineering examples are then used to demonstrate the computational efficiency and accuracy of the proposed method compared with double-loop method using the direct second-order reliability method (SORM/DL) and double-loop method with FORM (FORM/DL). The accuracy is assessed

by the probability of failure obtained from MCS at the optimal point while the efficiency is measured by the number of function calls. The percentage error is computed by

$$\varepsilon = \frac{|p_f - p_f^{\text{MCS}}|}{p_f^{\text{MCS}}} \times 100\% \quad (39)$$

where p_f is the result from a non-MCS method while p_f^{MCS} is from MCS.

6.4.1 Example 1: A Mathematical Problem

Two independent random variables X_1 and X_2 are normally distributed with $X_1 \sim N(\mu_{X_1}, 0.6)$ and $X_2 \sim N(\mu_{X_2}, 0.6)$. The time t varies over the interval $[0,1]$, and the spatial variable s changes over the interval $[172]$. The design variables are μ_{X_1} and μ_{X_2} . The limit-state function is defined by

$$g(\mathbf{X}, s, t) = \frac{80}{(s^2 - s + X_1^2 + 8X_2 + t - \sin(t) + 5)} - 1 \quad (40)$$

The RBD model is defined as follows:

$$\begin{cases} \min_{\mu_{X_1}, \mu_{X_2}} f = -(\mu_{X_1} + \mu_{X_2}) \\ \text{s. t. } \Pr\{g(\mathbf{X}, s, t) > 0\} \geq \Phi(\beta) \\ \quad -5 \leq \mu_{X_1} \leq 10 \\ \quad -5 \leq \mu_{X_2} \leq 10 \end{cases} \quad (41)$$

The allowable reliability index β is 3. The problem is solved by the proposed method, SORM/DL and FORM/DL. The results are given in Table 6.1.

Table 6.1 Results of Example 1

Methods	New method	SORM/DL	FORM/DL
Obj	-7.2867	-7.2867	-7.3096
$\boldsymbol{\mu}$	(2.7177, 4.5691)	(2.7177, 4.5691)	(2.7275, 4.5821)
p_f^{MCS} ($\times 10^{-3}$)	1.3679	1.3666	1.4942
Error (%)	1.33	1.23	10.68
N_{calls}	341	4317	747

The optimal result with the proposed method is shown in Fig. 6.3, which shows the optimal result is stable after 5 iterations.

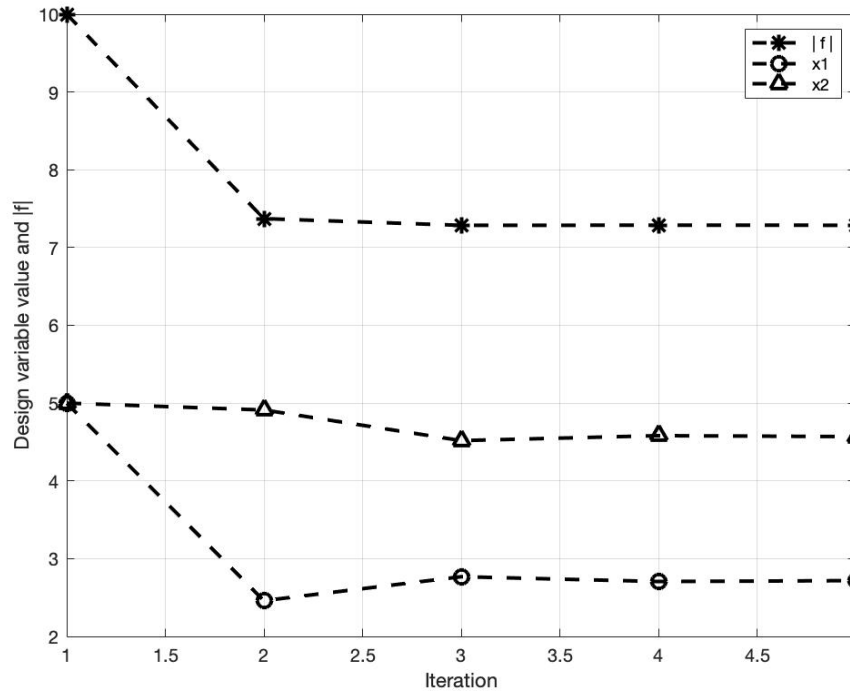


Figure 6.3 Iterative process of the objective function and design variables

6.4.2 Example 2: Three Bar System

A truss structure is shown in Fig. 6.4. Each bar of the system has its cross-sectional area A_i and modulus of elasticity, E_i , $i = 1,2,3$. The coefficient of thermal expansion of all bars is $\alpha = 12 \times 10^{-6} \text{C}^{-1}$. The temperature change is related to the installation height of the truss structure and is given by $\Delta T = T e^{-0.01(\Delta h^2 + 2\Delta h - 2)^2}$, where $\Delta h \in [1,6]$ m is the difference between two different installation heights. A downward force $P = P_0(0.9 + 0.1 \cos(0.2t))$ is applied at joint A , where $t \in [0,10]$ years. All the random variables are given in Table 6.2. The design variables are the cross-section areas of the bars μ_{A_1} , μ_{A_2} and μ_{A_3} .

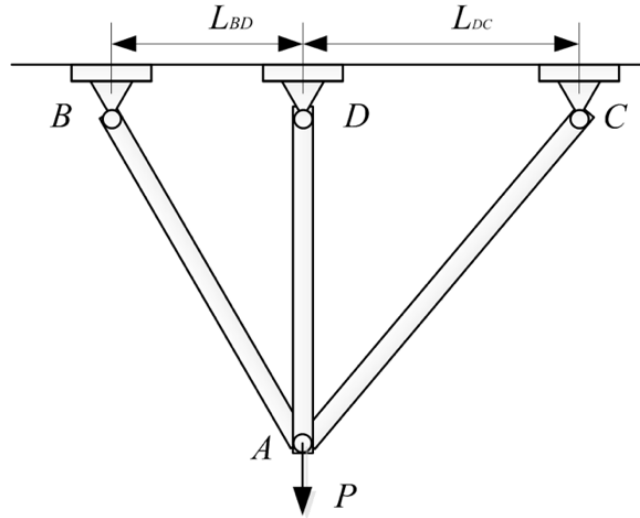


Figure 6.4 A truss structure

Table 6.2 Random variables of Example 2

Variable	Mean	Standard deviation	Distribution
$A_1(\text{mm}^2)$	μ_{A_1}	0.6	Normal
$A_2(\text{mm}^2)$	μ_{A_2}	0.6	Normal
$A_3(\text{mm}^2)$	μ_{A_3}	0.6	Normal
$E_1(\text{GPa})$	200	20	Normal
$E_2(\text{GPa})$	200	20	Normal
$E_3(\text{GPa})$	200	20	Normal
$P_0(\text{KN})$	40	6	Normal
$L_{AB}(\text{mm})$	200	2	Normal
$L_{AD}(\text{mm})$	231	2.31	Normal
$L_{AC}(\text{mm})$	283	2.83	Normal
$T(^{\circ}\text{C})$	35	7	Normal
$\sigma_{yield}(\text{GPa})$	7.5×10^8	4×10^7	Normal

The objective function is to minimize the weight given by

$$f = \mu_{A_1}\mu_{L_{AC}} + \mu_{A_2}\mu_{L_{AD}} + \mu_{A_3}\mu_{L_{AC}}$$

There are two failure modes for this truss structure. The first failure mode is that the perpendicular displacement of joint A , denoted as $\Delta\delta$, is greater than the allowable displacement δ_0 , and the limit-state function is defined by

$$g_1(\mathbf{X}, s, t) = \delta_0 - \Delta\delta \quad (42)$$

where $\delta_0 = 0.64$, and the perpendicular displacement of joint A is calculated by

$$\Delta\delta = \frac{A}{B}$$

where

$$\begin{aligned} A &= L_{AD}(PA_1E_1L_{AC}\cos\theta_1^2 + PA_2E_2L_{AB}\cos\theta_2^2 + A_1A_3E_1E_3L_{AC}T\alpha\cos\theta_1^2 \\ &\quad + A_2A_3E_2E_3L_{AB}T\alpha\cos\theta_2^2 + A_1A_2E_1E_2T\alpha(L_{AB}\sin\theta_1\cos\theta_2^2 + L_{AC}\sin\theta_2\cos\theta_1^2 \\ &\quad + L_{AC}\sin\theta_1\cos\theta_2\cos\theta_1 + L_{AB}\sin\theta_2\cos\theta_2\cos\theta_1)) \\ B &= A_1A_3E_1E_3L_{AC}\cos\theta_1^2 + A_2A_3E_2E_3L_{AB}\cos\theta_2^2 \\ &\quad + A_1A_2E_1E_2L_{AD}(\sin\theta_2^2\cos\theta_1^2 + \sin\theta_1^2\cos\theta_2^2 + 2\sin\theta_1\sin\theta_2\cos\theta_1\cos\theta_2) \\ \theta_1 &= \arctan\left(\frac{L_{AD}}{\sqrt{L_{AB}^2 - L_{AD}^2}}\right) \\ \theta_2 &= \arctan\left(\frac{L_{AD}}{\sqrt{L_{AC}^2 - L_{AD}^2}}\right) \end{aligned}$$

The second failure mode occurs when the stress at the joint is greater than the yield strength, and the limit-state function is defined by

$$g_2(\mathbf{X}, s, t) = \sigma_y - \sigma \quad (43)$$

where

$$\sigma = \frac{C}{D}$$

$$\begin{aligned} C &= A_1A_2A_3^2E_1E_2E_3T\alpha(L_{AC}\cos\theta_1^2\sin\theta_2 + L_{AB}\cos\theta_2^2\sin\theta_1 - 2L_{AD}\sin\theta_1\sin\theta_2\cos\theta_1\cos\theta_2 \\ &\quad + L_{AC}\cos\theta_1\cos\theta_2\sin\theta_1 + L_{AB}\cos\theta_1\cos\theta_2\sin\theta_2 - L_{AD}\cos\theta_2^2\sin\theta_1^2 \\ &\quad - L_{AD}\cos\theta_1^2\sin\theta_2^2) + A_2A_3E_2E_3FL_{AB}L_{AB}\cos\theta_2^2 + A_1A_3E_1E_3FL_{AC}\cos\theta_1^2 \\ D &= A_1A_2E_1E_2L_{AD}(\cos\theta_1^2\sin\theta_2^2 + \cos\theta_2^2\sin\theta_1^2) + A_1A_3E_1E_3L_{AC}\cos\theta_1^2 + A_2A_3E_2E_3L_{AB}\cos\theta_2^2 \\ &\quad + 2A_1A_2E_1E_2L_{AD}\sin\theta_1\sin\theta_2\cos\theta_1\cos\theta_2 \end{aligned}$$

The RBD model is given by

$$\left\{ \begin{array}{l} \min_{\mu_{A_1}\mu_{A_2}\mu_{A_3}} f = \mu_{A_1}\mu_{L_{AC}} + \mu_{A_2}\mu_{L_{AD}} + \mu_{A_3}\mu_{L_{AC}} \\ \text{s. t. } \Pr\{g_1(\mathbf{X}, s, t) = \delta_0 - \Delta\delta > 0\} \geq \Phi(\beta_1) \\ \Pr\{g_2(\mathbf{X}, s, t) = \sigma_y - \sigma > 0\} \geq \Phi(\beta_2) \\ 10 \leq \mu_{A_1} \leq 80 \\ 10 \leq \mu_{A_2} \leq 80 \\ 10 \leq \mu_{A_3} \leq 60 \end{array} \right. \quad (44)$$

The allowable reliability indexes are $\beta_i = 2.3, i = 1, 2$. The optimal results shown in Table 6.3. The proposed method is more accurate than SORA/DL and FORM/DL.

Table 6.3 Results of Example 2

Method	New method	DL/SORM	DL/FORM
Obj ($\times 10^4 \text{mm}^3$)	3.6616	3.6624	3.7189
$\mu(\text{mm})$	(53.41,38.83,60)	(53.31,38.95,60)	(53.05,38.57,60)
p_{f1}^{MCS}	0.0107	0.0107	0.0148
$\varepsilon_{p_{f1}}(\%)$	0.25	0.46	4.89
p_{f2}^{MCS}	0.0107	0.0107	0.0112
$\varepsilon_{p_{f2}}(\%)$	0.24	0.46	4.89
N_{calls}	2194	23500	7264

6.4.3 Example 3: A Cantilever Beam

Figure 6.5 shows that the end of cantilever beam is subjected to two forces F_1 and F_2 . The length of the cantilever beam L is 100 in. The objective is to minimize the volume $f = \mu_w\mu_h L$, where w and h represent the width and height of the beam cross section, respectively. There are two failure modes. The first failure mode is that the stress at the fixed end is greater than the allowable yield stress S_y , and the second failure mode is that the tip displacement of the beam is greater than the allowable displacement $D_0 = 2.5$ in. The two limit-state functions are given by

$$g_1(\mathbf{X}, s, t) = S_y - \frac{6L}{wh} \left(\frac{F_1}{h} - \frac{F_2}{w} \right) \quad (45)$$

$$g_2(\mathbf{X}, s, t) = D_0 - \frac{4L^3}{Ewh} \sqrt{\left(\frac{F_1}{h^2}\right)^2 + \left(\frac{F_2}{w^2}\right)^2} \quad (46)$$

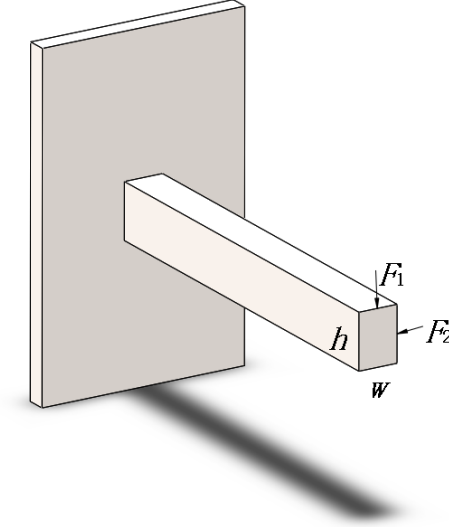


Figure 6.5 A cantilever beam

The distributions of the random design variables and random parameters are in Table 6.4. The force F_1 is a non-stationary Gaussian random field, whose mean is $\mu_{F_1} = 500e^{0.01\left(\left(s-\frac{1}{2}\right)^2 + (t-6)^2\right)}$ lbs and standard deviation is $\sigma_{F_1} = 50$ lbs. The spatial variable is $s \in [0,1]$ in and temporal variable is $t \in [0,10]$ years. The autocorrelation coefficient function of the Gaussian field is given by

$$\rho_{F_1}(s_1, t_1; s_2, t_2) = \exp\left[-\left(\frac{s_1 - s_2}{10}\right)^2 - \left(\frac{t_1 - t_2}{10}\right)^2\right] \quad (47)$$

The RBDO model is formulated as

$$\begin{cases} \min_{\mu_w, \mu_h} & f = \mu_w \mu_h L \\ \text{s. t.} & \Pr\{g_1(\mathbf{X}, s, t) > 0\} \geq \Phi(\beta_1) \\ & \Pr\{g_2(\mathbf{X}, s, t) > 0\} \geq \Phi(\beta_2) \\ & 1 \leq \mu_w \leq 4 \\ & 1 \leq \mu_h \leq 4 \end{cases} \quad (48)$$

The allowable reliability indexes are $\beta_i = 3, i = 1, 2$. The results are listed in Table 6.5. The optimal design variables are $w = 3.9541$ in and $h = 2.2531$ in, and the objective function value is $f = 890.9152$ in³ by the proposed method. The probabilities of failure obtained at the optimal

design variables by MCS are $p_{f_1}^{MCS} = 1.3633 \times 10^{-4}$ and $p_{f_1}^{MCS} = 1.3645 \times 10^{-4}$. The results are more accurate than those of DL/SORM and DL/FORM methods. In terms of the efficiency, the proposed method is the most efficient method as the number of function calls is 1358 compared with the function of calls of DL/SORM and DL/FORM are 12904 and 2098. In general, the proposed method is the best method due to high the accuracy and efficiency.

Table 6.4 Distributions of variables in Example 3

Variable	Mean	Standard deviation	Distribution
w(in)	μ_w	5×10^{-4}	Normal
h(in)	μ_h	5×10^{-4}	Normal
F_1 (lb)	1×10^{-1}	1×10^{-3}	Normal
E (psi)	2.9×10^7	1×10^5	Normal
S_y (psi)	3.9×10^4	500	Normal

Table 6.5 Results of Example 3

Method	New method	DL/SORM	DL/FORM
Obj (in ³)	890.9152	890.9183	890.8754
μ (in)	(3.9541,2.2531)	(3.9539,2.2533)	(3.9578,2.2509)
$p_{f_1}^{MCS}$ ($\times 10^{-4}$)	1.3633	1.3623	1.3623
$\varepsilon_{p_{f_1}}$ (%)	0.992	0.992	0.918
$p_{f_2}^{MCS}$ ($\times 10^{-4}$)	1.3645	1.3600	1.4397
$\varepsilon_{p_{f_2}}$ (%)	0.748	1.081	6.652
N_{calls}	1358	12904	2098

6.4.4 Example 4: Thermal Deflection of a Bimetallic Beam

Thermal expansion or contraction of a bimetallic beam occurs due to temperature change. The temperature in the operating room varies during the day and night and is given by $\Delta T = T(0.01 \sin(0.1t) + 1)$, where $t \in [0,24]$ hours. The typical bimetallic beam consists of two materials bonded together copper and invar. E_C is the young's modulus of the copper and E_I is the young's modulus of the invar. The length of the beam depends on the location of the installation, which is given by $L = L_0(-s^2 + s + 1)$, where $s \in [0,1]$ m. When the temperature change as a thermal load applies on the beam, the beam will deflect in the perpendicular direction at the right end side shown in Fig. 6.6. The design variables are $\mathbf{d} = (h, w)$, where h and w represent the height and width of the cross-sectional area of the beam, and their means are μ_h and μ_w , which are to be determined. All the random variables are listed in Table 6.6.

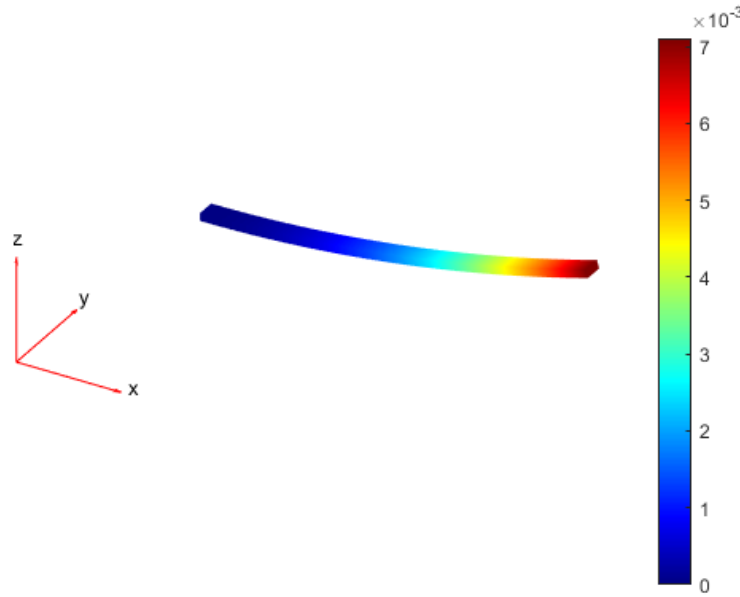


Figure 6.6 Deflection of the Bimetallic Beam

The failure mode is that the deflection exceeds $\delta = 8 \times 10^{-3}$. The limit-state function is given by

$$g(\mathbf{X}, s, t) = \delta - \Delta(\mathbf{d}, E_C, E_I, \Delta T) \quad (49)$$

where $\Delta(\mathbf{d}, E_C, E_I, \Delta T)$ is solved by the finite element method (FEM), which proves that the proposed method can be used for black-box simulations.

The objective is to minimize the weight of this beam. The RBD model is defined by

$$\begin{cases} \min_{\mu_w, \mu_h} f = \mu_w \mu_h \\ \text{s. t. } \Pr\{g(\mathbf{X}, s, t) > 0\} \geq \Phi(\beta) \\ 8 \times 10^{-4} \leq \mu_w \leq 2 \times 10^{-3} \\ 1 \times 10^{-4} \leq \mu_h \leq 1 \times 10^{-2} \end{cases} \quad (50)$$

All the results are listed in Table 6.7. The proposed method is the most efficient and accurate method among three methods as the error is only 3.04% and the number of function calls is 332.

Table 6.6 Random variables

Variable	Mean	Standard deviation	Distribution
$w(\text{m})$	μ_w	5×10^{-4}	Normal
$h(\text{m})$	μ_h	5×10^{-4}	Normal
$L(\text{m})$	1×10^{-1}	1×10^{-3}	Normal
$E_C(\text{Pa})$	1.37×10^{11}	1.37×10^7	Lognormal
$E_I(\text{Pa})$	1.30×10^{11}	1.3×10^7	Lognormal
$T(^{\circ}\text{C})$	130	13	Lognormal

Table 6.7 Results of Example 4

Method	New method	DL/SORM	DL/FORM
Obj ($\times 10^{-6}\text{m}^2$)	1.9197	1.9181	1.9312
μ ($\times 10^{-4}\text{m}$)	(8,2.3996)	(8,2.3975)	(8,2.4319)
pf^{MCS}	0.0013	0.0014	0.0012
Error (%)	3.04	5.71	10.43
N	332	3645	573

6.5 Summary

This paper develops a new sequential RBDO with the envelope method for time- and space-dependent reliability. The challenge in this work is to search for the equivalent most probable point

(MPP), which can be found by iterating MPP search and updating the equivalent reliability index. When the limit-state functions are inputted with only random variables and random fields, the single loop inverse MPP search can be used instead of sequentially inverse MPP search. Once the equivalent MPP is available, the time- and space-dependent problem is transformed into a static counterpart and the second-order saddlepoint approximation is used to estimate the reliability with higher accuracy. The equivalent MPP assures that the overall optimization is performed sequentially in cycles of deterministic optimization and reliability analysis. The proposed strategy has been proven to be effective in four examples.

The proposed method is more accurate than the first order methods since it uses second-order saddlepoint approximation to estimate the reliability. The new method, however, suffers from the same limitations as other MPP-based reliability methods. For instance, a local MPP, instead of the global MPP, may be found, thereby resulting in lower accuracy in the reliability prediction. The other limitation is that the proposed method cannot handle the case where the MPP occurs on boundaries of the time and space domain. In this case, the accuracy of reliability prediction will deteriorate. Our future work will focus how to accommodate MPPs on the boundaries of the time and space domain.

7. CONCLUSIONS AND FUTURE WORK

7.1 Conclusions

The objective of this dissertation is to predict reliability in the design phase and reliability-based design with Kriging and Envelope methods. This dissertation includes five research tasks. In the first task, an accurate method based on the Gaussian regression with active learning method is developed to predict the system reliability. In the second task, we propose the second-order saddlepoint approximation method to predict the system reliability. In the third task, an accurate method based on envelope function, efficient global optimization, and the second-order approximation is developed to predict time-dependent system reliability. In the fourth task, we extend the envelope method to deal with the time- and space-dependent reliability analysis. In the last task, the envelope method for time- and space-dependent reliability-based design is proposed. This task uses the idea of sequential optimization to decouple the double loop optimization into deterministic optimization and reliability analysis. Based on results of the above research tasks, we provide conclusions as follows.

The results of research task I (system reliability system with Kriging method) show that accounting for the dependence between responses at different input points can improve the accuracy and efficiency of the system reliability prediction. The use of active learning also helps reduce the computational time. The proposed method is more accurate than the independent kriging method giving the same computational time. The proposed method is also more efficient than the independent kriging method giving the same accuracy requirement. However, the proposed method does not consider the dependence among components. Considering the dependence among components could further improve accuracy and efficiency of the system reliability prediction.

The results of research task II (system reliability analysis with second order approximation) indicate that second-order saddlepoint approximation method (SOSPA) is more accurate than second order reliability method (SORM) and first-order reliability method (FORM) with increasing function calls. SOSPA accurately produces the marginal distributions of all component responses. The dependences between component responses are considered with only the first-order

approximation for the sake of efficiency. The accuracy of the proposed method can be furtherly improved if we estimate component correlations more accurately by a second order approximation.

The results of research task III (time-dependent system analysis with envelope method) show that the envelope method is an alternative method for predicting time-dependent system reliability. The envelope method with second-order approximation is in general more accurate than the first-order approximation method. The proposed method works well if the envelope function is convex. It does not work for a special case where the worst-case MPP occurs at the boundary of a time interval as the envelope function is not differentiable at the end points of an interval.

The results of research task VI (time- and space-dependent reliability analysis with envelope method) prove that the proposed method can efficiently produce an accurate time- and space-dependent reliability prediction with second-order approximation. The worst-case MPP can be found quickly by combining sequential efficient global optimization with the first-order reliability method. The major computational cost is the MPP search and second derivative calculations of the envelope function.

The last task demonstrates that the new method can achieve the most accurate design result among all methods by employing the envelope method for time- and space-dependent reliability-based design. The proposed method also shows that the sequential-loop method is much more efficient than the double-loop reliability-based design method. The new method still suffers from the same limitation as other MPP-based reliability methods. It may not work when multiple MPPs exist.

7.2 Future Work

This dissertation mainly focuses on series system reliability analysis. Our future work will address the following areas. (1) The accuracy of the system reliability analysis can be furtherly improved if we estimate the component correlations with the second-order approximation method. Besides, since the envelope function might have multiple MPPs, developing advanced methods to identify all important MPPs might achieve more accurate prediction results. (2) In terms of the applications of developed methods, we can apply our developed methods to more complicated engineering systems, such as parallel systems and mixed systems with multiple types of random variables, stochastic processes, and random processes.

REFERENCES

- [1] Zio, E., 2009, "Reliability engineering: Old problems and new challenges," *Reliability Engineering & System Safety*, 94(2), pp. 125-141.
- [2] Wu, H., Khan, M., Du, X., Sawchuk, A. P., and Yu, H. W., 2019, "Reliability Analysis for Image-based Non-invasive Pressure Quantification in Aortorenal Artery Systems," *Circulation Research*, 125(Suppl_1), pp. A122-A122.
- [3] Yu, H., Khan, M., Wu, H., Zhang, C., Du, X., Chen, R., Fang, X., Long, J., and Sawchuk, A. P., 2022, "Inlet and Outlet Boundary Conditions and Uncertainty Quantification in Volumetric Lattice Boltzmann Method for Image-Based Computational Hemodynamics," *Fluids*, 7(1), p. 30.
- [4] Yin, J., and Du, X., "Uncertainty Quantification by Convolutional Neural Network Gaussian Process Regression with Image and Numerical Data," *Proc. AIAA SCITECH 2022 Forum*, p. 1100.
- [5] Yin, J., Shen, D., Du, X., and Li, L., 2022, "Distributed Stochastic Model Predictive Control With Taguchi's Robustness for Vehicle Platooning," *IEEE Transactions on Intelligent Transportation Systems*.
- [6] Barone, G., and Frangopol, D. M., 2014, "Reliability, risk and lifetime distributions as performance indicators for life-cycle maintenance of deteriorating structures," *Reliability Engineering & System Safety*, 123, pp. 21-37.
- [7] Rausand, M., and Høyland, A., 2003, *System reliability theory: models, statistical methods, and applications*, John Wiley & Sons.
- [8] Hohenbichler, M., and Rackwitz, R., 1982, "First-order concepts in system reliability," *Structural Safety*, 1(3), pp. 177-188.
- [9] Gollwitzer, S., and Rackwitz, R., 1983, "Equivalent components in first-order system reliability," *Reliability Engineering*, 5(2), pp. 99-115.
- [10] Hu, Z., Zhu, Z., and Du, X., 2017, "Time-Dependent System Reliability Analysis for Bivariate Responses," *ASCE-ASME J Risk and Uncert in Engrg Sys Part B Mech Engrg*, 4(3).
- [11] Maier, H. R., Lence, B. J., Tolson, B. A., and Foschi, R. O., 2001, "First-order reliability method for estimating reliability, vulnerability, and resilience," *Water Resources Research*, 37(3), pp. 779-790.
- [12] Yin, J., and Du, X., 2022, "High-Dimensional Reliability Method Accounting for Important and Unimportant Input Variables," *Journal of Mechanical Design*, 144(4).

- [13] Du, X., and Zhang, J., 2010, "A Second-Order Reliability Method With First-Order Efficiency," *Journal of Mechanical Design*, 132(10).
- [14] Wu, H., and Du, X., 2020, "System Reliability Analysis With Second-Order Saddlepoint Approximation," *ASCE-ASME J Risk and Uncert in Engrg Sys Part B Mech Engrg*, 6(4).
- [15] Lim, J., Lee, B., and Lee, I., 2014, "Second-order reliability method-based inverse reliability analysis using Hessian update for accurate and efficient reliability-based design optimization," *International Journal for Numerical Methods in Engineering*, 100(10), pp. 773-792.
- [16] Daniels, H. E., 1954, "Saddlepoint Approximations in Statistics," *The Annals of Mathematical Statistics*, 25(4), pp. 631-650.
- [17] Butler, R. W., 2007, *Saddlepoint approximations with applications*, Cambridge University Press.
- [18] Guo, S., 2014, "An efficient third-moment saddlepoint approximation for probabilistic uncertainty analysis and reliability evaluation of structures," *Applied Mathematical Modelling*, 38(1), pp. 221-232.
- [19] Du, X., 2010, "System reliability analysis with saddlepoint approximation," *Structural and Multidisciplinary Optimization*, 42(2), pp. 193-208.
- [20] Wu, H., and Du, X., "System Reliability Analysis With Second Order Saddlepoint Approximation," *Proc. ASME 2019 International Design Engineering Technical Conferences and Computers and Information in Engineering Conference*V02BT03A039.
- [21] Mooney, C. Z., 1997, *Monte carlo simulation*, Sage Publications.
- [22] Binder, K., Heermann, D., Roelofs, L., Mallinckrodt, A. J., and McKay, S., 1993, "Monte Carlo simulation in statistical physics," *Computers in Physics*, 7(2), pp. 156-157.
- [23] Cadini, F., and Gioletta, A., 2016, "A Bayesian Monte Carlo-based algorithm for the estimation of small failure probabilities of systems affected by uncertainties," *Reliability Engineering & System Safety*, 153, pp. 15-27.
- [24] Melchers, R. J. S. s., 1989, "Importance sampling in structural systems," *Structural Safety*, 6(1), pp. 3-10.
- [25] Moarefzadeh, M., and Melchers, R., 1999, "Directional importance sampling for ill-proportioned spaces," *Structural Safety*, 21(1), pp. 1-22.
- [26] Huang, X., Chen, J., and Zhu, H., 2016, "Assessing small failure probabilities by AK-SS: An active learning method combining Kriging and Subset Simulation," *Structural Safety*, 59, pp. 86-95.

- [27] Au, S.-K., and Beck, J. L., 2001, "Estimation of small failure probabilities in high dimensions by subset simulation," *Probabilistic engineering mechanics*, 16(4), pp. 263-277.
- [28] Wang, Z., Mourelatos, Z. P., Li, J., Baseski, I., and Singh, A., 2014, "Time-Dependent Reliability of Dynamic Systems Using Subset Simulation With Splitting Over a Series of Correlated Time Intervals," *Journal of Mechanical Design*, 136(6).
- [29] Shi, Y., Lu, Z., and He, R., 2020, "Advanced time-dependent reliability analysis based on adaptive sampling region with Kriging model," *Proceedings of the Institution of Mechanical Engineers, Part O: Journal of Risk and Reliability*, p. 1748006X20901981.
- [30] Ulaganathan, S., Couckuyt, I., Dhaene, T., Degroote, J., and Laermans, E., 2016, "High dimensional Kriging metamodelling utilising gradient information," *Applied Mathematical Modelling*, 40(9-10), pp. 5256-5270.
- [31] Moustapha, M., Bourinet, J.-M., Guillaume, B., and Sudret, B., 2018, "Comparative Study of Kriging and Support Vector Regression for Structural Engineering Applications," *ASCE-ASME Journal of Risk and Uncertainty in Engineering Systems, Part A: Civil Engineering*, 4(2), p. 04018005.
- [32] Wang, Z., and Wang, P., 2012, "A Nested Extreme Response Surface Approach for Time-Dependent Reliability-Based Design Optimization," *Journal of Mechanical Design*, 134(12), pp. 121007-121014.
- [33] Dai, H., Zhang, H., and Wang, W., 2015, "A Multiwavelet Neural Network-Based Response Surface Method for Structural Reliability Analysis," *Computer-Aided Civil and Infrastructure Engineering*, 30(2), pp. 151-162.
- [34] Chengying, L., Hao, W., Liping, W., and Zhi, Z., 2017, "Tool wear state recognition based on LS-SVM with the PSO algorithm," *Journal of Tsinghua University (Science and Technology)*, 57(9), pp. 975-979.
- [35] Yin, J., and Du, X., 2022, "Active learning with generalized sliced inverse regression for high-dimensional reliability analysis," *Structural Safety*, 94, p. 102151.
- [36] Jiang, C., Li, W., Han, X., Liu, L., and Le, P., 2011, "Structural reliability analysis based on random distributions with interval parameters," *Computers & Structures*, 89(23-24), pp. 2292-2302.
- [37] Wu, H., Zhu, Z., and Du, X., 2020, "System Reliability Analysis With Autocorrelated Kriging Predictions," *Journal of Mechanical Design*, 142(10).
- [38] Yang, R., and Gu, L., 2004, "Experience with approximate reliability-based optimization methods," *Structural and multidisciplinary optimization*, 26(1), pp. 152-159.

- [39] Liang, J., Mourelatos, Z. P., and Nikolaidis, E., 2007, "A single-loop approach for system reliability-based design optimization." *Journal of Mechanical Design*, 129(12): 1215–1224.
- [40] Du, X., Guo, J., and Beeram, H., 2008, "Sequential optimization and reliability assessment for multidisciplinary systems design," *Structural and Multidisciplinary Optimization*, 35(2), pp. 117-130.
- [41] Yin, J., and Du, X., 2021, "A safety factor method for reliability-based component design," *Journal of Mechanical Design*, 143(9).
- [42] Hu, Z., Mansour, R., Olsson, M., and Du, X., 2021, "Second-order reliability methods: a review and comparative study," *Structural and Multidisciplinary Optimization*, 64(6), pp. 3233-3263.
- [43] Moustapha, M., Marelli, S., and Sudret, B., 2022, "Active learning for structural reliability: Survey, general framework and benchmark," *Structural Safety*, p. 102174.
- [44] Der Kiureghian, A., and Zhang, Y., 1999, "Space-variant finite element reliability analysis," *Computer methods in applied mechanics and engineering*, 168(1-4), pp. 173-183.
- [45] Hu, Z., and Du, X., 2015, "Mixed efficient global optimization for time-dependent reliability analysis," *Journal of Mechanical Design*, 137(5), p. 051401.
- [46] Hu, Z., and Du, X., 2013, "Time-dependent reliability analysis with joint upcrossing rates," *Structural and Multidisciplinary Optimization*, 48(5), pp. 893-907.
- [47] Zhang, J., and Du, X., 2011, "Time-dependent reliability analysis for function generator mechanisms." *Journal of Mechanical Design*, 133(3): 031005.
- [48] Wu, H., Hu, Z., and Du, X., 2021, "Time-Dependent System Reliability Analysis With Second-Order Reliability Method," *Journal of Mechanical Design*, 143(3), p. 031101.
- [49] Wu, H., and Du, X., "Time-Dependent System Reliability Analysis With Second Order Reliability Method," *Proc. ASME 2020 International Design Engineering Technical Conferences and Computers and Information in Engineering Conference*V11BT11A045.
- [50] Rice, S. O., 1944, "Mathematical analysis of random noise," *Bell System Technical Journal*, 23(3), pp. 282-332.
- [51] Ponte, R. V. d. M., 1985, "The theory of statistics of extremes and el nino phenomena: a stochastic approach," *Massachusetts Institute of Technology*.
- [52] Hu, Z., and Mahadevan, S., 2016, "A single-loop kriging surrogate modeling for time-dependent reliability analysis," *Journal of Mechanical Design*, 138(6), p. 061406.

- [53] Shi, Y., and Lu, Z., 2019, "Dynamic reliability analysis for structure with temporal and spatial multi-parameter," *Proceedings of the Institution of Mechanical Engineers, Part O: Journal of Risk and Reliability*, 233(6), pp. 1002-1013.
- [54] Wei, X., and Du, X., 2019, "Uncertainty Analysis for Time-and Space-Dependent Responses With Random Variables," *Journal of Mechanical Design*, 141(2), p. 021402.
- [55] Hao, W., and Du, X., 2022, "Envelope Method for Time-and Space-Dependent Reliability Prediction," *ASCE-ASME J Risk and Uncert in Engrg Sys Part B Mech Engrg*.
- [56] Singh, A., Mourelatos, Z. P., and Li, J., 2010, "Design for Lifecycle Cost Using Time-Dependent Reliability," *Journal of Mechanical Design*, 132(9), pp. 091008-091008-091011.
- [57] Hu, Z., and Du, X., 2014, "Lifetime cost optimization with time-dependent reliability," *Engineering Optimization*, 46(10), pp. 1389-1410.
- [58] Lee, I., Choi, K. K., and Gorsich, D., 2010, "Sensitivity analyses of FORM-based and DRM-based performance measure approach (PMA) for reliability-based design optimization (RBDO)," *International Journal for Numerical Methods in Engineering*, 82(1), pp. 26-46.
- [59] Du, X., and Hu, Z., 2012, "First order reliability method with truncated random variables," *Journal of Mechanical Design*, 134(9), p. 091005.
- [60] Zhu, Z., Hu, Z., and Du, X., 2015, "Reliability Analysis for Multidisciplinary Systems Involving Stationary Stochastic Processes," *Proceedings of the ASME 2015 International Design Engineering Technical Conferences and Computers and Information in Engineering Conference. Volume 2B: 41st Design Automation Conference. Boston, Massachusetts, USA. August 2–5, 2015. V02BT03A050. ASME*.
- [61] Ditlevsen, O., and Madsen, H. O., 1996, *Structural reliability methods*, Wiley, Chichester; New York.
- [62] Zio, E., 2013, *The Monte Carlo Simulation Method for System Reliability and Risk Analysis*, Springer London.
- [63] Balesdent, M., Morio, J., and Marzat, J., 2013, "Kriging-based adaptive Importance Sampling algorithms for rare event estimation," *Structural Safety*, 44, pp. 1-10.
- [64] Dubourg, V., Sudret, B., and Deheeger, F., 2013, "Metamodel-based importance sampling for structural reliability analysis," *Probabilistic Engineering Mechanics*, 33, pp. 47-57.
- [65] Echard, B., Gayton, N., Lemaire, M., and Relun, N., 2013, "A combined Importance Sampling and Kriging reliability method for small failure probabilities with time-demanding numerical models," *Reliability Engineering & System Safety*, 111, pp. 232-240.

- [66] Wang, Z., and Wang, P., 2015, "An Integrated Performance Measure Approach for System Reliability Analysis," *Journal of Mechanical Design*, 137(2), pp. 021406-021406-021411.
- [67] Helton, J. C., Johnson, J. D., Sallaberry, C. J., and Storlie, C. B., 2006, "Survey of sampling-based methods for uncertainty and sensitivity analysis," *Reliability Engineering & System Safety*, 91(10), pp. 1175-1209.
- [68] Hurtado, J., and Barbat, A., 1998, "Monte Carlo techniques in computational stochastic mechanics," 5(1), p. 3.
- [69] Viana, F. A. C., Simpson, T. W., Balabanov, V., and Toropov, V., 2014, "Special Section on Multidisciplinary Design Optimization: Metamodeling in Multidisciplinary Design Optimization: How Far Have We Really Come?," *AIAA Journal*, 52(4), pp. 670-690.
- [70] Picheny, V., 2009, "Improving accuracy and compensating for uncertainty in surrogate modeling," University of Florida Gainesville.
- [71] Sacks, J., Welch, W. J., Mitchell, T. J., and Wynn, H. P., 1989, "Design and Analysis of Computer Experiments," *Statistical Science*, 4(4), pp. 409-423.
- [72] Youn, B. D., and Choi, K. K., 2004, "A new response surface methodology for reliability-based design optimization," *Computers & Structures*, 82(2), pp. 241-256.
- [73] Bucher, C. G., and Bourgund, U., 1990, "A fast and efficient response surface approach for structural reliability problems," *Structural Safety*, 7(1), pp. 57-66.
- [74] Hurtado, J. E., Alvarez, D., and engineering, 2001, "Neural-network-based reliability analysis: a comparative study," *Computer methods in applied mechanics and engineering*, 191(1-2), pp. 113-132.
- [75] Elhewy, A. H., Mesbahi, E., and Pu, Y., 2006, "Reliability analysis of structures using neural network method," *Probabilistic Engineering Mechanics*, 21(1), pp. 44-53.
- [76] Xiao, N.-C., Zuo, M. J., and Zhou, C., 2018, "A new adaptive sequential sampling method to construct surrogate models for efficient reliability analysis," *Reliability Engineering & System Safety*, 169, pp. 330-338.
- [77] Basudhar, A., Dribusch, C., Lacaze, S. and Missoum, S., 2012. "Constrained efficient global optimization with support vector machines," *Structural and Multidisciplinary Optimization*, 46(2), pp.201-221.
- [78] Bourinet, J. M., Deheeger, F., and Lemaire, M., 2011, "Assessing small failure probabilities by combined subset simulation and Support Vector Machines," *Structural Safety*, 33(6), pp. 343-353.

- [79] Basudhar, A. and Missoum, S., 2013. "Reliability assessment using probabilistic support vector machines," *International Journal of Reliability and Safety*, 7(2), pp.156-173.
- [80] Schöbi, R., Sudret, B., and Marelli, S., 2017, "Rare Event Estimation Using Polynomial-Chaos Kriging," *ASCE-ASME Journal of Risk and Uncertainty in Engineering Systems, Part A: Civil Engineering*, 3(2), p. D4016002.
- [81] Lophaven, S. N., Nielsen, H. B., and Sondergaard, J., 2002, "DACE-A Matlab Kriging toolbox, version 2.0," Technical University of Denmark.
- [82] Martin, J. D., and Simpson, T. W., 2005, "Use of Kriging Models to Approximate Deterministic Computer Models," *AIAA Journal*, 43(4), pp. 853-863.
- [83] Kleijnen, J. P. C., "Design and Analysis of Simulation Experiments," Springer International Publishing, pp. 3-22.
- [84] Jones, D. R., Schonlau, M., and Welch, W., 1998, "Efficient global optimization of expensive black-box functions," *Journal of Global optimization*, 13(4), pp. 455-492.
- [85] Bichon, B. J., Eldred, M. S., Swiler, L. P., Mahadevan, S., and McFarland, J. M., 2012, "Efficient Global Reliability Analysis for Nonlinear Implicit Performance Functions," *Aiaa Journal*, 46(10), pp. 2459-2468.
- [86] Bichon, B. J., McFarland, J. M., and Mahadevan, S., 2011, "Efficient surrogate models for reliability analysis of systems with multiple failure modes," *Reliability Engineering & System Safety*, 96(10), pp. 1386-1395.
- [87] Echard, B., Gayton, N., and Lemaire, M., 2011, "AK-MCS: An active learning reliability method combining Kriging and Monte Carlo Simulation," *Structural Safety*, 33(2), pp. 145-154.
- [88] Fauriat, W., and Gayton, N., 2014, "AK-SYS: An adaptation of the AK-MCS method for system reliability," *Reliability Engineering & System Safety*, 123, pp. 137-144.
- [89] Zhu, Z., and Du, X., 2016, "Reliability analysis with Monte Carlo simulation and dependent Kriging predictions," *Journal of Mechanical Design*, 138(12), p. 121403.
- [90] Viana, F. A. C., Venter, G., and Balabanov, V., 2010, "An algorithm for fast optimal Latin hypercube design of experiments," *International Journal for Numerical Methods in Engineering*, 82(2), pp. 135-156.
- [91] Sadoughi, M., Li, M., and Hu, C., 2018, "Multivariate system reliability analysis considering highly nonlinear and dependent safety events," *Reliability Engineering & System Safety*, 180, pp. 189-200.
- [92] McDonald, M., and Mahadevan, S., 2008, "Design Optimization With System-Level Reliability Constraints," *Journal of Mechanical Design*, 130(2), pp. 021403-021403-021410.

- [93] Smith, N., and Mahadevan, S., 2005, "Integrating System-Level and Component-Level Designs Under Uncertainty," *Journal of Spacecraft and Rockets*, 42(4), pp. 752-760.
- [94] Hu, Z., and Du, X., 2018, "Integration of Statistics- and Physics-Based Methods—A Feasibility Study on Accurate System Reliability Prediction," *Journal of Mechanical Design*, 140(7), pp. 074501-074501-074507.
- [95] Hu, Z. and Du, X., 2014. "Lifetime cost optimization with time-dependent reliability," *Engineering Optimization*, 46(10), pp.1389-1410.
- [96] Rausand, M., and Høyland, A., 2004, *System reliability theory: models, statistical methods, and applications*, John Wiley & Sons.
- [97] Ditlevsen, O., 1979. "Narrow reliability bounds for structural systems," *Journal of structural mechanics*, 7(4), pp.453-472.
- [98] Song, J., and Der Kiureghian, A., 2003, "Bounds on system reliability by linear programming," *Journal of Engineering Mechanics*, 129(6), pp. 627-636.
- [99] Youn, B. D., and Wang, P., 2009, "Complementary intersection method for system reliability analysis," *Journal of Mechanical Design*, 131(4), p. 041004.
- [100] Du, X., 2010. "System reliability analysis with saddlepoint approximation," *Structural and Multidisciplinary Optimization*, 42(2), pp.193-208.
- [101] Kang, W.-H., Song, J., Gardoni, P., and Safety, S., 2008, "Matrix-based system reliability method and applications to bridge networks," *Reliability Engineering & System Safety*, 93(11), pp. 1584-1593.
- [102] Hu, C., Youn, B., and Optimization, M., 2011, "Adaptive-sparse polynomial chaos expansion for reliability analysis and design of complex engineering systems," *Structural and Multidisciplinary Optimization*, 43(3), pp. 419-442.
- [103] Rocco, C.M. and Moreno, J.A., 2002. "Fast Monte Carlo reliability evaluation using support vector machine," *Reliability Engineering & System Safety*, 76(3), pp.237-243.
- [104] Bichon, B., Eldred, M., Swiler, L., Mahadevan, S., and McFarland, J., 2007, "Multimodal reliability assessment for complex engineering applications using efficient global optimization," AIAA Paper No. AIAA-2007-1946.
- [105] Bichon, B. J., McFarland, J. M., and Mahadevan, S., 2011, "Efficient surrogate models for reliability analysis of systems with multiple failure modes," *Reliability Engineering and System Safety*, 96(10), pp. 1386-1395.

- [106] Fauriat, W., and Gayton, N., 2014, "AK-SYS: An adaptation of the AK-MCS method for system reliability," *Reliability Engineering and System Safety*, 123, pp. 137-144.
- [107] Madsen, H. O., Krenk, S., and Lind, N. C., 2006, *Methods of structural safety*, Courier Corporation.
- [108] Du, X., and Sudjianto, A., 2004, "First order saddlepoint approximation for reliability analysis," *AIAA journal*, 42(6), pp. 1199-1207.
- [109] Der Kiureghian, A., and Dakessian, T., 1998, "Multiple design points in first and second-order reliability," *Structural Safety*, 20(1), pp. 37-49.
- [110] Madsen, H., 1985, "First order vs. second order reliability analysis of series structures," *Structural Safety*, 2(3), pp. 207-214.
- [111] Du, X., 2008, "Saddlepoint approximation for sequential optimization and reliability analysis," *Journal of Mechanical Design*, 130(1), p. 011011.
- [112] Hohenbichler, M., and Rackwitz, R., 1982, "First-order concepts in system reliability," *Structural Safety*, 1(3), pp. 177-188.
- [113] Hu, Z., and Du, X., 2018, "Saddlepoint approximation reliability method for quadratic functions in normal variables," *Structural Safety*, 71, pp. 24-32.
- [114] Papadimitriou, D.I., Mourelatos, Z.P. and Hu, Z., 2019. "Reliability analysis using second-order saddlepoint approximation and mixture distributions," *Journal of Mechanical Design*, 141(2): 021401.
- [115] Der Kiureghian, A., Lin, H.Z. and Hwang, S.J., 1987. "Second-order reliability approximations," *Journal of Engineering mechanics*, 113(8), pp.1208-1225.
- [116] Konishi, S., Niki, N. and Gupta, A.K., 1988. Asymptotic expansions for the distribution of quadratic forms in normal variables. *Annals of the Institute of Statistical Mathematics*, 40(2), pp.279-296.
- [117] Tanizaki, H., 2004, *Computational methods in statistics and econometrics*, CRC Press.
- [118] Lugannani, R. and Rice, S., 1980. "Saddle point approximation for the distribution of the sum of independent random variables," *Advances in applied probability*, 12(2), pp.475-490.
- [119] Zeng, P., Jimenez, R., Li, T., Chen, Y., and Feng, X., 2017, "Application of Quasi-Newton Approximation-Based SORM for System Reliability Analysis of a Layered Soil Slope," *Geo-Risk* 2017, pp. 111-119.
- [120] Gollwitzer, S. and Rackwitz, R., 1988. "An efficient numerical solution to the multinormal integral," *Probabilistic Engineering Mechanics*, 3(2), pp.98-101.

- [121] Pandey, M.D., 1998. "An effective approximation to evaluate multinormal integrals," *Structural safety*, 20(1), pp.51-67.
- [122] Genz, A., 1992. "Numerical computation of multivariate normal probabilities," *Journal of computational and graphical statistics*, 1(2), pp.141-149.
- [123] Wei, P., Liu, F. and Tang, C., 2018. "Reliability and reliability-based importance analysis of structural systems using multiple response Gaussian process model," *Reliability Engineering & System Safety*, 175, pp.183-195.
- [124] Du, X., and Chen, W., 2004, "Sequential Optimization and Reliability Assessment Method for Efficient Probabilistic Design," *Journal of Mechanical Design*, 126(2), pp. 225-233.
- [125] Gu, L., Yang, R. J., Tho, C. H., Makowskit, M., Faruquet, O., and Y.Li, Y. L., 2001, "Optimisation and robustness for crashworthiness of side impact," *International Journal of Vehicle Design*, 26(4), pp. 348-360.
- [126] Singh, A., Mourelatos, Z. P., and Li, J., 2010, "Design for lifecycle cost using time-dependent reliability," *Journal of Mechanical Design*, 132(9).
- [127] Zhang, J., and Du, X., 2011, "Time-dependent reliability analysis for function generator mechanisms," *Journal of Mechanical Design*, 133(3).
- [128] Caprani, C. C., and OBrien, E. J., 2010, "The use of predictive likelihood to estimate the distribution of extreme bridge traffic load effect," *Structural safety*, 32(2), pp. 138-144.
- [129] Hu, Z., and Du, X., 2012, "Reliability analysis for hydrokinetic turbine blades," *Renewable Energy*, 48, pp. 251-262.
- [130] Andrieu-Renaud, C., Sudret, B., and Lemaire, M., 2004, "The PHI2 method: a way to compute time-variant reliability," *Reliability Engineering & System Safety*, 84(1), pp. 75-86.
- [131] Jiang, C., Wei, X. P., Huang, Z. L., and Liu, J., 2017, "An Outcrossing Rate Model and Its Efficient Calculation for Time-Dependent System Reliability Analysis," *Journal of Mechanical Design*, 139(4), pp. 041402-041402-041410.
- [132] Hu, Z., Li, H., Du, X., and Chandrashekhara, K., 2013, "Simulation-based time-dependent reliability analysis for composite hydrokinetic turbine blades," *Structural and Multidisciplinary Optimization*, 47(5), pp. 765-781.
- [133] Hu, Z., and Mahadevan, S., 2016, "A single-loop kriging surrogate modeling for time-dependent reliability analysis," *Journal of Mechanical Design*, 138(6).
- [134] Hu, Z., and Du, X., 2015, "Mixed efficient global optimization for time-dependent reliability analysis," *Journal of Mechanical Design*, 137(5).

- [135] Wang, Z., and Wang, P., 2013, "A new approach for reliability analysis with time-variant performance characteristics," *Reliability Engineering & System Safety*, 115, pp. 70-81.
- [136] Du, X., 2014, "Time-dependent mechanism reliability analysis with envelope functions and first-order approximation," *Journal of Mechanical Design*, 136(8).
- [137] Li, J., Chen, J.-b., and Fan, W.-l., 2007, "The equivalent extreme-value event and evaluation of the structural system reliability," *Structural safety*, 29(2), pp. 112-131.
- [138] Singh, A., and Mourelatos, Z. P., 2010, "On the time-dependent reliability of non-monotonic, non-repairable systems," *SAE International Journal of Materials and Manufacturing*, 3(1), pp. 425-444.
- [139] Hu, Z., and Du, X., "Second Order Reliability Method for Time-Dependent Reliability Analysis Using Sequential Efficient Global Optimization," *Proc. ASME 2019 International Design Engineering Technical Conferences and Computers and Information in Engineering Conference*, American Society of Mechanical Engineers Digital Collection.
- [140] Song, J., and Der Kiureghian, A., 2006, "Joint first-passage probability and reliability of systems under stochastic excitation," *Journal of Engineering Mechanics*, 132(1), pp. 65-77.
- [141] Radhika, B., Panda, S., and Manohar, C., 2008, "Time variant reliability analysis of nonlinear structural dynamical systems using combined Monte Carlo simulations and asymptotic extreme value theory," *Computer Modeling in Engineering and Sciences*, 27(1/2), p. 79.
- [142] Yu, S., Wang, Z., and Meng, D., 2018, "Time-variant reliability assessment for multiple failure modes and temporal parameters," *Structural and Multidisciplinary Optimization*, 58(4), pp. 1705-1717.
- [143] Gong, C., and Frangopol, D. M., 2019, "An efficient time-dependent reliability method," *Structural Safety*, 81, p. 101864.
- [144] Hu, Z., and Mahadevan, S., 2015, "Time-dependent system reliability analysis using random field discretization," *Journal of Mechanical Design*, 137(10), p. 101404.
- [145] Jiang, C., Wei, X., Wu, B., and Huang, Z., 2018, "An improved TRPD method for time-variant reliability analysis," *Structural and Multidisciplinary Optimization*, 58(5), pp. 1935-1946.
- [146] Jones, D. R., Schonlau, M., and Welch, W. J., 1998, "Efficient global optimization of expensive black-box functions," *Journal of Global optimization*, 13(4), pp. 455-492.
- [147] Wang, Z., and Wang, P., 2012, "A nested extreme response surface approach for time-dependent reliability-based design optimization," *Journal of Mechanical Design*, 134(12).
- [148] Goutis, C., and Casella, G., 1999, "Explaining the Saddlepoint Approximation," *American Statistician*, 53(3), pp. 216-224.

- [149] Hu, Z., and Du, X., 2018, "Saddlepoint approximation reliability method for quadratic functions in normal variables," *Structural Safety*, 71, pp. 24-32.
- [150] Gollwitzer, S., and Rackwitz, R., 1988, "An efficient numerical solution to the multinormal integral," *Probabilistic Engineering Mechanics*, 3(2), pp. 98-101.
- [151] Genz, A., 1992, "Numerical computation of multivariate normal probabilities," *Journal of computational and graphical statistics*, 1(2), pp. 141-149.
- [152] Genz, A., 2004, "Numerical computation of rectangular bivariate and trivariate normal and t probabilities," *Statistics and Computing*, 14(3), pp. 251-260.
- [153] Genz, A., and Bretz, F., 2009, *Computation of multivariate normal and t probabilities*, Springer Science & Business Media.
- [154] Li, C.-C., and Der Kiureghian, A., 1993, "Optimal discretization of random fields," *Journal of engineering mechanics*, 119(6), pp. 1136-1154.
- [155] Lemieux, C., 2009, *Monte Carlo and Quasi-Monte Carlo Sampling*, Springer, New York.
- [156] Binder, K., Heermann, D., Roelofs, L., Mallinckrodt, A. J., and McKay, S., 1993, "Monte Carlo simulation in statistical physics," 7(2), pp. 156-157.
- [157] Zhang, X., Lu, Z., Cheng, K., and Wang, Y., 2020, "A novel reliability sensitivity analysis method based on directional sampling and Monte Carlo simulation," *Proceedings of the Institution of Mechanical Engineers, Part O: Journal of Risk and Reliability*, p. 1748006X19899504.
- [158] Du, X., 2008, "Unified uncertainty analysis by the first order reliability method," *Journal of mechanical design*, 130(9).
- [159] Du, X., 2008, "Saddlepoint Approximation for Sequential Optimization and Reliability Analysis," *Journal of Mechanical Design*, 130(1), pp. 842-849.
- [160] Jeong, S., Murayama, M., and Yamamoto, K., 2005, "Efficient optimization design method using kriging model," *Journal of aircraft*, 42(2), pp. 413-420.
- [161] Zhou, C., Xiao, N.-C., Zuo, M. J., and Huang, X., 2020, "AK-PDF: An active learning method combining kriging and probability density function for efficient reliability analysis," *Proceedings of the Institution of Mechanical Engineers, Part O: Journal of Risk and Reliability*, 234(3), pp. 536-549.
- [162] Basudhar, A., Missoum, S., and Sanchez, A. H., 2008, "Limit state function identification using support vector machines for discontinuous responses and disjoint failure domains," *Probabilistic Engineering Mechanics*, 23(1), pp. 1-11.

- [163] Xiao, N.-C., Duan, L., and Tang, Z., 2017, "Surrogate-model-based reliability method for structural systems with dependent truncated random variables," *Proceedings of the Institution of Mechanical Engineers, Part O: Journal of Risk and Reliability*, 231(3), pp. 265-274.
- [164] Mohammad-Djafari, A., 1992, "A Matlab program to calculate the maximum entropy distributions," *Maximum Entropy and Bayesian Methods*, Springer, pp. 221-233.
- [165] Hu, Z., and Du, X., "Efficient Global Optimization Reliability Analysis (EGORA) for Time-Dependent Limit-State Functions," *Proc. ASME 2014 International Design Engineering Technical Conferences and Computers and Information in Engineering Conference*, American Society of Mechanical Engineers, pp. V02BT03A044-V002BT003A044.
- [166] Zhang, D., Han, X., Jiang, C., Liu, J., and Li, Q., 2017, "Time-dependent reliability analysis through response surface method," *Journal of Mechanical Design*, 139(4).
- [167] Hu, Z., and Du, X., 2013, "A sampling approach to extreme value distribution for time-dependent reliability analysis," *Journal of Mechanical Design*, 135(7), p. 071003.
- [168] Du, X., 2014, "Time-dependent mechanism reliability analysis with envelope functions and first-order approximation," *Journal of Mechanical Design*, 136(8), p. 081010.
- [169] Hu, Z., and Mahadevan, S., 2017, "A surrogate modeling approach for reliability analysis of a multidisciplinary system with spatio-temporal output," *Structural and Multidisciplinary Optimization*, 56(3), pp. 553-569.
- [170] Shi, Y., Lu, Z., Zhang, K., and Wei, Y., 2017, "Reliability analysis for structures with multiple temporal and spatial parameters based on the effective first-crossing point," *Journal of Mechanical Design*, 139(12), pp. 121403-121403.
- [171] Wei, X., and Du, X., 2019, "Robustness Metric for Robust Design Optimization Under Time- and Space-Dependent Uncertainty Through Metamodeling," *Journal of Mechanical Design*, 142(3).
- [172] Dering, M. L., and Tucker, C. S., 2017, "A Convolutional Neural Network Model for Predicting a Product's Function, Given Its Form," *Journal of Mechanical Design*, 139(11).

VITA

Hao Wu was born in Chengdu, Sichuan, the People's Republic of China. He received his Bachelor of Science degree in Mechanical Engineering in 2013 from Anhui University of Technology, Anhui, China. Then he continued his master education and obtained his Master of Science degree in Mechanical Engineering from University of Electronic Science and Technology of China in 2017. Hao Wu started pursuing the degree of Doctor of Philosophy in the school of Mechanical Engineering at Purdue University. He worked with Prof. Xiaoping Du and Prof. Ilias Bilonis in probabilistic design and system reliability analysis.